UNIVERSITY OF OKLAHOMA

GRADUATE COLLEGE

DETERMINATION OF SEISMIC ATTENUATION FROM SURFACE AND DOWNHOLE MEASUREMENTS

A Dissertation

SUBMITTED TO THE GRADUATE FACULTY

in partial fulfillment of the requirements for the

degree of

Doctor of Philosophy

By

SHENGJIE SUN

Norman, Oklahoma

2000

UMI Number: 9988511

Bell & Howell Information and Learning Company
300 North Zeeb Road
P.O. Box 1346
Ann Arbor, MI 48106-1346

DETERMINATION OF SEISMIC ATTENUATION FROM SURFACE AND DOWNHOLE MEASUREMENTS

A Dissertation APPROVED FOR THE
SCHOOL OF GEOLOGY AND GEOPHYSICS

BY

ACKNOWLEDGEMENTS

I would like to express my deepest gratitude to my advisor, Dr. John P. Castagna, for all his guidance, advice, support and patience throughout my Ph.D. program. I wish to thank all of my committee members, Drs. Robert W. Siegfried, Anuj Gupta, Roger Young, Alan Witten, James Forgotson for their advice, suggestion on my research, and their reviewing the manuscript. My thanks to Dr. Daniel J. O'Meara, Director of Institute of Reservoir Characterization for his support, help when I was in difficulties.

I would like to thank Dr. Bill Lamb of Institute of Exploration and Development Geoscience, OU, Ray Brown of Oklahoma Geological Survey, Antonio Ramos, visiting scientist from Brazil for their advice on my study. I would like to thank Dr. Claren Kidd of Youngblood library, University of Oklahoma for her assistance and encouragement. I would like to thank Dr. Ucan Sezai of Philip computer lab for his assistance.

My thanks to all the staff members, Donna Montgomery, Stephen Sandifer, Terry Brad and Kathy Socolic in particular, for their help and cooperation. I would like to thank my friends, Patrice Mahob, He Chen, Qiang Sun, Frederic Gallice and all others who helped me during my stay here.

Last but not the least, I thank my wife, Xiaojing Xie, for making all this possible through her many sacrifices and efforts. I also thank all other members of my family for their constant support and encouragement.

TABLE OF CONTENTS

LIST OF TABLES

LIST OF FIGURES

ABSTRACT

Attenuation is a potentially very important seismic attribute for seismic exploration and reservoir characterization. In order for attenuation to be utilized successfully as an attribute, it must first be reliably extracted from the seismic data and separated from scattering effects. Existing methods meet fatal difficulties in measuring attenuation from both surface seismic data and vertical seismic profile (VSP) data.

Intrinsic attenuation measurement from VSP using spectral ratios is seriously affected by scattering, coupling variations, and difficulties in first-arrival isolation. An algorithm to estimate intrinsic attenuation from VSP data where reliable seismic impedance logs are available effectively handles these problems. Using the available impedance profile calculated from well logs, VSP synthetics including up-going and down-going waves, multiples and attenuation are calculated. The scattering effect is removed iteratively by matching real spectral ratios with synthetic spectral ratios. Numerical modeling of infinite bandwidth and band limited cases shows that this method is accurate, effective and robust providing coupling variations are frequency-independent over the seismic bandwidth. Application to real VSP data from offshore Gulf of Mexico block Eugene island 354 shows high attenuation associated with potential gas pay.

Existing methods of attenuation estimation from surface seismic data suffer from wavelet extraction and scattering removal. An inversion method is developed to solve these problems. Instead of trying to extract the wavelet directly from the seismic trace and subsequently separate scattering effects, a full waveform forward modeling and damped

generalized linear inversion (GLI) algorithm to invert Q from the surface seismic trace are employed. The forward theory includes all the multiples and attenuation in the synthetic, thus allowing direct separation of the intrinsic Q from scattering effects. The employed forward inelastic wave theory also allows dispersion effects to be accounted for and does not require a constant Q model. Employment of the robust damped GLI algorithm produces a stable and accurate inversion result. Numerical modeling studies show that the Q profile can be recovered even if the initial model is not near the correct answer.

CHAPTER 1. INTRODUCTION

1.1 ATTENUATION AND ITS IMPORTANCE

It had been recognized that seismic attenuation can potentially be used as a direct hydrocarbon indicator (e.g. Mitchell, 1996) or as an indicator of fluid mobility (e.g., Castagna, 1998). However, related measurement of seismic attenuation in the field with surface seismic data has proven to be elusive. The purpose of this dissertation is to investigate new methods for seismic attenuation measurement.

Seismic attenuation is the amplitude decrease of the seismic wave with propagation distance. Attenuation of P-waves is a well-known seismic attribute and oil companies have used seismic attenuation as a direct hydrocarbon indicator for many years. Studies have been performed to understand the mechanism of the attenuation (e.g., Ricker, 1952; McDonal et al., 1958; Futterman, 1962; Jones 1986; Biot, 1956; White, 1975; O'Connel and Budiansky, 1977; Mavko and Nur, 1979; Palmer and Traviolia, 1980; Murphy et al., 1986; Dvorkin and Nur 1993) and its utility in reservoir characterization (e.g., Klimentos and McCann, 1990; Akbar et al., 1993). However, the attenuation mechanism in porous media is not completely understood. Laboratory measurements (Gardner et al. 1964; Frisillo and Stewart, 1980; Spencer, 1979 and 1981; Clark et al., 1980, 1981; Winkler and Nur, 1979 and 1982; Murphy, 1982 and 1983; Jones and Nur 1983; Jones, 1983 and 1986; Tittmann et al. 1983; Bourbie and Zinszner, 1984; Turgut et al., 1990; Frisillo and Thomsen 1992; Tutuncu et al., 1995; Batzle et al., 1996) and some of the field measurements (Meissner,1983; Kan et al., 1983; Raikes and White, 1984; Houck, 1987; Jacobsen, 1987; Yamamoto et al., 1995; Sames et al., 1997) indicate that the attenuation is frequency-dependent and closely related to the interaction between the pore fluid and the solid. In particular, the attenuation peaks at some frequency that depends on rock and fluid properties. However, it is generally not possible to predict the frequency at which this attenuation peak occurs from first principles and empirical observations must be relied upon. There is a growing body of evidence (Castagna, 1998) that this may occur between seismic and sonic frequencies in hydrocarbon reservoirs. Other lessons from the literature include:

1. Wave propagation is linear (independent of strain amplitude) at seismic strain and upper crustal conditions. This has been documented by several experiments at variable pressures, fluid saturations, and temperatures (Winkler and Nur, 1982; Murphy, 1983; Jones, 1983).

2. Attenuation in vacuum-dry rocks is negligible (Q of hundreds or thousands) compared to typical Q values from the upper crust, even at low pressures (Clark et al., 1980, 1981; Murphy, 1983). Attenuation is virtually independent of frequency in dry rocks (Spencer, 1981).

3. Attenuation is strongly affected by the fluid saturation, the properties of the pore fluid, and the seismic frequency (Gardner et al., 1964; Frisillo and Stewart, 1980; Spencer, 1981; Winkler and Nur, 1982; Murphy, 1983; Jones and Nur, 1983;

Tittmann et al. 1983; Bourbie and Zinszner, 1984; Jones, 1986; Turgut and Yamamoto, 1990; Frisillo and Thomsen 1992; Tutuncu et al., 1995; Batzle., 1996). In particular, attenuation peaks between seismic and sonic frequencies and the effect is most pronounced for rocks which are partially gas saturated.

4. Attenuation/dispersion can be significant enough to be detected above seismic frequency band. The effect is most pronounced for gas saturation. Seismic velocities in hydrocarbon reservoirs can be as much as 15% slower than sonic log velocities (Castagna, 1998), and related directly to fluid viscosity. In addition, *in situ* P-wave attenuation measurements compiled by Castagna et al. (1993) show a slight tendency for permeable sands to exhibit higher attenuation than impermeable shales. An attenuation profile in a South Texas clastic section measured by Kan et al. (1983) also exhibits anomalously high attenuation over an interval corresponding to a known gas reservoir.

5. Attenuation may be an important parameter in determining permeability. Klimentos and McCann (1990) measured the attenuation coefficients of compressional waves in 42 sandstones at confining pressure of 40 MPa (equivalent to a depth of burial of about 1.5 km). The results show that for these samples, compressional wave attenuation at 1 MHz and 40 MPa is related to clay content and porosity by an empirical formula. On the other hand, Klimentos and McCann show a strong systematic relation between clay content and permeability. Based on these results, Akbar et al. (1993) conclude that attenuation is the key factor in determining

permeability. They examined the relationship between attenuation and permeability using a 3-D theoretical model based on the squirt-flow mechanism. They find that the permeability-attenuation relation is characterized by an attenuation peak that shifts towards lower permeabilities as frequency decreases. Therefore the attenuation of a low-frequency wave decreases with increasing permeability. This result is similar to the experimental result of Klimentos and McCann (1990). However, Biot theory (1956) predicts the opposite effect.

Based on these theoretical and empirical studies, the following hypotheses appear to be reasonable: (1) attenuation can be a potential hydrocarbon indicator for seismic exploration, (2) seismic fluid mobility/permeability detection observation using the attenuation/dispersion may be possible, and (3) acoustic fluid mobility/permeability logging may be feasible.

1.2 DIFFICULTIES IN MEASURING ATTENUATION

Should the hypotheses presented in the previous section be proved true, attenuation has such important potential application that it must be considered a very promising seismic attribute for seismic exploration and reservoir characterization. However, the practical application of attenuation/dispersion is not so well developed. There are only a few unsuccessful attempts in seismic exploration (Mitchell et al., 1996; Dasgupta et al., 1998). For quantitative rock/fluid characterization, attenuation has only been demonstrated to be useful under very special circumstances (such as rock permeabilities much higher than the majority of oil reservoirs, see Yamamoto et al., 1995). The main reason for the failure of seismic attenuation as a geophysical attribute is the lack of a reliable estimation method from surface seismic data, VSP data and even full waveform well log data (Anderson, R. G. and Castagna, J. P., 1984).

Theoretically, there are at least five different methods to directly measure Q from seismic data: spectral amplitude ratio, peak-peak and first-peak amplitude ratio, rise time, pulse broadening, and the Futterman causal attenuation operator of an attenuating signal. In practice, attenuation measurement is measured mainly by spectral ratios. All these methods suffer the following difficulties:

We refer to attenuation caused by pore fluid and rock fabric as **intrinsic attenuation**; Attenuation caused by the fine layering effect (the O'Doherty and Anstey (1971) effect) is called **scattering attenuation**. What we are interested in is the intrinsic attenuation. However the attenuation we measure is generally the total effect of scattering and intrinsic attenuation. We call this **apparent attenuation**. Since both intrinsic and scattering attenuation have a very similar effect on wave propagation, the first difficulty is to separate them from each other. Although, many authors have addressed this problem (Kan, 1981; Spencer, 1985; Kang et al., 1994), no accurate methods have been proven. Another difficulty is the extraction of the wavelet spectra because of the effect of earth response and the limited resolution of classical spectral analysis.

For the seismic frequency range, there are two means of measuring seismic attenuation in the field: (1) from vertical seismic profiles (VSP), and (2) from surface seismic data. Both of these methods have similar problems.

1.3 PURPOSES

With respect to the above difficulties in measureing attenuation from seismic data, in this dissertation, methods for measuring attenuation from surface and VSP data will be investigated. For VSP data, an iterative scattering removal method is proposed. For the surface seismic data, the Generalized Linear Inversion (GLI) method is proposed. The proposed algorithms will try to properly separate intrinsic and layering induced attenuation, and try to solve the wavelet extraction difficulty.

In the GLI method, we will use the proposed synthetic theory to account for the scattering effects by assuming the impedance profile is known (from a well log) as is the source wavelet, and use a damped generalized linear inversion (GLI) method to invert for the intrinsic attenuation. This synthetic theory is applicable to 1-D media and can include all the multiples and attenuation in the synthetic trace. We will call it full waveform forward modeling in the following sections. This method will address two classical difficulties: the separation of intrinsic and layering induced attenuation and wavelet extraction. Modeling studies show this method is effective even with AGC filtered seismic data. In Chapter 4, the method and its modeling results will be detailed.

In the iterative scattering removal method for VSP data, the current spectral ratio method is improved to extract intrinsic attenuation from VSP data. Usually, VSP spectral ratio methods are seriously affected by scattering, coupling variations, and difficulties in first arrival isolation. Our method solves these problems, using the available impedance profile calculated from well logs. We calculate VSP synthetics which include up-going and down-going waves, multiples, geometrical spreading and attenuation. The scattering effect is removed iteratively by matching real spectral ratios with synthetic spectral ratios. This method does not have the first arrival isolation problem because it allows up and down-going and multiple arrivals within the analysis window. It also effectively reduces the coupling variation effects. In Chapter 5, we will describe the method, test it with synthetic data and apply it to real data.

1.4 OUTLINE OF DISSERTATION

There are 6 chapters in this dissertation. Chapter 1 is the introduction.

In Chapter 2, wave propagation theory in an attenuating medium is presented. The wave equation in attenuating media is derived, and the plane wave solution is given. Then scattering and intrinsic attenuation and their features are discussed. Finaly, the boundary conditions of plane wave propagation are derived. This chapter is the theoretical foundation of this dissertation.

In Chapter 3, the existing Q measurement techniques and existing difficulties are reviewed. First, the five basic techniques principally available are introduced. These methods are: (1) the measurement of spectral amplitude ratio, (2) peak-peak and first-peak amplitude ratios, (3) rise time, (4) pulse broadening, and (5) the Futterman causal attenuation operator of an attenuating signal. The current progress and remaining problems in Q estimation are reviewed. The representative methods for VSP data are: (1) the spectral ratio method by Kan et al. (1981) attempts to solve the scattering problem; (2) the inversion algorithm by Kang and McMechan (1994) tries to separate scattering attenuation by using an assumed additive relation; (3) the inversion method by Amundsen and Mittet (1994) addresses the coupling problem. The representative methods for surface seismic data are: (1) the power spectral ratio method (Raikes and White, 1984) and (2) the matching (inversion) technique (White, 1980; Lamb, 1998).

In Chapter 4, a full waveform GLI inversion method is proposed to solve the difficulties in measuring attenuation from surface seismic data. First, the full waveform synthetic theory is presented. Then, the GLI inversion technique is introduced. Finally, the numerical modeling is carried out. Since the forward theory includes all the multiples and attenuation in the synthetic, the new method allows direct extraction of the intrinsic Q from the seismic trace while taking into account scattering effects. The employment of the robust damped GLI algorithm will produce more stable and accurate inversion results. The numerical modeling verifies the correctness and feasibility of this method.

In Chapter 5, an iterative scattering-removal method to measure intrinsic attenuation from Vertical Seismic Profile (VSP) data is introduced. The full waveform VSP synthetic theory is briefly described. Then the detailed iterative procedure is given. This is following by numerical modeling and real application. This method greatly improved the existing spectral ratio method by allowing scattered events in the analysis window, thereby avoiding the first-arrival-isolation problem. This method, using the linear properties of seismic spectral ratios, is free from receiver sonde coupling problems unless the variations in coupling are frequency dependent over the seismic bandwidth. By using VSP synthetics that include up-going and down-going waves, multiples and attenuation, the scattering effect is removed iteratively by matching real spectral ratios with synthetic spectral ratios. Numerical modeling shows the accuracy and advantages of this method. Application to real VSP data confirms that high attenuation is associated with potential gas pay.

Chapter 6 contains discussion and conclusions. The complementary features, importance and potential of VSP and surface seismic methods are discussed.

CHAPTER 2. WAVE PROPAGATION IN AN ATTENUATING MEDIUM

In this chapter, the basic theory of seismic attenuation is introduced. The plane wave equation in an attenuating medium is derived. Intrinsic and scattering attenuation are defined and their relationship with other seismic and rock physics parameters such as the velocity, dispersion, frequency, quality factor etc., is discussed. Finally a derivation of boundary conditions in a 1-D elastic medium is given, which will be very important for forward synthetic modeling.

2.1 WAVE EQUATION IN ATTENUATING MEDIUM

2.1.1 Stress

Stress is the force per unit area exerted on a particle in a medium (Aki and Richards, 1980). It is a tensor, with 9 components; six of which are independent.

A particle within a medium can be considered as a tetrahedral volume (Figure 2.1). Three of the faces are normal to the rectangular coordinates axes and the fourth face has its outward-directed normal **n** in an arbitrary direction. The nine components of stress (T_{ij}) are defined as the three stress components acting on each of the three faces normal to the axes. T_{ij} is the j component of the stress that act on the face normal to the i axes. Due to symmetry: $T_{ij} = T_{ji}$, there are six independent components expressed in the matrix

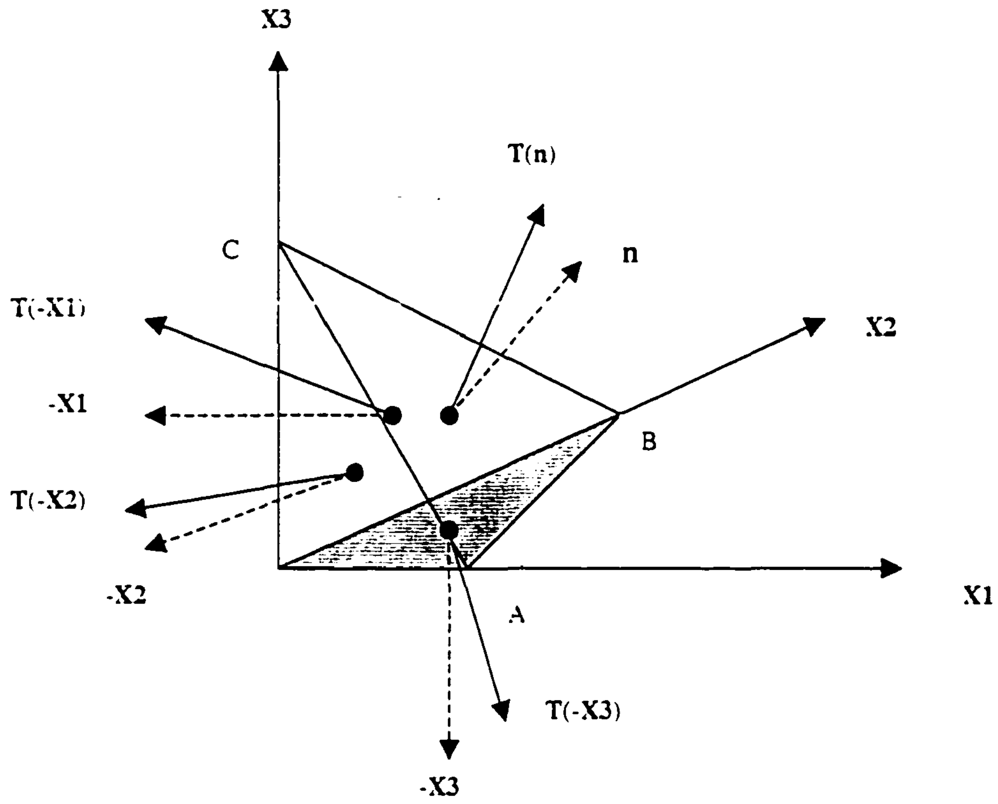

Figure 2.1 Tetrahedral volume in the rectangular coordinates system, **T** is stress, $-\mathbf{X}_j$ (j=1,2,3) is the normal to the face, the normal of the fourth face is **n**.

$$\mathbf{T} = \begin{bmatrix} T_{xx} & T_{xy} & T_{xz} \\ T_{yx} & T_{yy} & T_{yz} \\ T_{zx} & T_{zy} & T_{zz} \end{bmatrix} \tag{2.1}$$

In abbreviated subscript notation:

$$\mathbf{T} = \begin{bmatrix} T_1 & T_6 & T_5 \\ T_6 & T_2 & T_4 \\ T_5 & T_4 & T_3 \end{bmatrix} \quad \text{or} \tag{2.2}$$

$$\mathbf{T}^T = \begin{bmatrix} T_1 & T_2 & T_3 & T_4 & T_5 & T_6 \end{bmatrix} \tag{2.3}$$

2.1.2 Strain

In regular Cartesian coordinates, the strain (S_{ij}) is defined as (Aki and Richards, 1980):

$$S_{ij} = \frac{1}{2}\left(\frac{\partial U_i}{\partial x_j} + \frac{\partial U_j}{\partial x_i} \right) \tag{2.4}$$

where i,j=1,2,3, and U_i or U_j is the component of the particle displacement along axes i or j.

Due to symmetry, the strain tensor can also be expressed in similar abbreviated subscript notation as stress:

$$\mathbf{S} = \begin{bmatrix} S_1 & S_6 & S_5 \\ S_6 & S_2 & S_4 \\ S_5 & S_4 & S_3 \end{bmatrix} \quad \text{or} \tag{2.5}$$

$$\mathbf{S}^T = \begin{bmatrix} S_1 & S_2 & S_3 & S_4 & S_5 & S_6 \end{bmatrix} \tag{2.6}$$

Strain components in abbreviated subscripts are related in a simple way to particle displacement components:

$$\begin{bmatrix} S_1 \\ S_2 \\ S_3 \\ S_4 \\ S_5 \\ S_6 \end{bmatrix} = \begin{bmatrix} \dfrac{\partial U_x}{\partial x} \\ \dfrac{\partial U_y}{\partial y} \\ \dfrac{\partial U_z}{\partial z} \\ \dfrac{\partial U_y}{\partial z} + \dfrac{\partial U_z}{\partial y} \\ \dfrac{\partial U_x}{\partial z} + \dfrac{\partial U_z}{\partial x} \\ \dfrac{\partial U_x}{\partial y} + \dfrac{\partial U_y}{\partial x} \end{bmatrix} \tag{2.7}$$

or

$$\mathbf{S} = \nabla_s \mathbf{U} \tag{2.8}$$

where

$$\mathbf{U} = \begin{bmatrix} U_x & U_y & U_z \end{bmatrix} \tag{2.9}$$

and

$$\nabla_s = \begin{bmatrix} \dfrac{\partial}{\partial x} & 0 & 0 \\ 0 & \dfrac{\partial}{\partial y} & 0 \\ 0 & 0 & \dfrac{\partial}{\partial z} \\ 0 & \dfrac{\partial}{\partial z} & \dfrac{\partial}{\partial y} \\ \dfrac{\partial}{\partial z} & 0 & \dfrac{\partial}{\partial x} \\ \dfrac{\partial}{\partial y} & \dfrac{\partial}{\partial x} & 0 \end{bmatrix} \tag{2.10}$$

2.1.3 Newton's law

Consider a vibrating material particle of arbitrary shape with volume δv and surface area δs. The forces associated with its vibration are body force **f**δ**v** and surface force

$$\int_{\delta s} \mathbf{T} \cdot \mathbf{ds} = \int_{\delta v} \nabla \mathbf{T} dv \tag{2.11}$$

From Newton's second law (force = mass times acceleration), then:

$$\begin{aligned} &\int_{\delta s} \mathbf{T} \cdot \mathbf{ds} + \int_{\delta v} \mathbf{F} dv = \int_{\delta v} \rho \frac{\partial^2 \mathbf{U}}{\partial t^2} dv \\ &\Rightarrow \int_{\delta v} (\nabla \mathbf{T} + \mathbf{F}) dv = \int_{\delta v} \rho \frac{\partial^2 \mathbf{U}}{\partial t^2} dv \\ &\Rightarrow \nabla \mathbf{T} + \mathbf{F} = \rho \frac{\partial^2 \mathbf{U}}{\partial t^2} \end{aligned} \tag{2.12}$$

2.1.4 Hooke's law

According to Hooke's law, in an elastic medium, stress is linearly proportional to the strain

$$T_{ij} = C_{ijkl} S_{kl}\ ,\ \mathrm{i,j,k,l=x,y,z}\ . \tag{2.13}$$

where **C** is the stiffness tensor, **T** is stress and **S** is strain. The symmetry: $C_{ijkl} = C_{ijlk} = C_{jikl}$, will reduce the number of independent constants to 36. And with the symmetry: $C_{ijkl} = C_{klij}$, the constants are further reduced to 21. This is the maximum number of constants for any medium.

In abbreviated subscripts:

Abbreviated subscript	original subscript: ij
1	xx
2	yy
3	zz
4	yz, zy
5	zx, xz
6	xy, yx

The general form of Hooke's law is therefore

$$T_i = C_{ij}S_j, \quad i,j = 1,2,3,4,5,6 \quad \text{or} \quad \mathbf{T} = \mathbf{CS} \qquad (2.14)$$

2.1.5 Extension of Hooke's law in attenuating medium

Materials observing Hooke's law, do not have internal energy loss. Ideal materials of this kind do not exist in nature, let alone in the solid earth. where the attenuation of seismic energy is an established fact.

A material is said to be linearly viscoelastic if stress components are linearly related to strain components at a given time and the principle of linear superposition holds. Rocks are generally linear viscoelastic for strains induced by far-field seismic waves. The ideal Hooke's law relation: $T_i = C_{ij}S_j$, can be modified to include damping by adding terms containing time derivatives of strain. That is:

$$T_i = C_{ij} S_j + \eta_{ij} \frac{\partial S_i}{\partial t} \tag{2.15}$$

where η_{ij} are viscosity constants.

2.1.6 Wave equation in attenuating medium

From Newton's law

$$\nabla \mathbf{T} + \mathbf{F} = \rho \frac{\partial^2 \mathbf{U}}{\partial t^2} = \rho \frac{\partial \mathbf{W}}{\partial t} \tag{2.16}$$

From Hooke's law

$$\mathbf{T} = \mathbf{C}\,\mathbf{S} + \eta \frac{\partial \mathbf{S}}{\partial t} \tag{2.17}$$

Let: $\tau = \mathrm{C} + \eta \dfrac{\partial}{\partial t}$, then Hooke's law is

$$\mathbf{T} = \tau \mathbf{S} \quad \text{and} \quad \frac{\partial \mathbf{T}}{\partial t} = \tau \frac{\partial \mathbf{S}}{\partial t} \tag{2.18}$$

Since

$$\mathbf{S} = \nabla_s \mathbf{U} \rightarrow \frac{\partial \mathbf{S}}{\partial t} = \nabla_s \mathbf{W} \tag{2.19}$$

Then

$$\frac{\partial \mathbf{T}}{\partial t} = \tau \; \nabla_s \mathbf{W} \tag{2.20}$$

where **W** is the particle velocity. Equation (2.16) and (2.20) constitute the acoustic field (t, v) equations, from where we can get the field wave equation.

From the equation (2.16), we have

$$\nabla \frac{\partial \mathbf{T}}{\partial t} + \frac{\partial \mathbf{F}}{\partial t} = \rho \frac{\partial^2 \mathbf{W}}{\partial t^2} \tag{2.21}$$

Substituting this equation (2.21) into (2.20), yields the velocity wave equation:

$$\frac{\partial \mathbf{F}}{\partial t} + \nabla (\tau \;\; \nabla_s \mathbf{W}) = \rho \frac{\partial^2 \mathbf{W}}{\partial t^2}$$

(2.22)

2.2 PLANE WAVE SOLUTION IN ATTENUATING MEDIUM

In a 1-D medium, assuming body force **F** =0, the wave equation (2.22) become:

$$\frac{\partial}{\partial x}(c + \eta \frac{\partial}{\partial t}) \frac{\partial}{\partial x} W = \rho \frac{\partial^2 W}{\partial t^2} \tag{2.23}$$

where c is the Young's modules, η is the viscosity, ρ is the density. Assume $W = X(x)T(t)$. According to Fourier transformation principle, $T(t)$ is the superposition of $e^{i\omega t}$ over frequency, where ω is angular frequency. Substituting $e^{i\omega t}$ into the equation (2.23) for $T(t)$, gives:

$$(c + i\omega\eta) \frac{\partial^2}{\partial x^2} X(x) = -\rho\omega^2 X \tag{2.24}$$

The solution to this equation obtained using the root method is:

$$X(x) = e^{\pm ikx} \tag{2.25}$$

where $k = \sqrt{\rho\omega^2 / (c + i\omega\eta)}$ is the wave number as in the elastic case, but here k is complex and is called the complex wave number.

Thus, the single plane wave solution for the wave equation (2.22) can be written in the form of

$$W(x,t) = W_0 e^{i(\omega t - kx)} \tag{2.26}$$

The complex wave number can be written in the format

$$k = \beta - i\alpha \tag{2.27}$$

where β is the real wave number defined as

$$\beta = \frac{\omega}{V_{phase}} \tag{2.28}$$

and V_{phase} is the phase velocity. Then the solution is

$$W(x,t) = W_0 e^{-\alpha x} e^{i(\omega t - \beta x)} \tag{2.29}$$

Thus, in an attenuating (linear viscoelastic) medium, the wave will propagate along the x direction with exponentially attenuated amplitude. The attenuation factor will be the form of exp(-αx).

2.3 ATTENUATION/DISPERSION AND Q

In an attenuating medium, the attenuation (amplitude decay) of a plane-wave seismic pulse as a function of position, z , can be described by:

$$A(z) = A(0)e^{-\alpha z} \tag{2.30}$$

where A(z) = signal amplitude at position z, A(0) = initial amplitude, and α = attenuation coefficient.

The attenuation of a seismic wave results from the viscoelasticity of the material. The mechanism for this viscoelasticity is not yet fully understood. General experience is that, a propagating seismic wave will lose energy as a result of internal friction and the amplitude will be attenuated. The total effect of the internal friction that can occur within a material is described by the unitless parameter Q, called the Quality Factor, defined as (Aki and Richards, 1980)

$$\frac{1}{Q(\omega)} = -\frac{\Delta E}{2\pi E} \tag{2.31}$$

where E is the energy stored in one cycle, ω is the angular frequency and $-\Delta E$ is the energy lost in one cycle. For a medium with linear stress-strain relationship, the wave energy is proportional to its amplitude squared. Then

$$\frac{1}{Q(\omega)} = -\frac{\Delta A}{\pi A} \tag{2.32}$$

From this definition, the attenuating solution of a wave propagating in attenuating medium with Q can be derived. Assuming V is the phase velocity and ω is the angle frequency

$$\lambda = \frac{2\pi V}{\omega} \tag{2.33}$$

and

$$\Delta A = \frac{dA}{dz}\lambda \tag{2.34}$$

Then

$$\frac{dA}{dz} = -\frac{\omega}{2VQ}A \tag{2.35}$$

The attenuating solution to the above equation is

$$A(z) = A_0 \exp\left[-\frac{\omega z}{2VQ}\right] \tag{2.36}$$

comparing the equation (2.36) and (2.30), the Q and attenuation relationship in a linearly viscoelastic medium is:

$$Q = \frac{\omega}{2V\alpha} = \frac{\beta}{2\alpha} \tag{2.37}$$

Dispersion is the frequency dependence of seismic velocity. If the seismic phase velocity in a medium is a function of frequency, i.e. $V=V(\omega)$, we say the medium is dispersive. It has been shown (Futterman, 1962) that in a medium where wave propagation is linear and causal, the presence of attenuation requires the phase velocity to be a function of frequency, i.e. attenuation is a necessary and sufficient condition for dispersion.The relationship of frequency-dependent phase velocity to frequency-dependent attenuation is known as the dispersion-attenuation relationship. If a function is causal, its real and imaginary parts are related by the Hilbert relationship (Bracewell, 1965), and the dispersion-attenuation relationship may be written in terms of the Kramers-Kronig integrals (Kanamori and Anderson, 1977) as

$$\frac{1}{V(\omega)} = \frac{1}{V_\infty}\left(\frac{1}{2\pi} P \int_{-\infty}^{\infty} \frac{1/Q(\omega')d\omega'}{(\omega' - \omega)}\right) \tag{2.38}$$

where V_∞ is the high-frequency value of phase velocity, and P stands for the Cauchy principal value of the integral.

For the constant Q model, the real part of the complex wavenumber in equation (2.27) is expressed as the sum (Bickel and Natarajan, 1985)

$$\beta = \frac{\omega}{V_0} - \frac{\omega}{\pi Q V_0}\ln\left(\frac{\omega}{\omega_0}\right) \tag{2.39}$$

where ω / V_0 is a pure delay term with phase velocity V_0 associated with the reference frequency ω_0.

Therefore, to measure the attenuation coefficient, amplitudes of Fourier frequency components are typically measured at two locations. The ratio of these amplitude spectra eliminates the initial amplitude dependence. Thus, at a given frequency:

$$A(z_1) / A(z_2) = e^{-\alpha(z_1/z_2)} \tag{2.40}$$

hence,

$$\alpha = (z_2 - z_1)^{-1} \ln\left[A(z_1) / A(z_2)\right] \tag{2.41}$$

It is often assumed that the quality factor (Q) is constant across the seismic frequency band. This assumption is generally supported for P-waves by spectral ratio measurements which indicate that the attenuation coefficient is linearly proportional to frequency (McDonal et al.; 1958). This requires that the product Q times velocity be constant (see equation 2.37). If velocity is only slowly varying with frequency (Spencer, 1981;

Murphy, 1982) as is commonly assumed for the seismic frequency band. Q is approximately constant. Then from equation 2.37, Q is obtained from

$$\alpha = \frac{1}{2VQ}\omega \tag{2.42}$$

because $\frac{1}{2VQ}$ is the linear slope of α over angular frequency. This slope can be estimated from equation (2.41). If we assume V and Q are approximately frequency independent over the bandwidth of the data, Q can then be obtained from the slope if V is known.

2.4 SCATTERING ATTENUATION/DISPERSION AND Q

It has long been recognized that sediment layers with thickness much less than a seismic wavelength affect a wave by slowing it slightly and decreasing its amplitude. This effect is similar to inelastic attenuation. We refer to this effect as scattering induced attenuation/dispersion. A beautifully written paper by O'Doherty and Anstey (1971) provides the best introduction to this subject.

There are five factors that affect the amplitude of a seismic wave signal. They are (1) spherical divergence, (2) absorption, (3) the reflection coefficient of the reflecting interface, (4) the cumulative transmission loss at all interfaces above this, and (5) the effect of multiple reflections. Among the five, the absorption causes the intrinsic attenuation and the last three causes the scattering attenuation. Scattering attenuation and qualify factor are defined in similar way as for intrinsic attenuation and Q.

Of the five factors affecting amplitude, spherical divergence is easy to correct in a structurally simple earth. The familiar law of conservation of energy, when applied to a spherical wavefront emanating from a point source in uniform lossless material, tells us that the intensity diminishes as the inverse square of the radius of the wavefront. Translated into the type of measurements made in seismic work, this says that the pressure amplitude of the seismic wave is inversely related to the distance traveled.

The process of reflection and transmission at interfaces do not involve any loss of energy, merely a redistribution of it in the forward and backward directions. We know that energy reflected from an interface is not available to be transmitted through it. If the reflection coefficient of an interface is R, the transmission coefficient will be 1-R for particle velocity amplitude (see next section about boundary condition). Clearly, the larger the reflection coefficient, the greater is the transmission loss. The transmission loss is not the only reason for scattering attenuation (if it is, the signal will be decayed away to nothing so quickly as to be useless). In fact, multiples, especially the fine layer multiples, offset most of the transmission losses. The effect of multiple reflections is the least well understood of the factors affecting amplitude. However, observation shows that multiple paths having an even number of bounces can have the effect of delaying, shaping and magnifying the pulse transmitted through a layered sequence and transmission loss with multiples causes the similar amplitude decay to intrinsic attenuation. O'Doherty and Anstey (1971) gave an approximate relationship between the amplitude spectrum $T(\omega)$ of the transmitted pulse and the power spectrum $R(\omega)$ of the reflection coefficient series:

$$T(\omega) = e^{-R(\omega)t} \tag{2.43}$$

where t is travel time. This is the well-known O'Doherty-Anstey formula, which has been rederived by Banik etc. (1985) and Shapiro etc. (1993) in different ways.

Generally we are interested in the attenuation caused by internal friction, which is called intrinsic attenuation. But what we can measure from spectra ratios is the total attenuation. Separating the two attenuations is necessary if measured attenuation is to be related directly to rock properties.

2.5 BOUNDARY CONDITIONS OF PLANE WAVE PROPAGATION

2.5.1 General definition of boundary conditions

In acoustic problems, we assume the interfaces between different solid media are usually firmly bonded together, so that there is no slippage or separation of one with respect to the other. This means the particle displacement velocity must be continuous across the discontinuity surface. That is

$$\mathbf{W} = \mathbf{W}' \tag{2.44}$$

where $\mathbf{W}$ is the particle displacement velocity just above the surface and $\mathbf{W}'$ the particle displacement just below.

Boundary conditions of stress field can be derived by assuming a small dislike volume, enclosing an area ds of the interface surface (Figure 2.2).

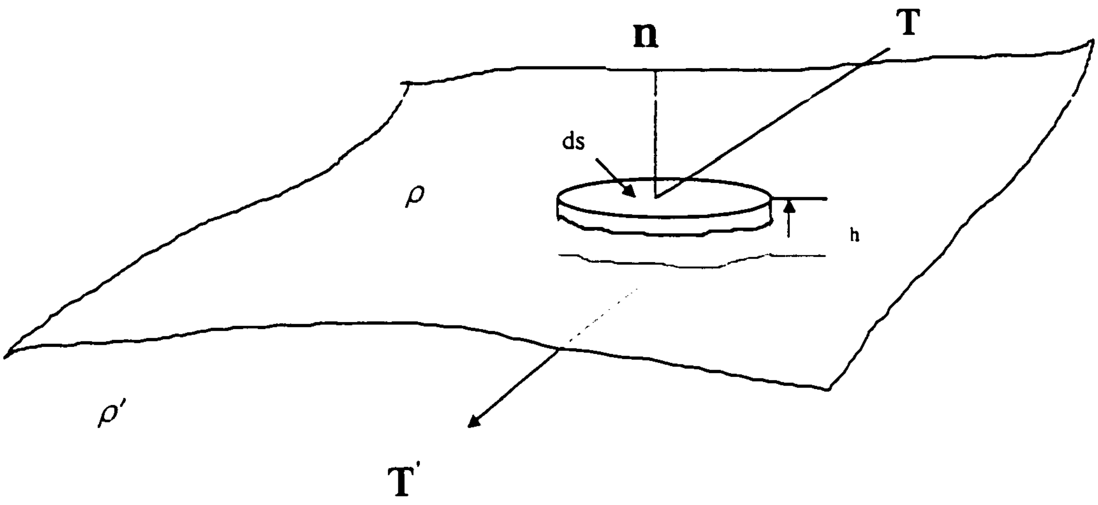

Figure 2.2. Continuous stress model

Assuming body force **F** and particle velocity **W**, Newton's law gives:

$$(\mathbf{T} - \mathbf{T}')\mathbf{n}\,ds + \mathbf{F}\,h\,ds = \left(\frac{\rho + \rho'}{2}\right)\frac{\partial \mathbf{W}}{\partial t}h\,ds$$

(2.45)

As $h \to 0$,

$$Fhds \to 0$$

$$\left(\frac{\rho + \rho'}{2}\right)\frac{\partial \mathbf{W}}{\partial t}hds \to 0 \tag{2.46}$$

So

$$\mathbf{T} \bullet \mathbf{n} = \mathbf{T'} \bullet \mathbf{n} \tag{2.47}$$

2.5.2 Plane wave solution in isotropic and homogenous media

In isotropic and homogeneous media, the constitutional relation is

$$\mathbf{C} = \begin{bmatrix} C_{11} & C_{12} & C_{12} & 0 & 0 & 0 \\ C_{12} & C_{11} & C_{12} & 0 & 0 & 0 \\ C_{12} & C_{12} & C_{11} & 0 & 0 & 0 \\ 0 & 0 & 0 & C_{44} & 0 & 0 \\ 0 & 0 & 0 & 0 & C_{44} & 0 \\ 0 & 0 & 0 & 0 & 0 & C_{44} \end{bmatrix} \tag{2.48}$$

And $C_{12} = C_{11} - 2C_{44}$. Assuming a plane wave propagating along the x direction, since the field can vary only with x, only the partial derivative $\frac{\partial}{\partial x}$ is non zero in field equation

$$\begin{cases} \nabla \mathbf{T} + \mathbf{F} = \rho \dfrac{\partial \mathbf{W}}{\partial t} \\ \dfrac{\partial \mathbf{T}}{\partial t} = \tau \bullet \left(\nabla_s \mathbf{W} \right) \end{cases} \tag{2.49}$$

So the equations can be reduced as follows:

From

$$\nabla \mathbf{T} = \rho \frac{\partial \mathbf{W}}{\partial t}$$

Then

$$\begin{aligned} &\frac{\partial T_1}{\partial x} = \rho \frac{\partial W_x}{\partial t} \\ \Rightarrow\ &\frac{\partial T_6}{\partial x} = \rho \frac{\partial W_y}{\partial t} \\ &\frac{\partial T_5}{\partial x} = \rho \frac{\partial W_z}{\partial t} \end{aligned} \tag{2.50}$$

From

$$\frac{\partial \mathbf{T}}{\partial t} = \tau\ \nabla_s \mathbf{W} \Rightarrow \frac{\partial \mathbf{T}}{\partial t} = \mathbf{C}(\ \nabla_s \mathbf{W}\ )$$

Then

$$\Rightarrow\ \frac{\partial T}{\partial t} = C \begin{bmatrix} \frac{\partial W_x}{\partial x} \\ 0 \\ 0 \\ 0 \\ \frac{\partial W_z}{\partial x} \\ \frac{\partial W_y}{\partial x} \end{bmatrix} \tag{2.51}$$

and

$$\begin{aligned} \frac{\partial T_1}{\partial t} &= C_{11} \frac{\partial W_x}{\partial x} \\ \frac{\partial T_2}{\partial t} &= C_{12} \frac{\partial W_x}{\partial x} \\ \frac{\partial T_3}{\partial t} &= C_{12} \frac{\partial W_x}{\partial x} \\ \frac{\partial T_4}{\partial t} &= 0 \\ \frac{\partial T_5}{\partial t} &= C_{44} \frac{\partial W_z}{\partial x} \\ \frac{\partial T_6}{\partial t} &= C_{44} \frac{\partial W_y}{\partial x} \end{aligned} \tag{2.52}$$

From: $\dfrac{\partial T_4}{\partial t} = 0 \rightarrow T_4 = 0$ (2.53)

From:

$$\begin{cases} \dfrac{\partial T_1}{\partial x} = \rho \dfrac{\partial W_x}{\partial t} \\ \dfrac{\partial T_1}{\partial t} = C_{11} \dfrac{\partial W_x}{\partial x} \end{cases} \Rightarrow \frac{C_{11}}{\rho} \frac{\partial^2 W_x}{\partial x^2} = \frac{\partial^2 W_x}{\partial t^2} \tag{2.54}$$

This is the compressional wave equation, thus

$$W_x(x,t) = W_{x0} e^{i\omega(t - \frac{x}{V_p})} \tag{2.55}$$

with phase velocity

$$(V_p)_x = \sqrt{\frac{C_{11}}{\rho}} \tag{2.56}$$

and

$$\begin{aligned} \pm T_1 &= \mp W_x \sqrt{C_{11}\rho} \\ \pm T_2 &= \mp \sqrt{\rho C_{12}} \\ \pm T_3 &= \mp W_x \sqrt{\rho C_{12}} \end{aligned} \tag{2.57}$$

From :

$$\begin{cases} \dfrac{\partial T_6}{\partial x} = \rho \dfrac{\partial W_y}{\partial z} \\ \dfrac{\partial T_6}{\partial t} = C_{44} \dfrac{\partial W_y}{\partial x} \end{cases}$$

Then

$$\Rightarrow \frac{C_{44}}{\rho}\frac{\partial^2 W_y}{\partial x^2} = \frac{\partial^2 W_y}{\partial t^2} \tag{2.58}$$

This is the y-polarization wave equation with velocity

$$\left(V_p\right)_y = \sqrt{\frac{C_{44}}{\rho}} \quad \text{and} \quad \pm T_6 = \mp W_y \sqrt{\rho C_{44}} \tag{2.59}$$

From:

$$\begin{cases} \dfrac{\partial T_5}{\partial x} = \rho \dfrac{\partial W_z}{\partial t} \\ \dfrac{\partial T_5}{\partial t} = C_{44} \dfrac{\partial W_z}{\partial x} \end{cases}$$

Then

$$\Rightarrow \frac{C_{44}}{\rho}\frac{\partial^2 W_z}{\partial x^2} = \frac{\partial^2 W_z}{\partial t^2} \tag{2.60}$$

This is the z-polarization wave equation with velocity

$$\left(V_p\right)_z = \sqrt{\frac{C_{44}}{\rho}} \quad and \quad \pm T_5 = \mp W_y \sqrt{\rho C_{44}} \tag{2.61}$$

2.5.3 Boundary conditions of plane wave propagation in a 1-D medium

Applying the above boundary conditions (2.44) and 2.47) to a plane interface with normally incident plane compressional waves, boundary conditions are simplified.

For the incident wave (2.55-2.57)

$$
\begin{aligned}
(W_x)_I &= Ae^{i(\omega t-\kappa x)} \\
(T_1)_I &= -(\rho C_{11})^{\frac{1}{2}} Ae^{i(\omega t-\kappa x)} \\
(T_2)_I &= -\frac{C_{12}}{V_p} Ae^{i(\omega t-\kappa x)} \\
(T_3)_I &= -\frac{C_{12}}{V_p} Ae^{i(\omega t-\kappa x)}
\end{aligned}
\tag{2.62}
$$

The reflected waves are

$$
\begin{aligned}
(W_x)_R &= Be^{i(\omega t+\kappa x)} \\
(T_1)_R &= (\rho C_{11})^{\frac{1}{2}} Be^{i(\omega t+\kappa x)} \\
(T_2)_R &= \frac{C_{12}}{V_p} Be^{i(\omega t+\kappa x)} \\
(T_3)_R &= \frac{C_{12}}{V_p} Be^{i(\omega t+\kappa x)}
\end{aligned}
\tag{2.63}
$$

And the transmitted waves are

$$
\begin{aligned}
(W_x)_T &= B'e^{i(\omega t-\kappa' x)} \\
(T_1)_T &= -(\rho' C'_{11})^{\frac{1}{2}} B'e^{i(\omega t-\kappa' x)} \\
(T_2)_T &= -\frac{C'_{12}}{V'_p} B'e^{i(\omega t-\kappa' x)} \\
(T_3)_T &= -\frac{C'_{12}}{V'_p} B'e^{i(\omega t-\kappa' x)}
\end{aligned}
\tag{2.64}
$$

Since only one stress component, $T_1 = T_{xx}$, is involved in the boundary condition equation, from the equation (2.44) and (2.47)

$$
\begin{aligned}
(W_x(0))_I + (W_x(0))_R &= (W_x'(0))_T \\
(T_1(0))_I + (T_1(0))_R &= (T_1'(0))_T
\end{aligned}
\tag{2.65}
$$

That is

$$
\begin{aligned}
&A + B = B' \\
&-(\rho C_{11})^{\frac{1}{2}}(A - B) = -(\rho' C_{11})^{\frac{1}{2}} B'
\end{aligned}
\tag{2.66}
$$

Solution of these equations for B and B' gives the particle velocity reflection and transmission coefficients

$$
\begin{aligned}
R_W &= \frac{(W_t(0))_R}{(W_t(0))_I} = -\frac{(\rho' C_{11})^{\frac{1}{2}} - (\rho C_{11})^{\frac{1}{2}}}{(\rho' C_{11})^{\frac{1}{2}} + (\rho C_{11})^{\frac{1}{2}}} \\
T_W &= \frac{\left(W_t'(0)\right)_T}{(W_t(0))_I} = \frac{2(\rho C_{11})^{\frac{1}{2}}}{(\rho' C_{11})^{\frac{1}{2}} + (\rho C_{11})^{\frac{1}{2}}}
\end{aligned}
\tag{2.66}
$$

The stress reflection and transmission coefficients and

$$
\begin{aligned}
R_T &= \frac{(T_1(0))_R}{(T_1(0))_I} = -R_V \\
T_T &= \frac{\left(T_1'(0)\right)_T}{(T_1(0))_I} = \frac{(\rho' C_{11}')^{\frac{1}{2}}}{(\rho C_{11})^{\frac{1}{2}}} T_V
\end{aligned}
\tag{2.67}
$$

So, boundary conditions expressed in reflection and transmission coefficients are:

For the particle velocity case:

$$1 + R_W = T_W \tag{2.68}$$

For the stress case:

$$1 + R_T = T_T \tag{2.69}$$

Hence, if we define the reflection coefficient as

$$R = \frac{\sqrt{\rho' C_{11}} - \sqrt{\rho C_{11}}}{\sqrt{\rho' C_{11}} + \sqrt{\rho C_{11}}} \tag{2.70}$$

the boundary conditions are,

In the particle velocity case

$$T = 1 - R \tag{2.71}$$

In the stress case

$$T = 1 + R \tag{2.72}$$

CHAPTER 3. REVIEW OF Q MEASUREMENT TECHNIQUES

There are at least five different methods to directly measure Q from seismic data. These methods are: (1) the measurement of spectral amplitude ratio, (2) peak-peak and first-peak amplitude ratios, (3) rise time, (4) pulse broadening, and (5) the Futterman causal attenuation operator of an attenuating signal. Badri and Mooney (1987) analyze and compare these methods, and applied them to their experimental data in unconsolidated sediment near Wenover, Utah. They conclude that different computational techniques can result in different Q values for the same type of materials; rise-time and pulse-broadening methods are probably source-dependent; a correct geometrical spreading factor appears to be sufficient to account for the observed amplitude decay with distance, which makes the Q value computed from Futterman the operator in their study questionable. Their conclusions suggest that the Q values computed from the spectral-ratio method are probably the most reliable.

To measure Q, there are two typical difficulties. One is to separate intrinsic Q and scattering Q. The other is to extract the wavelet or isolate the arrival. Badri and Mooney (1987) did not address these difficulties in their paper. However, these difficulties are the key problems in application of the attenuation in hydrocarbon exploration and reservoir characterization. Spencer (1985) summarized and analyzed the difficulties in Q measurement from VSP data by examining related techniques to solve these problems. In this chapter, we will first introduce the basic techniques in Q measurement, then present progress in Q measurement techniques, strategies and finally discuss remaining difficulties in attacking these problems.

3.1 BASIC TECHNIQUES IN Q MEASUREMENT

From section 2.3, in an attenuating medium, the attenuation (amplitude decay) of a seismic pulse as a function of position, z, is described by:

$$A(z) = A(0)e^{-\alpha z} \tag{3.1}$$

where A(z) = signal amplitude at position z, A(0) = initial amplitude, and α = attenuation coefficient. In the above equation, we assume that the attenuation coefficient $\alpha(\omega)$ is linearly dependent upon frequency within a limited bandwidth. This linear dependence of α leads to a further assumption in which Q is approximately frequency-independent over the frequency range under consideration. If these assumptions are approximately valid, then the spectral components for angular frequency ω at depths z1 and z2 are related by the expression

$$A(z_1) \,/\, A(z_2) = e^{-\alpha(z_1/z_2)} \tag{3.2}$$

The expression (3.2) can be used either in the time domain or in the frequency domain. This gives us five possible methods to use in attempting to measure attenuation.

3.1.1 Peak amplitude ratio method

If we choose to apply equation (3.2) in the time domain, we can use either (a) the ratio of peak-to-peak amplitude of the first motion, or (b) the ratio of peak amplitude of the first motion of the waveform recorded at the more distant location to the amplitude at the reference location. Note that the time-domain application can be used only if we make some additional assumptions. The most important assumption is that the portion of the signal under consideration at the second location was originally the same portion of the signal at the first location. Also, it is assumed that factors such as geometrical divergence have been properly accounted for.

3.1.2 Spectral ratio method

In the frequency domain, the various methods of analysis all rely on equation (3.2) which can be manipulated in several ways. Converting to logarithms of the amplitude ratios, expression (3.2) can be written as

$$\alpha = (z_2 - z_1)^{-1} \ln\left[A(z_1) / A(z_2)\right] \tag{3.3}$$

With this equation, we can obtain α and hence

$$Q = \frac{\omega}{2V\alpha} \tag{3.4}$$

The Q value can be computed from the inverse slope of the line fitted through the data points within the specific bandwidth. Substituting expression (3.4) into equation (3.3), gives

$$(z_2 - z_1)^{-1} \ln\left[A(z_1) / A(z_2)\right] = \omega / 2VQ \tag{3.5}$$

Equation (3.5) is an equation of a straight line with slope $(1/2VQ)$. If the velocity of the medium is known and Q is assumed to be independent of frequency, Q can be determined from the following

$$Q = \frac{1}{2Vs} \tag{3.6}$$

where s is the slope of the line fit.

The spectral-ratio method requires at least a moderate bandwidth for the source waveform, since it requires measurement of spectral slope versus frequency and also requires a reasonably high signal-to-noise ratio in the frequency band for analysis.

3.1.3 Rise-time method

Q can also be computed from a rise-time method. Gladwin and Stacey (1974) defined the rise time as the ratio of the maximum peak amplitude to the maximum slope of the initial portion of the signal after the first arrival. This definition can be fitted with an equation of the form

$$T = (C / Q)t + T_0 \tag{3.7}$$

where T is the rise time at the point of measurement and T_0 is the rise time of the pulse at the source. C is a fixed constant close to 0.5, and t is the traveltime between the source and the point of measurement. Kjartansson (1979) has derived a value of 0.485 for C for signal detection.

Equation (3.7) simply represents a linear relationship between the rise time T and the travel time t, with (C/Q) as the slope and T_0 as the intercept. The Q value measured in this method is very sensitive to the slope of the fitted line through the data points.

3.1.4 Pulse-broadening method

The fourth method in computing Q in an attenuating medium is the pulse-broadening method. It is based on the assumption that pulse broadening is due to inelastic attenuation in the medium and that Q is approximately independent of frequency. As proposed by Gladwin and Stacy (1974) and Kjartansson (1979), the broadening is proportional to the traveltime and is related to Q by the equation

$$\lambda = (C / Q)t + \lambda_0 \tag{3.8}$$

where λ is the pulse width at the measurement point, λ_0 is the pulse width at the source, and t is the traveltime between the source and the point of measurement. C is a fixed constant with value C=0.5.

The pulse width can be measured in several ways. The first approach is based on measuring the pulse width of the first quarter of a cycle after the first break, which can be defined as the time lapse between the first break and first peak amplitude. The second approach is based on measuring the pulse width of the first half-cycle after the first break. The pulse width for a half-cycle can be defined as the time lapse between the first arrival of the first break and the first zero crossing. The first approach, pulse width of the first quarter-cycle, is preferable because some of the interference can be avoided. This approach is especially favorable if the signal under consideration includes several arrivals.

3.1.5 Futterman causal attenuation operator

A fifth method to estimate Q in an attenuation medium is the Futterman causal attenuation operator. This method is based on simulating a synthetic seismogram through an attenuating medium by propagating an observed signal through a perfectly elastic medium and modifying it with a filter. The filter is based on an operator proposed by Futterman (1962). It has the important characteristic of satisfying the physical condition of causality.

The ultimate goal of this method is to arrive at a Q value for which the shape and content of the synthesized waveform will match those of the observed waveform at some desired distance. This Q value is then considered to be a reasonable estimate of Q for the *in-situ* materials. The input parameters required for this filter are velocity, quality factor Q, distance to a reference receiver, waveform at the reference receiver, and distance to the receiver at the point of observation. If the computed waveform does not match the observed waveform at distance R, the input parameter Q is then modified. A typical corrective procedure would be to perturb the parameter Q of the filter to improve the match, keeping other parameters fixed. Such a procedure can be made systematic and thus suitable for implementation on the computer. The Q value used in this process can be limited to a geologically plausible range. This iterative procedure makes no effort to obtain a perfect match between the observed and computed signals, especially if the observed signals show a high degree of complexity in appearance. Nevertheless, by comparing the computed signals for a range of plausible Q values, one can arrive at an optimum match in shape, amplitude, and frequency content between the observed and synthetic signals.

The synthetic seismograms can be computed from the inverse Fourier transform of the expression

$$F_{syn}(R,\omega) = F_{obs}(R1,\omega)H(R,\omega) \tag{3.9}$$

where $H(R, \omega)$ is the transfer function of the Futterman operator and $F_{obs}(R1,\omega)$ is the Fourier transform of the observed signal at the reference station at distance R1 from the source. If a good match is observed, the Q value used to arrive at such a match will be considered a reasonable estimate of the attenuation property of the sediments at the site under consideration. The transfer function of the Futterman operator is given by the expression

$$
H(R,\omega)=\begin{cases}
(\dfrac{R1}{R2})\exp(-\dfrac{|\omega|R}{2Qv_0}) \\
\times\exp\left\{(i\dfrac{\omega R}{Qv_0})\left[\ln\left(\dfrac{\omega}{\omega'}\right)-2\right]\right\} \quad for \quad \omega_0<|\omega|<\omega' \\
1.0 \quad for \quad 0<|\omega|<\omega_0 \, . \\
0.0 \quad for \quad |\omega|>\omega' \quad .
\end{cases}
\tag{3.10}
$$

where v_0 is the wave velocity at frequency ω_0 which is the reference frequency taken at the lowest frequency value that can be resolved in the signal. ω' is the highest frequency for sampled data. The *R1/R2* term is a geometrical spreading factor to compensate for spherical-wave expansion.

3.2 PROGRESS IN Q ESTIMATION

The basic techniques in Q estimation described in the previous section are theoretically feasible. However, practical difficulties include scattering-removal (including multiples on local reflectivity), wavelet or first arrival isolation, and geophone coupling variations. Although these problems have not been completely solved since then, some important progress has been made. In this section, we describe present attempts to solve these problems for VSP and seismic data.

3.2.1 Progress in estimating Q from VSP

Three typical methods are introduced here. The spectral ratio method by Kan et al. (1981) attempts to solve the scattering problem. The inversion algorithm by Kang and McMechan (1994) tries to separate scattering attenuation by using an assumed additive relation. The inversion method by Amundsen and Mittet (1994) addresses the coupling and first arrival problem by directly inverting frequency-dependent complex wavenumber or propagation velocity.

Method by Kan et al. (1981)

By assuming that the earth is laterally homogeneous and that the offset of the VSP source is negligible, the frequency domain response of the direct P-wave arrival ($A(f, z)$) can be written as (Kan, 1981)

$$A(f,z) = S(f,z)E(f,z)/z \tag{3.11}$$

where f is frequency, z is the geophone depth, and $S(f, z)$ is the far field source spectrum which may vary from shot to shot. The earth response, $E(f, z)$ is written

$$E(f,z) = G(f,z)\exp[-\alpha(f,z)z] \tag{3.12}$$

Here, the effects of intrabed multiples and transmission losses are lumped together in $G(f,z)$. Using the Q-attenuation relation $\alpha(f) = \pi f / QV$ (equation 2.37), then

$$A(f,z) = \frac{1}{z} S(f,z) G(f,z) \exp\left(-\frac{\pi f z}{QV}\right) \tag{3.13}$$

The quality factor Q is the intrinsic Q which is assumed to be independent of frequency. Before estimating the attenuation, correction of the VSP data for spherical divergence (the z^{-1} factor in equation (3.11)) is applied and fixed depth monitor measurements of the source signatures are used to equalize the source variation to a common amplitude for all depths ($s(f)$). Converting the absolute values of these corrected data to a decibel scale, equation (3.13) becomes:

$$a(f,z) = \sigma(f) + g(f,z) - cfz / QV \tag{3.14}$$

where $\sigma(f) = 20\log_{10}[S(f)]$, $g = 20\log_{10}|G|$ *and* $c = 20\pi\log_{10} e$.

By assuming that multiple and transmission effects over a sufficiently large depth interval represent small modulations of the dominantly linear decrease of $a(f, z)$ with increasing z, the observations $a(f, z)$ may be fitted with equation (3.14) by neglecting these modulations thereby yielding the estimate of Q^{-1} which characterizes the attenuation.

The assumption that the multiple and transmission effect result only in a small modulation is a poor approximation ever over large intervals.

Method by Kang and McMechan (1994)

For estimation and separation of intrinsic and scattering Q contributions, the composite apparent Qp (or Qs) is first measured as a function of frequency (ω) from the primary P (or S) waves. This is done directly from the definition (Aki and Richards, 1980)

$$1/Q(\omega) = -\Delta E(\omega)/2\pi E(\omega) \tag{3.15}$$

where $E(\omega)$ is the energy in a propagating wave at any reference point in space and time. Multiple observations can be averaged at each ω to increase the measurement stability and reliability.

Separation of scattering and intrinsic contributions is based on the additive relation (Daninty, 1981; Rovelli, 1982; Richards and Menke, 1983; Hough et al., 1988; Hoshiba et al., 1991; Mayeda et al., 1992; Frazer, 1994)

$$\frac{1}{Q_t} = \frac{1}{Q_{st}} + \frac{1}{Q_{in}} \tag{3.16}$$

where Q_t is the total composite Q , Q_{sc} is the scattering Q contribution, and Q_{in} is the intrinsic Q contribution.

Kang et al. assumes that Q_{in} is frequency independent and that Q_{sc} is frequency dependent. Using the above equation, Kang et al. solve for the optimal model parameters from observations at different frequencies. Q_{in} as one of model parameters is estimated concurrently.

Estimation of scattering Q as a function of frequency, and subsequent estimation of the average scatterer size A and the velocity deviation σ associated with the scatterers, are based on the model of Blair (1990) as described by Tang and Burns (1992). The key relationship is

$$Q^{-1}(K,D) = \beta\sigma^2\gamma(D)^{1-D}\frac{(KA)^D}{\left[1+KA\gamma(D)\right]^{1-D}} \tag{3.17}$$

where K is wavenumber (=ω/V), D is the spatial dimension (=1, 2, 3), σ is the standard deviation of the medium fluctuations as a percentage of the unperturbed model values, A is the dominant scatterer size (which is analogous to the correlation distance in the fractal model), and β and γ are coefficients that depend on scatterer shape and D, respectively. Other less general representations of scattering Q have been used by Rovelli (1982), Richards and Menke (1983), and Hough et al. (1988).

The questionable validity of the assumptions involved in employing this method (the additive relation and the frequency dependency assumption) cast doubt on the validity of the estimations.

Method by Amundsen and Mittet (1994)

This method uses an inversion strategy to estimate the inelastic attenuation. The scheme is restricted to zero-offset vertical seismic profiling (VSP) data acquired in a medium with plane horizontal layers. The real VSP data are filtered to satisfy this assumption. The filter is designed to remove all energy except for the direct downgoing wave and the primary reflected wave from each interface.

The wavefield is determined uniquely by a frequency-dependent complex propagation velocity in each layer. Both frequency-dependent phase velocities and quality factors can be determined from the complex propagation velocities. If we know the complex velocities or the complex wavenumbers, then the complex wavenumber in layer n has the relationship

$$K_n = \frac{\omega}{c_n(\omega)} = \frac{\omega}{c_n^{ph}(\omega)} + i\alpha_n(\omega) \tag{3.18}$$

where c_n is the complex propagation velocity, c_n^{ph} is the phase velocity, and α_n is the absorption coefficient. Since the image and real part are respectably equal in complex equation (3.18), the phase velocity and attenuation coefficient (or quality factor) can be calculated. For example, if

$K_n = R_n + iI_n$, then

$$\alpha_n(\omega) = I_n \tag{3.19}$$

$$C_n^{ph}(\omega) = \frac{\omega}{R_n} \tag{3.20}$$

The complex propagation velocity is obtained by an inversion algorithm. The inverse problem in this method is formulated as an optimization problem where the least-squares objective function $F(\mathbf{m})$

$$F(\mathbf{m}) = \frac{1}{2}\left\|\Delta V^{(k)}\right\|_{l_2}^2 = \frac{1}{2}\sum_{i=1}^{N} \Delta V_i^{(k)*} \Delta V_i^{(k)} \tag{3.21}$$

is minimized in each iteration with respect to the model parameter vector $\mathbf{m}$ of length M.

$$\mathbf{m} = \left[m_1, m_2, \ldots\ldots, m_M\right]^T . \tag{3.22}$$

The asterisk (*) denotes complex conjugate and k the iteration index. The parameter vector $\mathbf{m}$ is partitioned to include the frequency-dependent propagation velocities $\mathbf{c}$ and frequency-independent coupling factors $\mathbf{a}$, that is, $\mathbf{m} = \left[\mathbf{c}^T, \mathbf{a}^T\right]^T$, where $(^T)$ denotes transpose. The number of elements in $\mathbf{c}$ is equal to [number of layers] times [number of the frequencies], and the number of elements in $\mathbf{a}$ is equal to [number of receivers]. Elements c_i represents complex propagation velocity element $c_\ell(\omega)$ in layer ℓ for a given frequency ω. Similarly, the data are represented as elements of a vector $\mathbf{V}$ of length N,

$$\mathbf{V} = \left[V_1, V_2, \ldots\ldots, V_N\right]^T , \tag{3.23}$$

where N is equal to [number of receivers] times [number of frequencies]. Element V_i represents particle velocity data element $V(z_r, \omega)$ at receiver position z_r for a given frequency ω. Since we assume that the geophone-to-formation coupling is unknown, this coupling may be included in the forward modeling. Then the difference between the observed data V^{obs} and the predicted data $\mathbf{A}^{(k)T}\mathbf{V}^{(k)}$ in iteration k is given by

$$\Delta\mathbf{V}^{(K)} = \mathbf{A}^{(k)T}\mathbf{V}^{(k)} - \mathbf{V}^{obs} \tag{3.24}$$

where $\mathbf{A}^{(k)}$ is a diagonal matrix with elements composed of the elements in vectors $\mathbf{a}^{(k)}$. Using a Gauss-Newton method to solve the minimization equation, the parameter update vector in iteration k is obtained as $\Delta\mathbf{m}^{(k)}$. The model parameters are given as

$$\mathbf{m}^{(k+1)} = \mathbf{m}^{k} + \Delta\mathbf{m}^{(k)}. \tag{3.25}$$

This method takes advantage of the parameterization technique in inversion theory. It estimates the frequency-dependent complex propagation velocity and the coupling factors by partitioning them into the to-be-inverted vectors. The frequency-dependent quality factor and the frequency-dependent phase velocity are calculated from the complex wavenumber. Since the coupling factors are included in the to-be-inverted variables, coupling effects are removed.

The disadvantage of this method is that it requires all the multiples and up-going waves in real data to be filtered to satisfy the assumption.

3.2.2 Progress in estimating Q from surface seismic data

Two methods are typically used in estimating Q from surface seismic data, the power spectral ratio method (Raikes and White, 1984) and the matching (inversion) technique (White, 1980; Lamb, 1998).

Estimation from power spectral ratios

This method estimates Q from the power spectral ratios of the reflection signals in two time intervals of surface seismic data. Assuming $P_1(f)$ and $P_2(f)$ are the power spectra in two separate time gates on the seismic section at t_1 and t_2, this method gives:

$$\ln\left(P_2(f)/P_1(f)\right) = 2\ln\left|A_2(f)/A_1(f)\right| \qquad (3.26)$$

$$= -2\pi f(t_2 - t_1)/Q$$

This equation follows from the relation:

$$P_s(f) = \left|A(f)\right|^2 P_r(f) \qquad (3.27)$$

between the power spectrum $P_s(f)$ of a seismic reflection signal $s_t = a_t * r_t$ and the power transfer function $\left|A(f)\right|^2$ of the seismic wavelet a_t and the power spectrum $P_r(f)$ of the reflectivity sequence r_t from which the signal derives. It is assumed that the spectral coloring of the reflectivity either does not change between the two intervals or is compensated and that no other frequency-dependent effects are operating.

The power spectra can be estimated in various ways. One way would be to use multiple coherence analysis (White, 1973). This separates the signal and noise spectra on the basis of the short-range, trace-to-trace coherence of their spectral components. Alternatively, the random noise in the data could be attenuated by applying a spatial filter such as a Karhunen-Loeve filter or a signal-preserving f-x filter (Harris and White, 1991) to the aligned reflection signal. The alignment of signals is very important because timing jitter would cause a loss of coherent spectral power at high frequencies. The other way to estimate power spectra is to use autocorrelations and timing jitter will not cause a loss of power spectra if autocorrelations are used.

Raikes and White (1984) think that the assumption that the spectrum of the reflection sequence is stationary over the analysis windows is a poor assumption and modified this method by using an estimate of the reflectivity from well log data. If the $R_1(f)$ and $R_2(f)$ are the calculated reflectivity spectrum from the portions of the reflectivity trace corresponding to gates 1 and 2, the spectral and spectral ratios can be corrected by

$$\frac{P_2'(f)}{P_1'(f)} = \frac{P_2(f)/R_2(f)}{P_1(f)/R_1(f)} \tag{3.28}$$

Although we do not extract the wavelet in this method, calculating the reflectivities over the corresponding window and selecting the proper window size are difficulties. Small windows will exhibit strong Gibbs phenomena and will be most colored by local reflectivity. Nulls in the reflectivity spectrum will be magnified for equation (3.28). This method also assumes the multiples are previously removed by processing.

Estimation by matching seismic data and synthetic seismograms

This method estimates attenuation by extracting the seismic wavelets in the two intervals by matching the seismic data to well-log synthetic seismograms. The matching technique is described by White (1980) and Lamb (1998).

Given the reflection coefficient time series and the processed seismic trace at the well position, D, we can attempt to find the wavelet by the objective function:

$$O\{W\} = \sum_{i=1}^{N_t} \left(S_i - D_i\right)^2 \omega_i \qquad (3.29)$$

where W represent the wavelet with a length of 2 N_w +1, the $\{\omega\}$ are user assigned weight functions, and S is the synthetic seismogram, given by

$$S_i = \sum_{j=-N_w}^{N_w} R_{i-j} Wj \qquad \text{for } 1 <= I <= N_t \qquad (3.30)$$

R is the refection coefficient series (expressed in time), N_t is the number of elements in the time series.

Setting $\frac{dO}{dW_i} = 0$ to get a least squares solution to the problem, yields the least square estimation of the wavelet. Transforming to the frequency domain, the spectral ratio is used to estimate the Q.

This method tries to extract the wavelet over a small window and will suffer from windowing problems. It also can not consider the scattering attenuation properly and it has the similar time matching problem as the power spectral method.

CHAPTER 4. FULL WAVEFORM GLI INVERSION METHOD FOR SURFACE SEISMIC DATA

4.1. INTRODUCTION

To properly measure attenuation from surface seismic data, scattering removal and time-varying wavelet extraction are necessary. From Chapter 3, it is evident that, due to the difficulty of scattering separation in surface seismic data, existing methods avoid doing so, by assuming multiple effects are removed by processing. Nevertheless, these methods still suffer from wavelet extraction problems. In this chapter, an inversion method designed to solve these difficulties is described.

Instead of trying to extract the wavelet directly from the seismic trace and subsequently separating scattering effects, a full waveform forward modeling and damped generalized linear inversion (GLI) is used to invert Q from the surface seismic trace. Since the forward theory includes all the multiples and attenuation in the synthetic, it allows direct extraction of the intrinsic Q from the seismic trace while taking into account scattering effects. The employment of the robust damped GLI algorithm will produce more stable and accurate inversion results. GLI has some powerful features that are very helpful to the estimation problem. It allows parameterization of known quantities and unknown variables in the inversion scheme. This feature allows the application of constraints to the inversion results. It can also reduce effects of some unknowns such as scale factors and filters by assuming they are to-be-inverted variables. The impedance profile and source wavelet are assumed to be known. In addition, the seismic trace should be specially processed to preserve the multiples and amplitude information.

In the following section, the details of the forward modeling theory, the GLI scheme, damping technique and parameterization are described. A feasibility study is conducted. The numerical modeling shows that attenuation can be recovered almost perfectly from the inversion method. Even AGC filtering will not affect the results.

4.2. FORWARD MODELING THEORY

Based on the general principles of delay, continuity, and energy conservation, elastic 1-D seismogram synthesis including multiples (Claerbout, 1976) can be combined with viscoelastic theory to produce synthetic seismograms including all the multiples and attenuation.

4.2.1 Assumptions

The following assumptions are made:

a. 1-D layered inelastic media.

b. Normally incident elastic waves of both pressure and shear type.

c. Constant Q.

4.2.2 Continuity principle and energy conservation

Consider a horizontal interface between two media, M1 and M2. If a plane wave of unit amplitude is incident on the boundary, there will be a transmitted wave of amplitude t (or t') and reflected amplitude c (or c') as depicted in Figure 4.1.

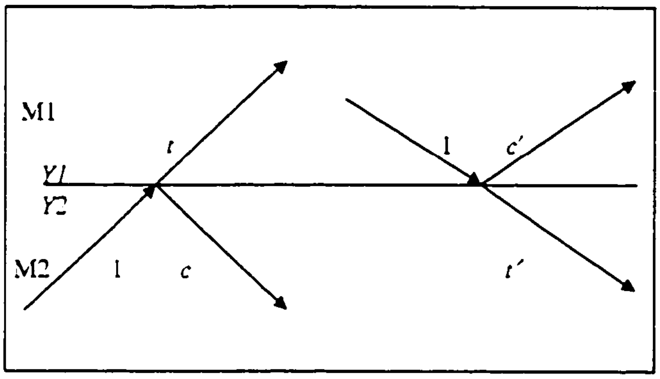

Figure 4.1. Waves incident on an interface, reflected t (or t'), transmitted c (or c')

Ordinarily there are two kinds of variables used to describe seismic waves, and both of these can be continuous at a material discontinuity. One is a scalar like pressure, or stress. The other is velocity which is a vector. In acoustic problems, we assume the interfaces between different solid media are usually firmly bonded together, so that there is no slippage of one with respect to the other. According to the **continuity principle**, the particle displacement velocity and the vertical component of the stress must be continuous across the discontinuity surface (for detailed derivation see, the boundary condition description in Chapter 2). The boundary condition across the interface in the case of Figure 4.1 can be given as

$$t = 1 + c \quad and \quad t' = 1 + c' \qquad \text{for the scalar variable (pressure)} \tag{4.1}$$

or $$1 = t + c \quad and \quad 1 = t' + c' \qquad \text{for the vector variable (velocity)} \tag{4.2}$$

Energy of the wave is proportional to the squared wave amplitude. The proportionality factor depends upon the medium in which it is measured. According to Claerbout (1976), when particle velocity is measured, the scale factor is called the impedance I. When pressure is measured, the scale factor is called the admittance Y. In the pressure case, if we denote the factor of the top medium by Y_1 and bottom by Y_2, then the statement of **energy conservation** that the energy before incidence equals the energy after incidence is

$$Y_2 1^2 = Y_2 c^2 + Y_1 t^2 \tag{4.3}$$

Solving for c from equation (4.1) and (4.3) gives

$$c = \frac{Y_2 - Y_1}{Y_2 + Y_1} \tag{4.4}$$

which gives two important equations for later use

$$c' = -c \quad \text{and} \quad 1 - c^2 = tt' \tag{4.5}$$

In Chapter 2, we also prove that in the particle velocity case, we will get the same results as (4.5), but

$$c = (I1-I2)/(I1+I2). \qquad (4.6)$$

4.2.3 Up and down going wave

We know that all waves obey the wave equation and the basic solution to the 1-D scalar equation (see wave equation in Chapter 2) is

$$U(t) = \sum_{-\infty}^{\infty} a_k e^{i(\omega t - kx)} + b_k e^{i(\omega t + kx)} \qquad (4.7)$$

where ω is angular frequency and k is the wave number. Mathematically we call the first part the downgoing wave if the x direction is downwards, the second is the upgoing wave, because the waves represented by the two parts will propagate in opposite directions.

Physically, in acoustics, one deals with pressure P and the vertical component of particle velocity W (not to be confused with wave velocity v). Another possible definition (Claerbout, 1976) for U (upgoing) and D (downgoing) is

$$D=(P+W/Y)/2 \qquad (4.8)$$

$$U=(P-W/Y)/2 \tag{4.9}$$

with the inverse relations

$$P=D+U \tag{4.10}$$

$$W=(D-U)Y \tag{4.11}$$

From this definition, we can see the relation $t=1+c$ associated with continuity of pressure and the relation $t=1-c$ associated with vertical component of particle velocity. The relation $t=1+c$ says the pressure P is the same on either of the interface. The relation $t=1-c$ says that D-U is the same on either side of the interface.

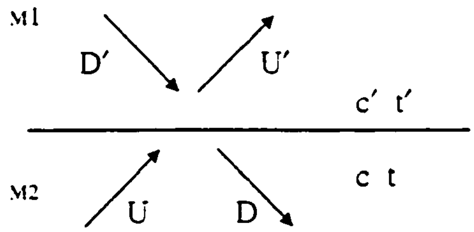

Figure 4.2. Waves incident and reflected from an interface in terms of up and down going waves.

No matter what definition of up and down going wave is used, the boundary conditions establish the relation between the waves across a boundary. Referring to Figure 4.2, we have

$$U' = tU + c'D \tag{4.12}$$

$$D = cU + t'D' \tag{4.13}$$

which may be arranged in matrix form

$$\begin{bmatrix} -t & 0 \\ -c & 1 \end{bmatrix}\begin{bmatrix} U \\ D \end{bmatrix} = \begin{bmatrix} -1 & c' \\ 0 & t' \end{bmatrix}\begin{bmatrix} U' \\ D' \end{bmatrix} \tag{4.14}$$

Now multiplying by the inverse of the left-hand matrix

$$\begin{aligned} \begin{bmatrix} U \\ D \end{bmatrix} &= \frac{1}{-t}\begin{bmatrix} 1 & 0 \\ c & -t \end{bmatrix}\begin{bmatrix} -1 & c' \\ 0 & t' \end{bmatrix}\begin{bmatrix} U' \\ D' \end{bmatrix} \\ &= \frac{1}{t}\begin{bmatrix} -1 & c' \\ -c & cc' - tt' \end{bmatrix}\begin{bmatrix} U' \\ D' \end{bmatrix} \end{aligned} \tag{4.15}$$

Finally substituting equation (4.5) into equation (4.15), yields an equation to extrapolate the waves from the medium M1 to the medium M2.

$$\begin{bmatrix} U \\ D \end{bmatrix} = \frac{1}{t}\begin{bmatrix} 1 & c \\ c & 1 \end{bmatrix}\begin{bmatrix} U' \\ D' \end{bmatrix} \tag{4.16}$$

Let us now consider the layered medium shown in Figure 4.3. For this arrangement of layers, equation (4.16) may be written

$$\begin{bmatrix} U \\ D \end{bmatrix}_{k-1} = \frac{1}{t_k}\begin{bmatrix} 1 & c_k \\ c_k & 1 \end{bmatrix}\begin{bmatrix} U' \\ D' \end{bmatrix}_k \tag{4.17}$$

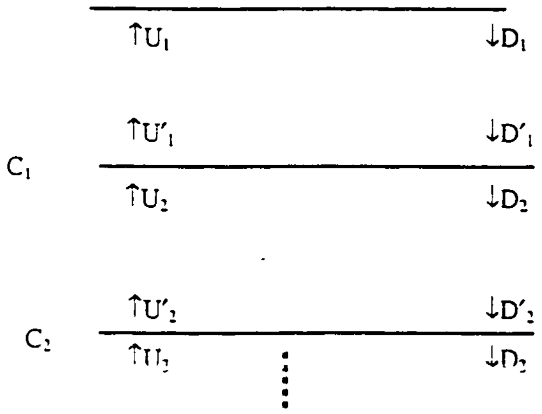

Figure 4.3. Layered medium model (different from Goupilaud-type layered medium, this model does not require that layers have equal travel time.)

4.2.4 Wave theory in an attenuating medium

With equation (4.17), if we also know how to extrapolate the primed wave to non-primed wave, we will be able to extrapolate the waves from the bottom to the top or verse versa layer by layer. Actually, this can be done by applying the wave theory in an attenuating medium described in Chapter 3.

As discussed in Chapter 3, in an attenuating medium, the one-dimensional solution to the scalar wave equation yields the following expression for a plane wave propagating along the x-axis

$$U(x,t) = e^{i(\omega t - kx)} \tag{4.18}$$

where the complex wavenumber is defined as

$$k = \beta - i\alpha = \beta(1 - \frac{i}{2Q}) \tag{4.19}$$

For different attenuation models, the complex wavenumber k has different expressions. For the constant Q model, the real part of the wavenumber in equation (4.19) is expressed as the sum (Bickel and Natarjan, 1985)

$$\beta = \frac{\omega}{V_0} - \frac{\omega}{\pi Q V_0} \ln(\frac{\omega}{\omega_0}) \tag{4.20}$$

where ω / V_0 is a pure delay term with phase velocity V_0 associated with the reference frequency ω_0.

Based on this theory, let us consider the layered medium shown in Figure 4.3 again. Suppose the thickness of kth layer is x_k. This gives the kth layer a relation between primed and unprimed waves (as shown in Figure 4.3) at any frequency.

$$\begin{aligned} U'_k &= U_k e^{-i\beta x_k} e^{\alpha x_k} \\ D'_k &= D_k e^{i\beta x_k} e^{-\alpha x_k} \end{aligned} \tag{4.21}$$

which may be arranged in the matrix form if we assume $z = e^{i\beta x_k} e^{-\alpha x_k}$.

$$\begin{bmatrix} U' \\ D' \end{bmatrix}_k = \begin{bmatrix} 1/z & 0 \\ 0 & z \end{bmatrix} \begin{bmatrix} U \\ D \end{bmatrix}_k \tag{4.22}$$

Combining equation (4.22) with equation (4.17), we get an equation to extrapolate the waves from one layer to another layer.

$$
\begin{aligned}
\begin{bmatrix} U \\ D \end{bmatrix}_{k+1} &= \frac{1}{t_k}\begin{bmatrix} 1 & c_k \\ c_k & 1 \end{bmatrix}\begin{bmatrix} 1/z_k & 0 \\ 0 & z_k \end{bmatrix}\begin{bmatrix} U \\ D \end{bmatrix}_k \\
&= \begin{bmatrix} 1/z_k t_k & c_k z_k / t_k \\ c_k / z_k t_k & z_k / t_k \end{bmatrix}\begin{bmatrix} U \\ D \end{bmatrix}_k
\end{aligned}
\tag{4.23}
$$

4.2.5. Z transform to Fourier transform

Equation (4.23) is derived in the time domain. To realize this extrapolation in the time domain, we need a specific assumption like an equal-time-interval layer model. Even so, it is still difficult to find a method to realize (4.23) for an attenuating medium. This section will show that equation (4.23) is also correct in terms of frequency domain.

The Z transform is defined as

$$B(Z) = \sum_t b_t Z^t \tag{4.24}$$

The substitution $Z = e^{i\omega}$ gives the Fourier transform in discretized form

$$B(\omega) = \sum_t b_t e^{i\omega t} \tag{4.25}$$

In the terms of the discretized function, the Z transform and the Fourier transform have the same properties. As in the Z transform, where the inverse Z transform merely identifies coefficients of various powers of Z with different points of time, the inverse Fourier transformation is just like identifying coefficients of powers of Z. So, when we write the expression

$$B(Z) = b_0 + b_1 Z + b_2 Z^2 + \cdots \tag{4.26}$$

we have both a time function and its Fourier transform. If we plot the coefficients (b_0, b_1, b_2, ...), we plot the time function. If we evaluate and plot (4.26) at numerous real ω, then we have plotted the transform. Thus, equation (4.23), the propagation equation, is correct in terms of both time and frequency domain. Here we understand that U and D are evaluated at given frequency ω in equation (4.23).

4.2.6 Getting the waves from the reflection coefficients

A layered material may be specified by giving the reflection coefficient at each interface. Considering the basic reflection seismic geometry shown in Figure 4.4, alternate descriptions are to give any one of the scattered waves R(z) and E(z).

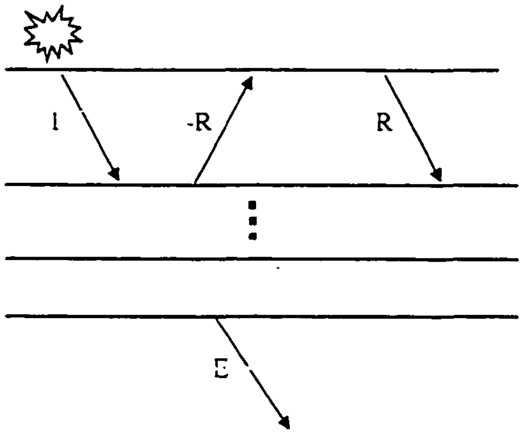

Figure 4.4. Basic reflection seismology geometry. Impulse of unit amplitude going downward is initiated. The earth sends back -R(z) to the surface. Since the surface is perfectly reflective, the surface sends R(z) back into the earth. Escaping from the bottom of the layers is a wave E(z).

Suppose there are k interfaces in the geometry. From the equation (4.23), we have

$$\begin{aligned}\begin{bmatrix}0\\E\end{bmatrix} &= \begin{bmatrix}1/z_k t_k & c_k z_k/t_k\\ c_k/t_k & z_k/t_k\end{bmatrix} \cdots \begin{bmatrix}1/z_1 t_1 & c_1 z_1/t_1\\ c_1/t_1 & z_1/t_1\end{bmatrix}\begin{bmatrix}-R\\1+R\end{bmatrix}\\ &= \prod_k \begin{bmatrix}1/z_k t_k & c_k z_k/t_k\\ c_k/t_k & z_k/t_k\end{bmatrix}\begin{bmatrix}-R\\1+R\end{bmatrix} \\ &= \begin{bmatrix}F_{11} & F_{12}\\ F_{21} & F_{22}\end{bmatrix}\begin{bmatrix}-R\\1+R\end{bmatrix}\end{aligned} \tag{4.27}$$

From the first simultaneous equation we may solve for R

$$R = \frac{F_{12}}{F_{11} - F_{12}} \tag{4.28}$$

The second equation of (4.27) gives the escaping wave as

$$E = \frac{F_{11}F_{22} - F_{12}F_{21}}{F_{11} - F_{12}} \tag{4.29}$$

R and E are evaluated at a given frequency, so it is understood that R(Z)=R(ω) and E(z)=E(ω). Using the inverse Fourier transformation gives the time functions for R and E.

$$\begin{aligned} R(t) &= \frac{1}{2\pi}\int_{-\infty}^{\infty} R(\omega)e^{-i\omega t}\,d\omega \\ E(t) &= \frac{1}{2\pi}\int_{-\infty}^{\infty} E(\omega)e^{-i\omega t}\,d\omega \end{aligned} \tag{4.30}$$

Note that since R(ω) and E(ω) are discrete and bandlimited when we realize the method, there will be sampling and windowing effects for both R(t) and E(t). These are classical signal analysis problems which can be mitigated somewhat by evaluating R(ω) and E(ω) at a sufficiently fine sampling rate and sufficiently broad bandwidth. Please also note that here R(t) is the response of the layered strata to an impulse. For a general source s(t), R(t) must be convolved with s(t).

4.2.7. Synthetic examples

Model studies were used to test the forward modeling algorithm. Figure 4.5-Figure 4.8 show both the models and their synthetic results.

Figure 4.5 shows a one-layer model. In this model, the source is an impulse and Q of the first layer is 50. We can see repeated multiples exhibiting the proper impulse response for wave propagation in a constant Q medium.

Figure 4.6 is also a one-layer model case, but with a theoretical mixed-phase wavelet as the source, and compared the two different cases when Q=1000 and Q=50. This comparison clearly shows the attenuation and dispersive properties of a wavelet traveling in constant Q medium. After passing the attenuating medium, the amplitude of the wavelet is seriously attenuated and the pulse is broadened and phase shifted.

Figure 4.7 is a three-layer model. The source is an impulse and Q for second layer is 30. This figure shows the repeated multiples and reasonable attenuation as well as dispersion. We also can see that some reflections wrap around when the window is too small.

Figure 4.8 is also a three-layer case with a theoretical mixed-phase wavelet as the source, the second layer designed as the potential reservoir and compute seismograms when Q is set to 1000 and to 10. This figure shows significant shift and attenuation of the wave after passing through the reservoir.

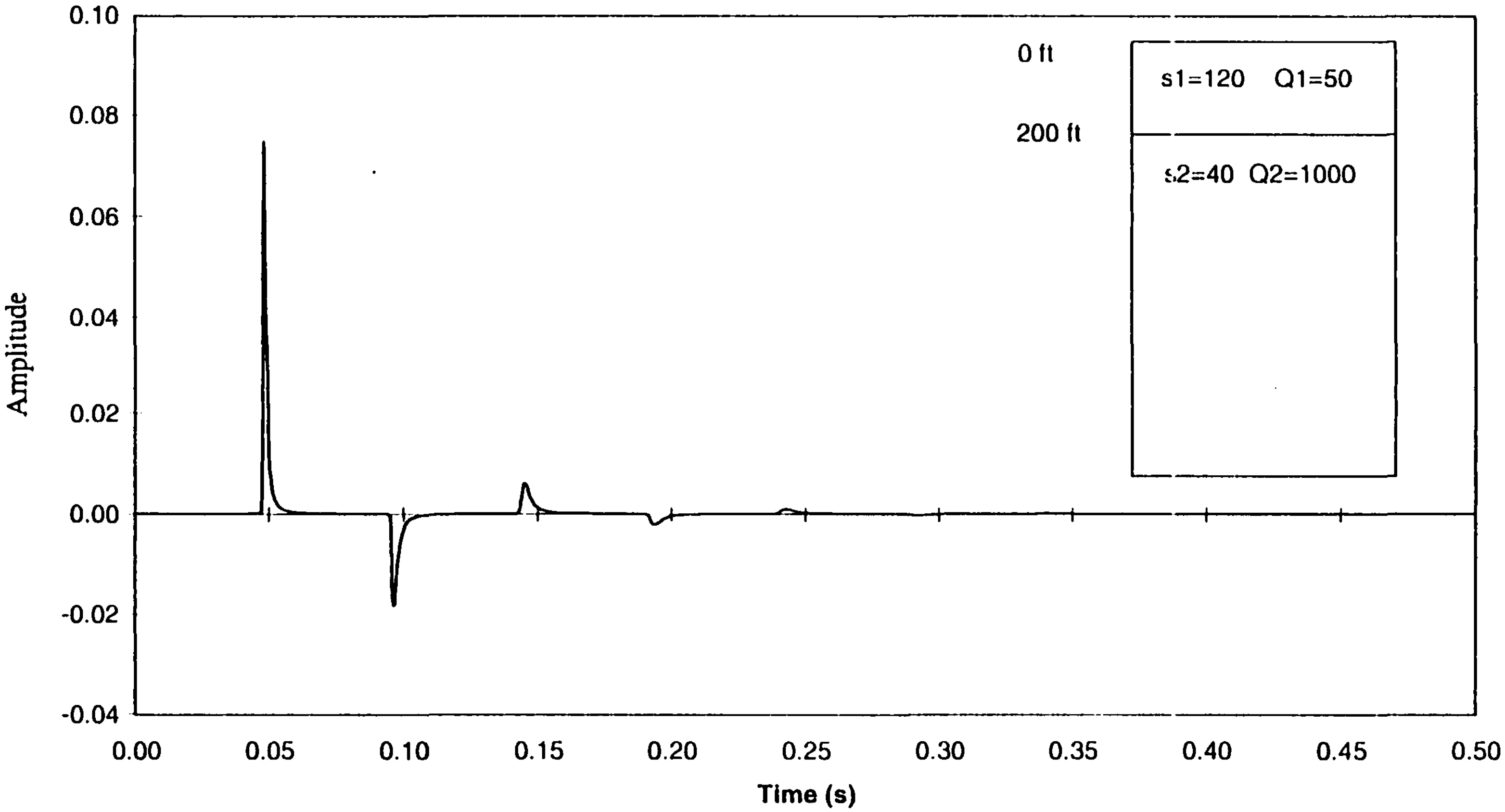

Figure 4.5. Synthetic trace for the one layer model , Impulse source, Q=50. s1, and s2 are slowness (μs/ft).

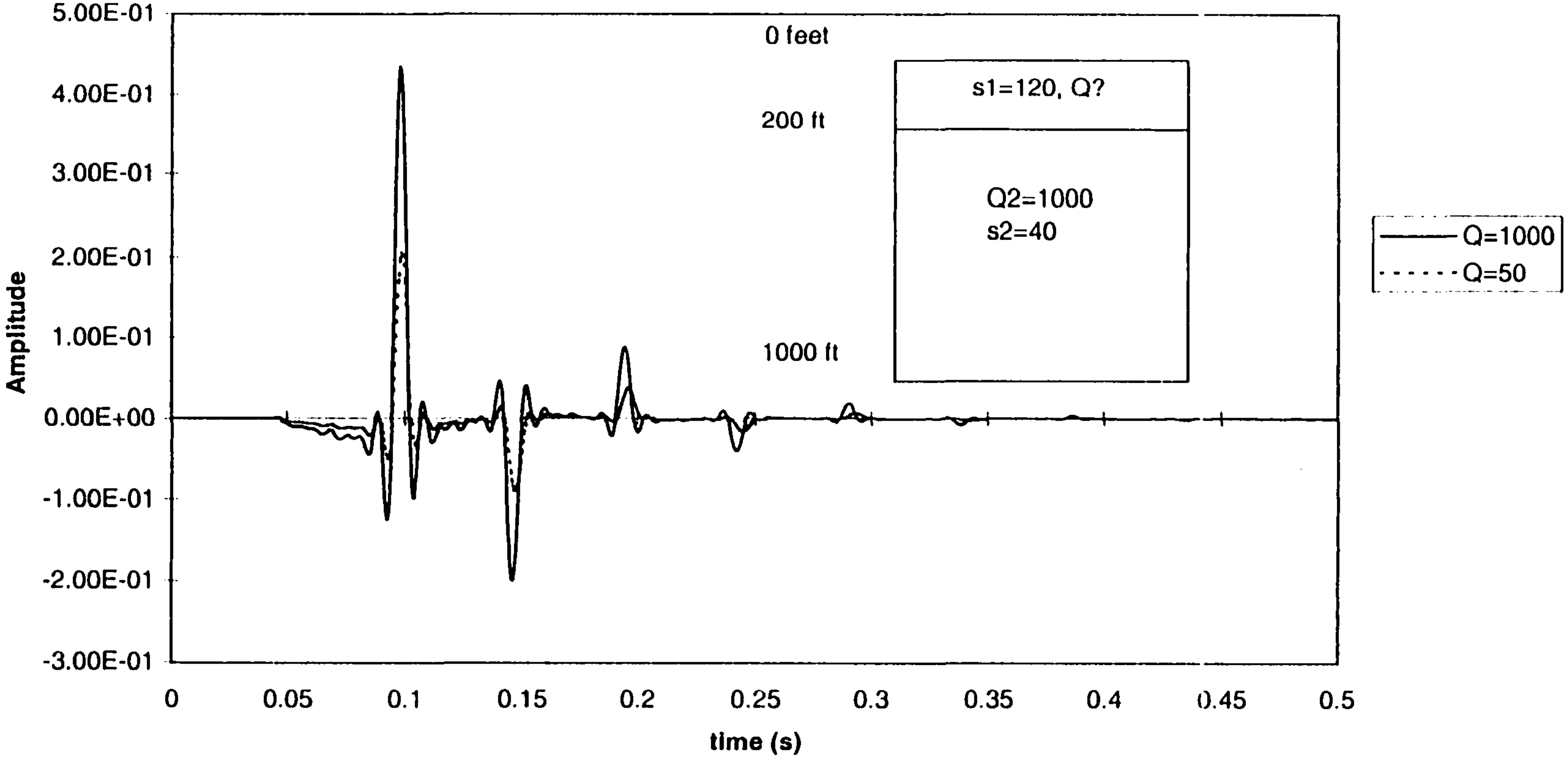

Figure 4.6. Comparison of one layer model when Q=1000 and Q=50. s1and s2 are slowness (μs/ft).

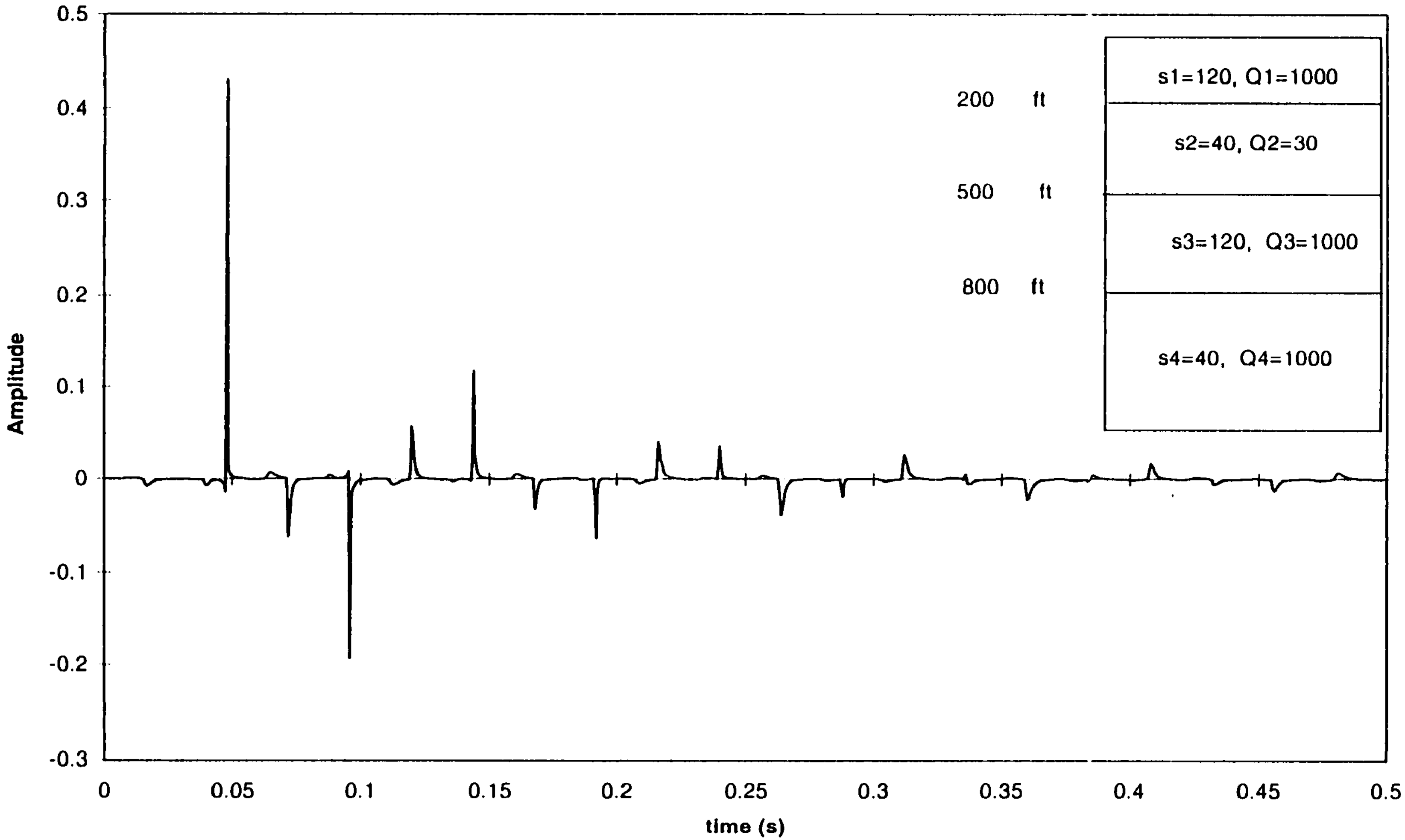

Figure 4.7. Impulse source, three layer model, Q=30. s1, s2, s3and s4 are slowness (μs/ft).

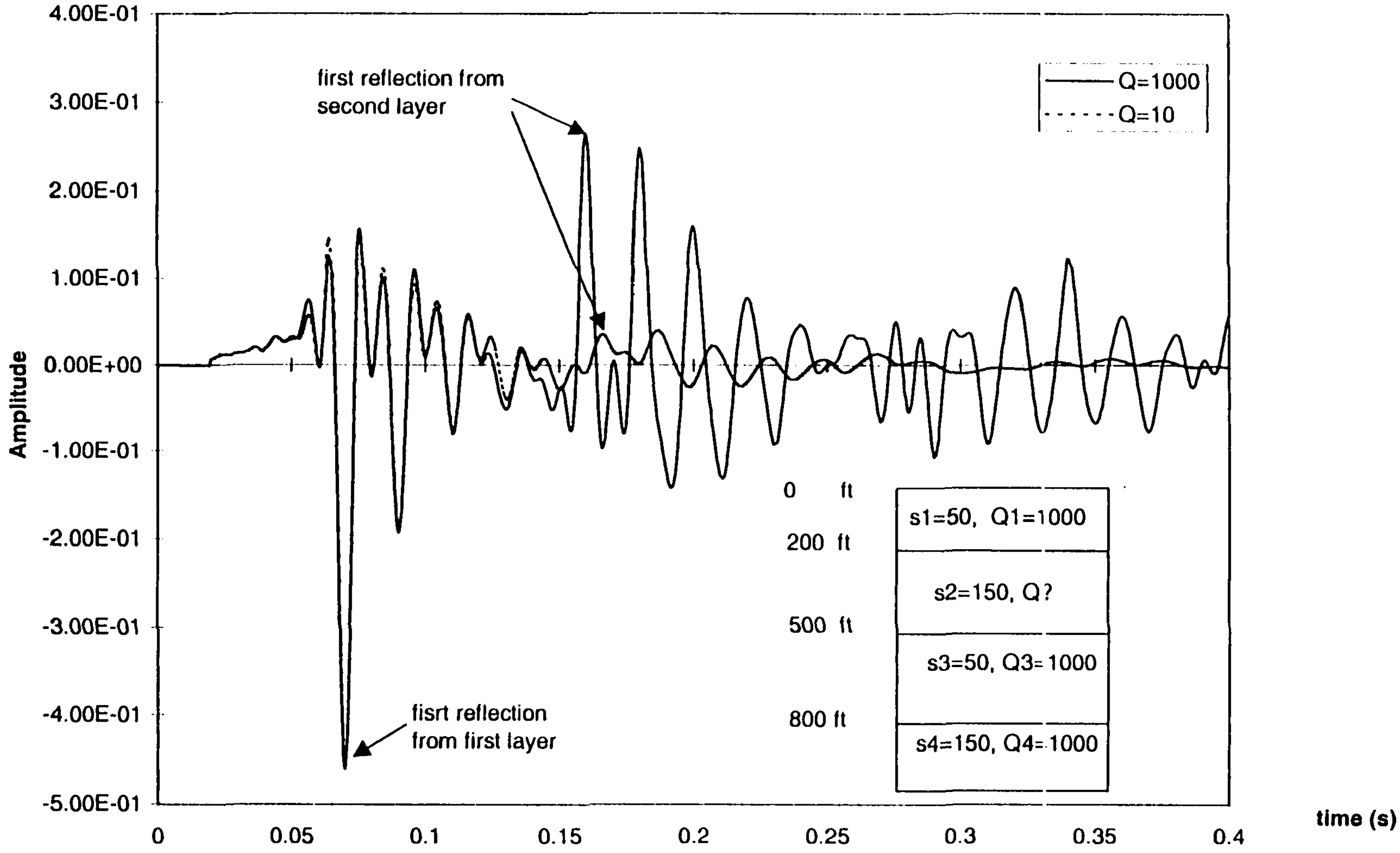

Figure 4.8. Comparison of three layer model when Q=1000 and 10. s1, s2, s3and s4 are slowness (μs/ft).

4.3 DAMPED GENERALIZED LINEAR INVERSION

4.3.1 Inversion problem definition

Our goal is to estimate Q from the seismic trace near a borehole. With our forward model, all we need is an inversion algorithm. The inverse problem is described as: given the observed seismic trace at the borehole, velocity profile (or impedance profile) and source wavelet, to invert the Q profile. Mathematically, this is equivalent to: minimize an objective function that can be defined by (Meju, 1994)

$$\Phi = \sum_{1}^{n}\left[Y_i - Y_i'\right]^2 = \|\mathbf{Y} - \mathbf{Y}'\|^2 \quad \text{I=1,2,3...,n} \tag{4.31}$$

where $\mathbf{Y} = (Y_1, Y_2, Y_3, ..., Y_n)$ is the observed seismic trace, and $\mathbf{Y}' = (Y_1', Y_2', Y_3', ..., Y_n')$ is the predicted trace by theoretical model. Theoretically, $\mathbf{Y}'$ is function of the independent parameter vector $\mathbf{m} = (m_1, m_2, ..., m_k)$, i.e. $\mathbf{Y}' = f(\mathbf{m})$. The independent parameter vector consists of all the unknown independent variables needed for forward modeling. In our model, the impedance profile and the source wavelet are known. The unknowns, **m**, constitute the Q profile. We may also want to put other parameters into m, such as scale factors, filters etc, if they are not known. The problem is that the more unknowns in inversion, the more uncertainty in the results. So, generally we intend to limit the unknowns to as few as we can.

The independent parameter vector, **m**, is inverted by iteratively minimizing the objective function. For the linear predictive function f, $\mathbf{Y}' = \mathbf{Gm}$ where **G** is the coefficient matrix. Then the objective function becomes

$$\Phi = (\mathbf{Y} - \mathbf{Gm})^T (\mathbf{Y} - \mathbf{Gm}) \tag{4.32}$$

where T means transpose of the matrix. The well known least-squares solution for the parameters estimates (denoted by $\mathbf{m}'$) is given by

$$\mathbf{m}' = \left[\mathbf{G}^{\mathrm{T}}\mathbf{G}\right]^{-1}\mathbf{G}^{\mathrm{T}}\mathbf{Y} \tag{4.33}$$

Q inversion is nonlinear, so, the predictive function can not be expressed in the form of $\mathbf{Y}' = \mathbf{Gm}$. To solve the nonlinear problem, we have to turn to a generalized method which linearizes the nonlinear problem by expanding function f in a Taylor series and writing the Taylor series through the linear terms

$$\mathbf{Y}' = f_0 + \mathbf{P}\delta \tag{4.34}$$

where f_0 is the initial prediction, δ is the first order correction vector to the initial parameter vector **m**, **P** is the sensitivity matrix and

$$\mathbf{P}^{[n \times k]} = \left(\frac{\partial f_i}{\partial m_j}\right) \qquad i = 1,2,\ldots,n, \quad j = 1,2,\ldots,k \tag{4.35}$$

Now δ appears linearly in the prediction of Y' and therefore can be found by the standard least-squares method of setting $\partial\Phi / \partial\delta_j = 0$, for all j. Thus δ is found by solving

$$(\mathbf{P}^T\mathbf{P})\delta = \mathbf{P}^T\mathbf{d} \quad \text{and} \quad \delta = (\mathbf{P}^T\mathbf{P})^{-1}\mathbf{P}^T\mathbf{d} \tag{4.36}$$

where $\mathbf{d} = (\mathbf{Y} - f_0)$.

Solving for correction vector δ from equation (4.36) gives the optimum correction. Once the correction vector is known, it is a simple matter to solve for the corrected parameter vector $\mathbf{m}$.

$$\mathbf{m} = \mathbf{m}_0 + \delta \tag{4.37}$$

where $\mathbf{m}_0$ represent the initial guess of the parameter vector $\mathbf{m}$.

Equation (4.37) is an approximation since the Taylor series predictive function is truncated to the first order to linearize the function. This makes the solution for the correction vector from equation (4.36) an approximation, and the solution for $\mathbf{m}$ in equation (4.37) must also be an approximation. This approximate error can be reduced by using the corrected initial guess from equation (4.37) as a next initial guess in equation (4.36) and iterating through the problem again. This iterative procedure is outlined in Figure 4.9. The iterative loop of Figure 4.9 will gave an error that is decreasing in a roughly exponential manner with each iteration if the initial guess lies within the region of convergence. The error computed with each iteration is defined by the new objective function Φ. The loop is continued until the error drops below some predetermined level or until a new correction vector fails to give an improvement over the previous iteration's error. This is called Generalized Linear Inversion (GLI) (Marquardt, 1963; Cooke et. al. 1983; Meju, 1994).

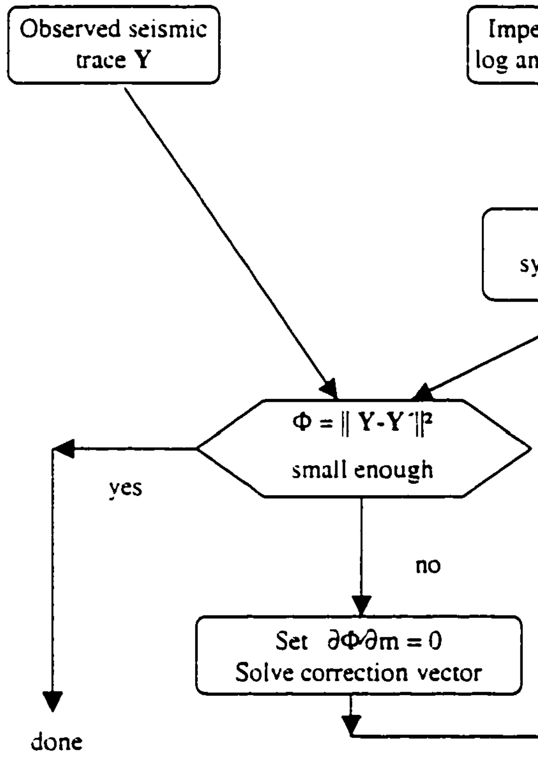

Figure 4.9. The chart flow for inversion iteration procedure

4.3.2 Parameterization

With the impedance and the wavelet known, the basic parameter left unknown is Q. The Q profile must be discretized into the independent parameter vector **m**. We will represent Q profile by a serious of Q value and interval thickness as shown in Figure 4.10.

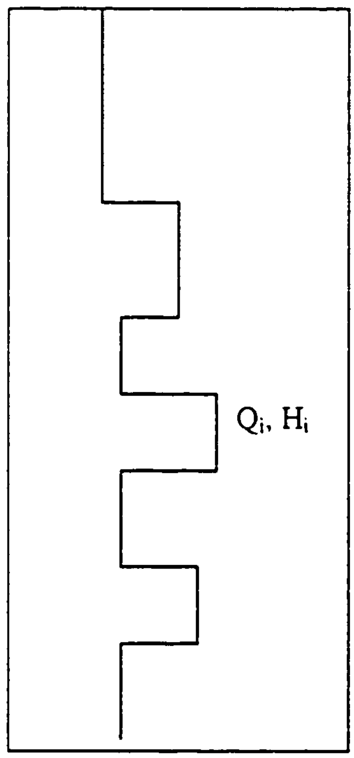

Figure 4.10. Example of a discrete Q profile

The Q profile is listed as Q value and interval pairs repeated from top to the bottom, i.e., **m** should be in the form of

$$\mathbf{m} = (Q_1, D_1, Q_2, D_2, \ldots, Q_k, D_k) \tag{4.38}$$

Since the seismic trace is affected by Q slightly, we will not use either the sonic interval or the seismic sample interval as the Q interval but rather will consider geological and geophysical data first to make the Q intervals as large as reasonable. The Q intervals are not required to be equal. Both the interval thickness and the interval Q will be inverted by the method.

4.3.3 Parameters other than Q profile

Since the forward modeling assumes that the reflectivity and the source wavelet are known, the only other parameters left are the scale factors. There are two types of scale factors, one is a constant factor generally caused by instrument gain and processing; another is time varient scale factors caused by processing such as AGC. Since the reflectivity and source wavelet are known, the constant scale factor can be incorporated into wavelet. The time variable factors will be circumvented by parameterizing them in the inversion. For example, we can assume the window length of the AGC as unknown and add that to parameter vector to be inverted. Then the independent parameter vector **m** becomes

$$\mathbf{m} = (Q_1, D1, Q2, D_2, \ldots, Q_k, D_k, L_{AGC}) \tag{4.39}$$

4.3.4 Sensitivity matrix

To compute the sensitivity matrix in the inversion method, it is necessary to take partial derivatives of the synthetic seismic trace with respect to each boundary location, and each interval Q value. Also needed are the partial derivatives of the synthetic with respect to the scale factor. Computation and storage of these derivatives is the most time and computer memory consuming operation encountered in generalized linear inversion. Sometimes it even is impossible to calculate the matrix analytically because the forward modeling theory is too complicated. Fortunately, generalized linear inversion is a very robust process and will allow one to use approximations to these partial derivatives that may not be exact, but are computationally more efficient than the exact derivatives. In fact, the error introduced by these approximations is probably less than the error due to truncating the Taylor series expansion. A number of different approximation techniques are available to generate the desired derivatives. Here we will use finite difference method. This numerical technique is a left-finite difference:

$$\frac{dS(t)}{dm_i} = \frac{\left(S(m_i + \Delta m_i) - S(m_i)\right)}{\Delta m_i} \tag{4.40}$$

where S(t) represents the trace value at time t. The m_i represent the ith parameter. Δm_i is the finite difference.

4.3.5 Damping technique

In practice, it is found helpful to correct the parameter vector, **m**, by only a fraction of the correction vector as $\beta\delta$, $0<\beta<=1$; where β is called the damping factor; otherwise the extrapolation may be beyond the region where the function f can be adequately represented by equation (4.34), and would cause divergence of the iterates. This is done by solving equation (4.36) with a modified least-squares-error procedure. The modification consists of the addition of the damping factor to the classical least-squares-error solution which gives

$$(\mathbf{P}^T\mathbf{P} + \beta\mathbf{I})\delta = \mathbf{P}^T\mathbf{d} \quad \text{and} \quad \delta = (\mathbf{P}^T\mathbf{P} + \beta\mathbf{I})^{-1}\mathbf{P}^T\mathbf{d} \tag{4.41}$$

where **I** is the identity matrix. The damping factor, β, reflects the local linearity of the error surface and can be calculated analytically as discussed by Marquardt (1963) or it can be chosen in an empirical manner. Here we determine our damping factor according to the suggestion by Marquardt (1963) as follows

1. let $C>1$, say $C=10$
2. let β denote the value of β from the previous iteration. Initially let $\beta=1.0$ for example.
3. compute $\Phi(\beta)$ and $\Phi(\beta / C)$
4. if $\Phi(\beta / C) <= \Phi(\beta)$, let $\beta=\beta/C$
5. if $\Phi(\beta / C) > \Phi(\beta)$, let $\beta=\beta C$

4.3.6 SVD solution to matrix equation

To solve the matrix equation, a widely used matrix solution method (singular value decomposition or SVD) developed by Lanczos(1961) is used here.

According to SVD, an $n \times n$ or $n \times k$ (n>=k) matrix **P**, say, can be factored into a product of three other matrices: $\mathbf{P} = \mathbf{U}\Lambda\mathbf{V}^{\mathrm{T}}$, where $\mathbf{U}_{(n \times k)}$ and $\mathbf{V}_{(k \times k)}$ are respectively the data space and parameter space eigenvectors, and Λ is a $k \times k$ diagonal matrix containing at most r nonzero eigenvalues of **P**, with $r \leq k$. These diagonal entries in $\Lambda(\lambda_1, \lambda_2, \ldots, \lambda_k)$ are termed the singular values of **P**. This factorization is known as the SVD of **P**. If the eigenvalues of a matrix are small, the matrix is said to be ill-conditioned. The SVD method is popular in geophysical data analysis because it is robust mathematically and stable numerically. It also provides other vital information on the state of the model and data thus enabling model resolution covariance studies.

Apply SVD to equation (4.41) in terms of the SVD of **P**

$$\mathbf{P}^{\mathrm{T}}\mathbf{P} + \beta\mathbf{I} = \mathbf{V}\Lambda\mathbf{U}^{T} \bullet \mathbf{U}\Lambda\mathbf{V}^{T} + \beta\mathbf{I} = \mathbf{V}(\Lambda^{2} + \beta\mathbf{I})\mathbf{V}^{\mathrm{T}} \tag{4.42}$$

and the least-squares generalized inverse is

$$(\mathbf{P}^{\mathrm{T}}\mathbf{P} + \beta\mathbf{I})^{-1}\mathbf{P}^{\mathrm{T}} = \mathbf{V}(\Lambda^{2} + \beta\mathbf{I})^{-1}\mathbf{V}^{\mathrm{T}} \bullet \mathbf{V}\Lambda\mathbf{U}^{\mathrm{T}} = \mathbf{V}(\Lambda^{2} + \beta\mathbf{I})^{-1}\Lambda\mathbf{U}^{\mathrm{T}} \tag{4.43}$$

so that the least-squares solution is given by

$$\delta = (\mathbf{P}^{\mathrm{T}}\mathbf{P} + \beta\mathbf{I})^{-1}\mathbf{P}^{\mathrm{T}}\mathbf{d} = \mathbf{V}(\Lambda^{2} + \beta\mathbf{I})^{-1}\Lambda\mathbf{U}^{\mathrm{T}}\mathbf{d} \tag{4.44}$$

4.3.7 Uniqueness and resolution

Once the correction vector has been computed from equation (4.44), it is possible to compute the resolution matrix as defined by Backus and Gilbert(1968):

$$\mathbf{R} = \mathbf{P}^{-1}\mathbf{P} \tag{4.45}$$

The matrix **R** is a measure of the uniqueness of the solution. When **R** is the identity matrix, the solution is unique. When **R** is not the identity matrix it indicates just which parameters are not well resolved. If the nth element of the nth row (that is the element that lies along the diagonal of **R**) is one, then the nth parameter in the solution is unique. When this element is not unity, the adjacent elements indicate just how well resolved the nth parameter is compared to its neighbors. For example, if the elements of the nth row of **R** is all zeros except for n-1, n, n+1 elements which are all 1/3, then the nth parameter in the solution is ill-resolved with respect to the n-1 and n+1 parameter.

4.4 FEASIBILITY STUDY

To test the performance of the inversion algorithm, we carried out model studies. As shown in Figure 4.11, this is a four layer 1-D model.

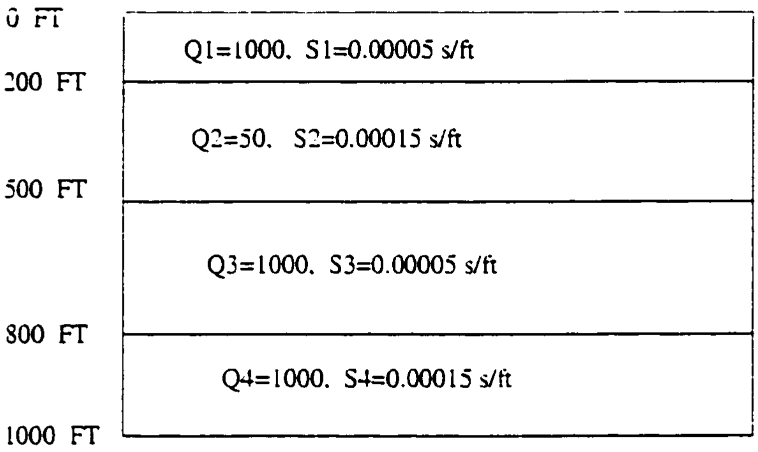

Figure 4.11. 1-D four layer model

In our test study, we generate synthetic traces based on the parameter profile shown in the Figure 4.11 using full waveform forward modeling. This synthetic will be treated as the original field trace. Then the following numerical inversions are carried out.

In first model inversion, we change Q2 and H2 from 10 and 300 to 50 and 250 respectively and other parameters do not change. Using the changed parameter profile as the initial model, we try to use the inversion algorithm to extract the original profile. This is to test how sensitive our inversion algorithm to both the interval thickness and the Q value. The result is shown on Figure 4.12. We see that for the model in Figure 4.11, if we just change the target layer parameters in certain reasonable range (Q from 10 to 20, $\Delta H = 50$), the Q profile can be perfectly recovered.

In the second, third and fourth model inversion examples, We just change Q of layer 2 and let the boundary free to see how well this algorithm can resolve the Q value. We change Q2 from 10 to 50 in second example. We can see the Q2 still can be recovered perfectly (Figure 4.13). Then we change the Q2 from 10 to 100 in third example. The results (Figure 4.14) show a little tradeoff in thickness identification and both the thickness and the Q value are recovered very well. Finally we just change the Q2 from 10 to 1000 in the fourth example. The results (Figure 4.15) show more tradeoff of thickness than does example 3, but both the thickness and Q value are still recovered very well.

The above four tests assume our seismic traces are not processed and that the multiples and the amplitude all are preserved. In fact, seismic field data are processed and generally the amplitude cannot be preserved. To model the facts, we add a "light" AGC to our forward model to simulate processed data. In the inversion process, it is supposed we just know that the seismic trace is AGC-filtered, but we do not know what AGC is used. In this case, we employ the powerful feature of the inversion algorithm, the parameterization. What we do is that we assume the length of the AGC filter used is an unknown and parameterize it into the parameter vector. Then we change the Q2 from 10 to 1000 as in example 4 and repeat the inversion procedure again. The inverted Q profile is shown on Figure 4.16 with the initial and original profile. Figure 4.16 shows that the inversion result of filtered data is as good as the result of unfiltered data in example 4.

This means our inversion algorithm will be very robust even working with filtered data if we parameterize variables of the processing methods into the independent parameter vector.

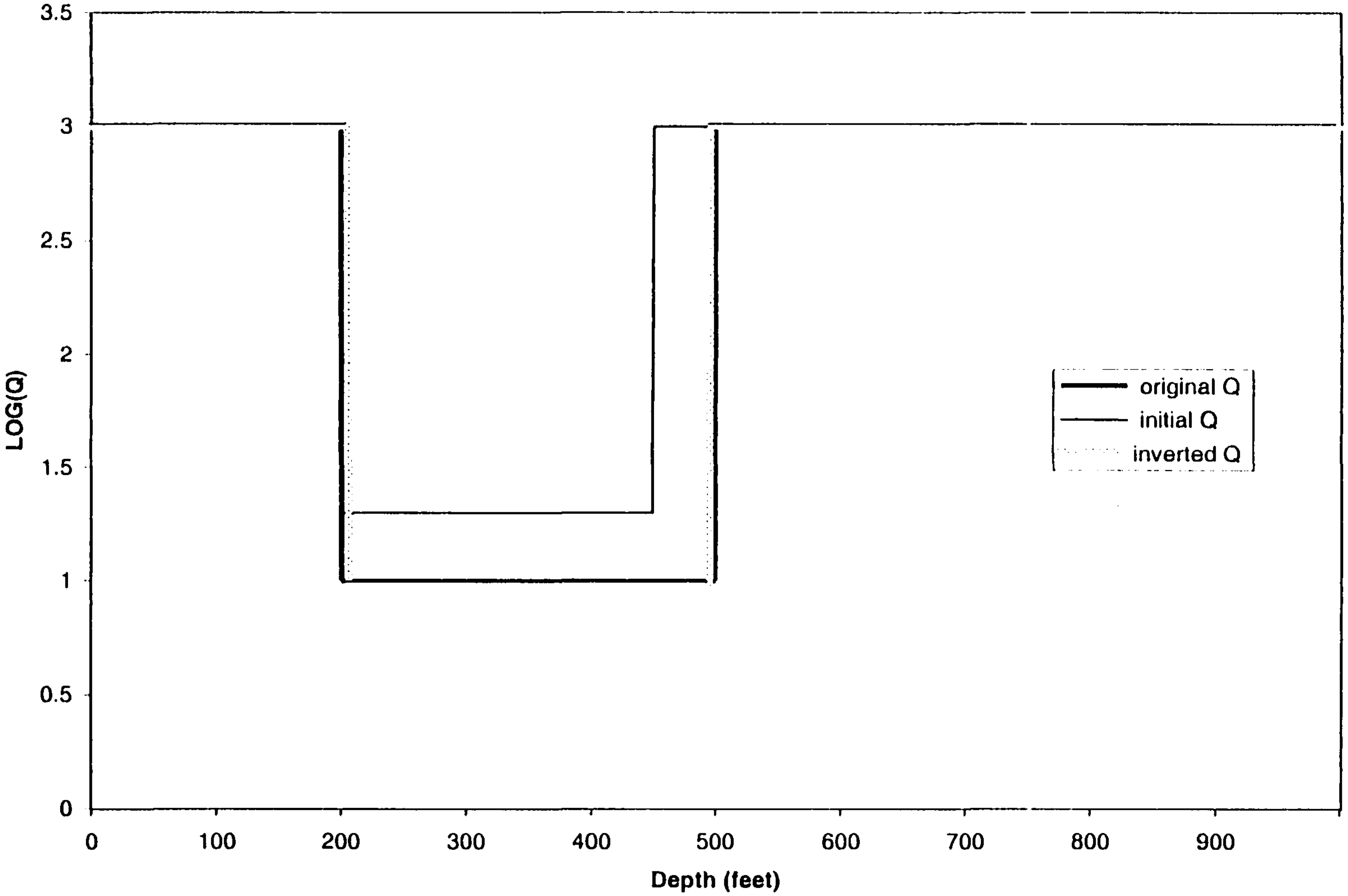

Figure 4.12. Q model inversion 1: Q2 and H2 are changed initially from 10 and 300 to 20 and 250

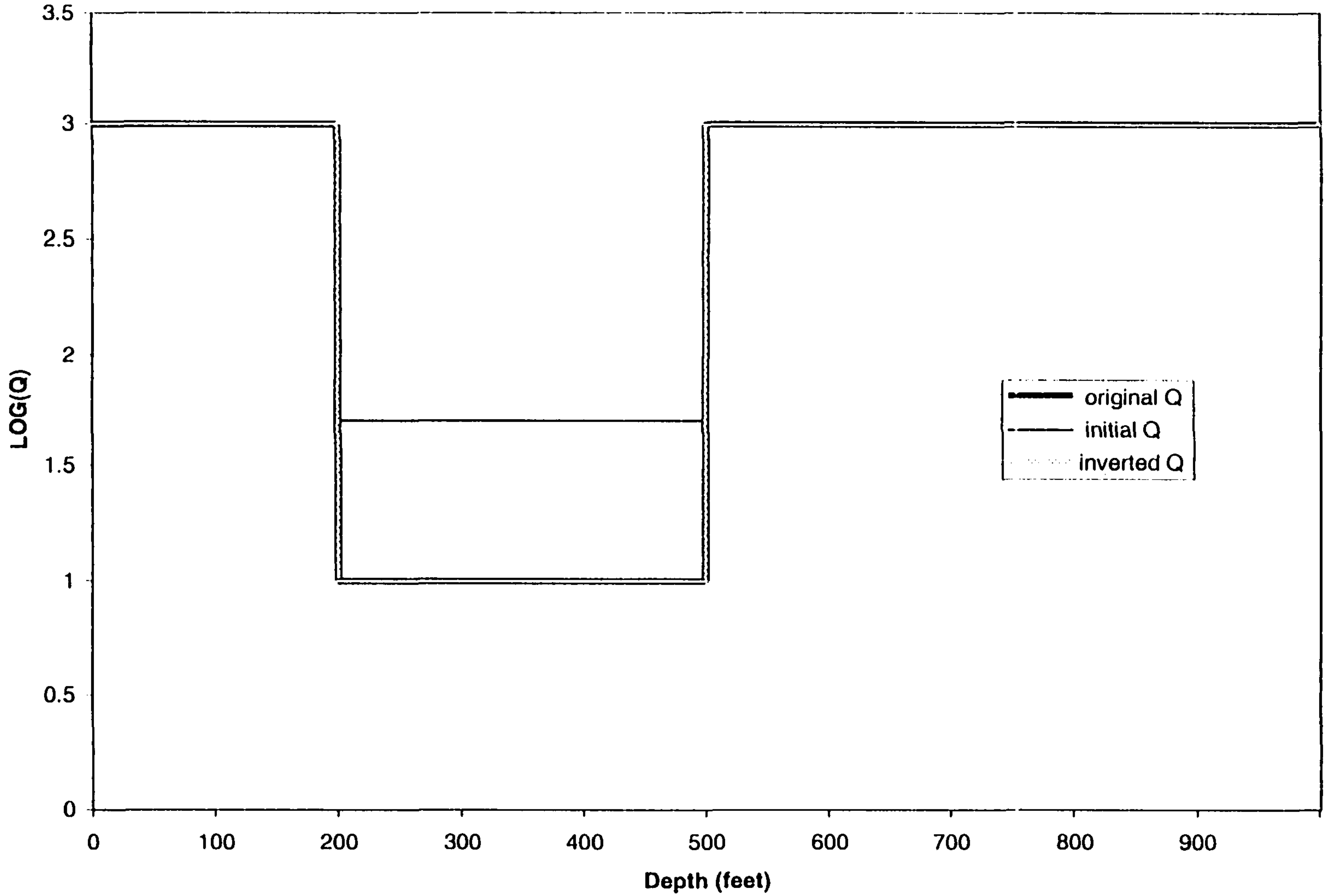

Figure 4.13. Q model inversion 2: Q2 is initially changed from 10 to 50

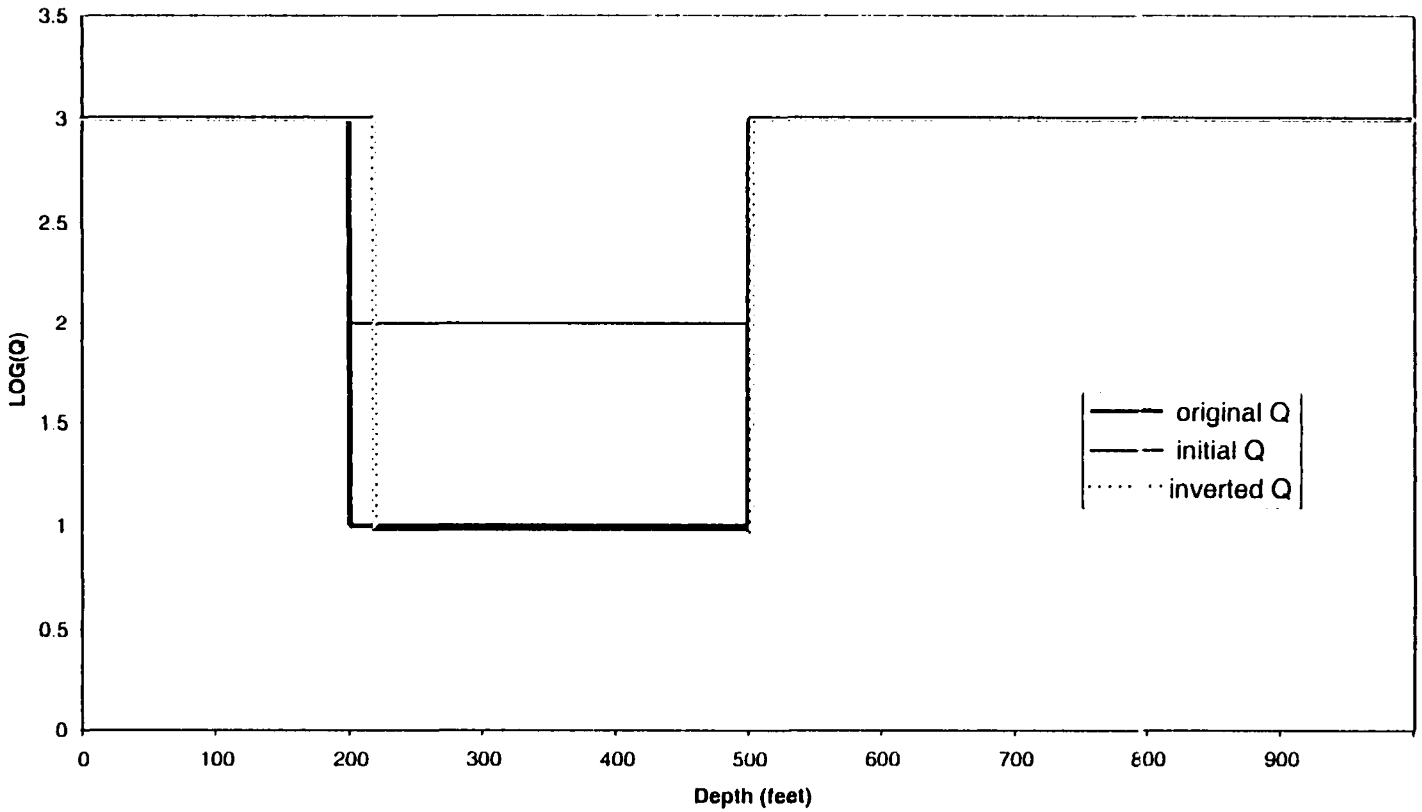

Figure 4.14. Q model inversion 3: Q2 is changed to 100, which originally is 10

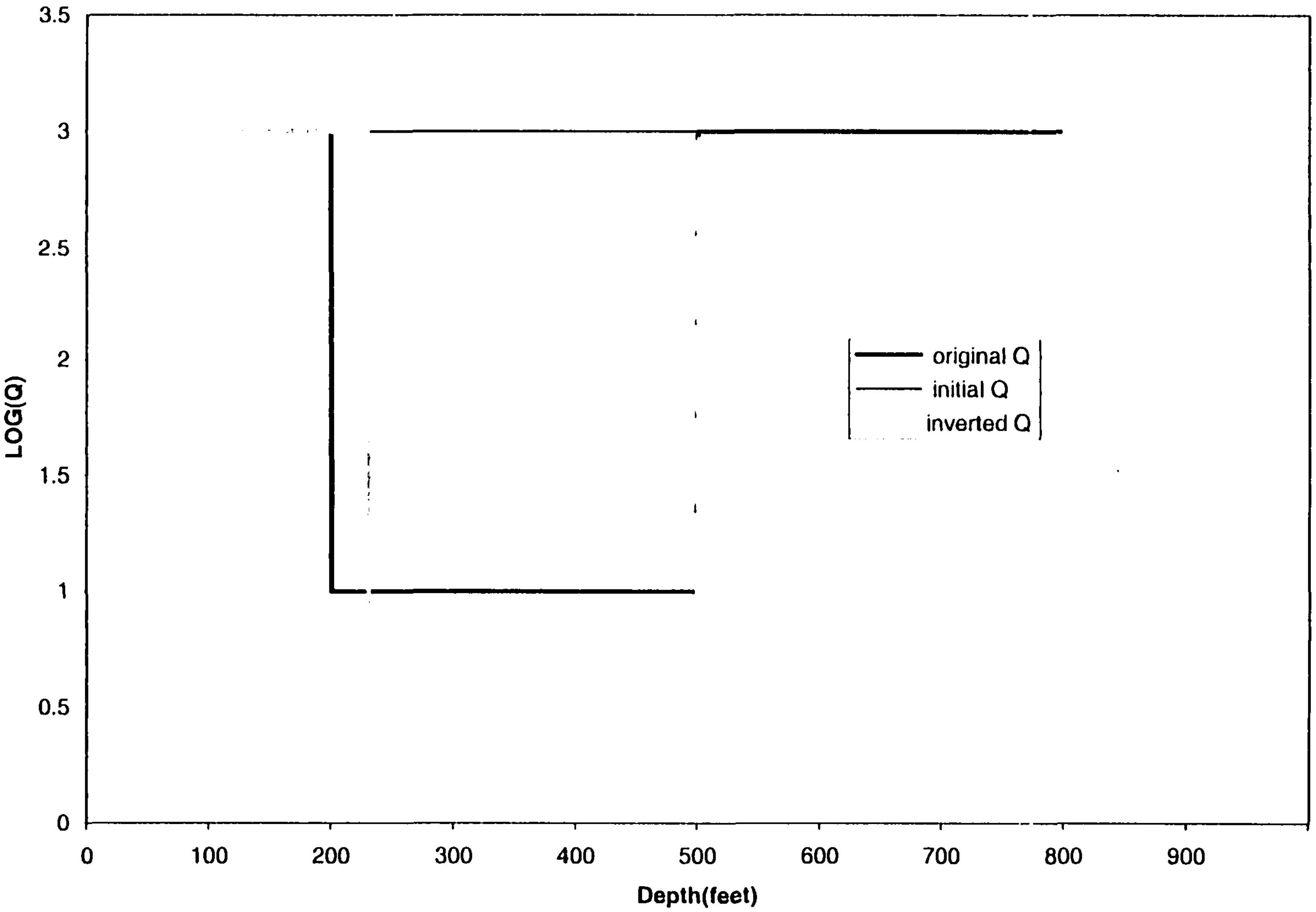

Figure 4.15. Q model inversion 4: Q2 is changed from 10 to 1000

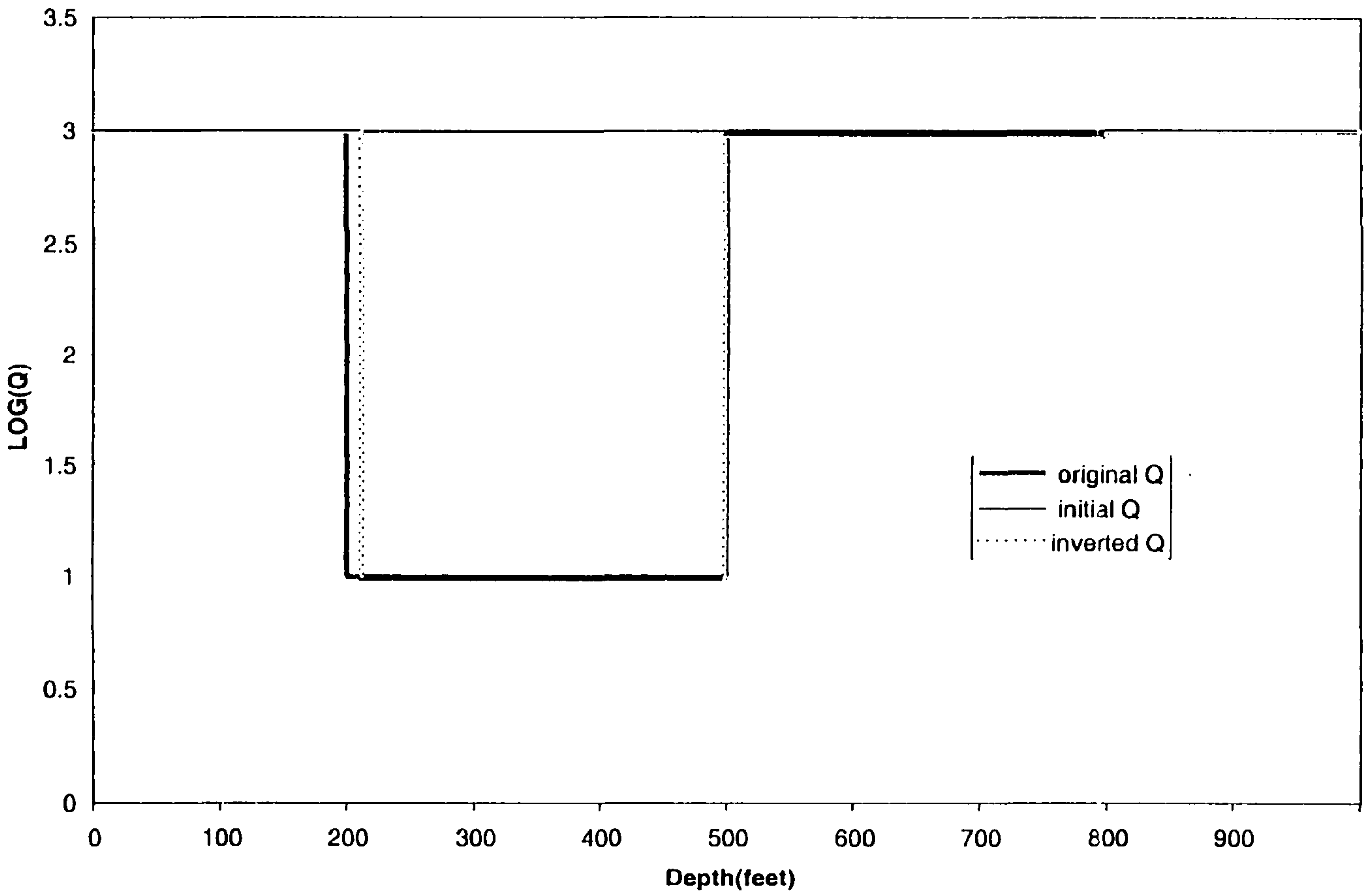

Figure 4.16. Q model inversion 5: Q2 is changed from 10 to 1000, but the seismic trace is filtered by "light" AGC

CHAPTER 5. ITERATIVE SCATTERING-REMOVAL METHOD FOR DOWNHOLE ATTENUATION MEASUREMENTS USING VSP'S

5.1 INTRODUCTION

In Chapter 3, a general description of the methods to measure attenuation from VSP data were given. Although these methods are feasible in theory, they have various difficulties when applied. Typical difficulties are scattering-removal, first arrival isolation and coupling variations. Existing methods include: (1) Spectral ratio method of Kan et al. (1981) which tries to solve the scattering problem by averaging spectra; (2) The inversion algorithm of Kang and McMechan (1994) which tries to separate scattering attenuation by using an additive relation (or assumption); (3) The inversion method of Amundsen and Mittet (1994) which address the coupling problem. All of these methods address certain aspects of the problem but none have completely solved the problem. Some of these methods have been improved in solving scattering problems. All these techniques suffer from the necessity to isolate the direct down-going arrival, although in principle, the inversion method could be extended to include the full VSP seismogram.

The method described here is a modification of Kan's spectral-ratio method in principle and in technique, but is akin to extension of the inversion method in that it allows scattered events in the analysis window, thereby avoiding the first-arrival-isolation problem. This method, using the linear properties of seismic spectral ratios, is free from receiver sonde coupling problems unless the variations in coupling are frequency dependent over the seismic bandwidth. Using the available impedance profile calculated from well logs, VSP synthetics that include up-going and down-going waves, multiples and attenuation are calculated. The scattering effect is removed iteratively by matching real spectral ratios with synthetic spectral ratios.

Numerical modeling of infinite bandwidth and band limited cases shows that this method is accurate, effective and robust. Application to real VSP data from offshore Gulf of Mexico block Eugene Island 354 shows high attenuation associated with potential gas pay.

In this chapter, the modified spectral ratio method will first be described as will the presentation of VSP synthetics. The attenuation extraction method will then be tested by numerical modeling. Finally, the method is applied to real data from offshore Gulf of Mexico block Eugene Island 354 and the attenuation profile is compared to the available well log data.

5.2 ITERATIVE SCATTERING REMOVAL METHOD

Supposing that the earth is laterally homogeneous and that the offset of the VSP source is negligible, the amplitude spectrum of a windowed VSP trace at depth z, $A(f,\alpha,z)$, can be written as

$$A(f,\alpha,z) = S(f,z)E(f,\alpha,z)T(f,z) \tag{5.1}$$

where f is frequency, α is the attenuation coefficient, z is the geophone depth, and $S(f, z)$ is the field source spectrum which may vary from shot to shot. $T(f, z)$ is the recording system transfer function. The earth response, $E(f, \alpha, z)$, is written as

$$E(f, \alpha, z) = G(f, \alpha, z)\exp[-\alpha(f, z)z] \tag{5.2}$$

Here, the effects of spreading, intrabed multiples and transmission losses are lumped together in $G(f, \alpha, z)$. Using the constant Q-attenuation relation where the attenuation coefficient, α, is given by $\alpha(f, z) = \pi f / Q(z)V(z)$, gives

$$A(f, Q, z) = S(f, z)T(f, z)G(f, Q, z)\exp\left(-\frac{\pi f z}{Q(z)V(z)}\right) \tag{5.3}$$

where V is velocity, and Q is the quality factor which can be assumed to be independent of frequency in the seismic frequency range (McDonal et al., 1958). In fact, Q need not be constant with frequency, only the product QV, however, we expect V to vary only slightly over the seismic band. The amplitude spectral ratio $a(f, Q)$ for depths z_1 and z_2 is given by:

$$a(f, Q) = \sigma(f) + t(f) + g(f, Q) + \pi f \Delta z / QV \tag{5.4}$$

where $a(f,Q) = \ln(A(f,Q,z_1) / A(f,Q,z_2))$,

$\Delta z = z_2 - z_1$,

$\sigma(f) = \ln[S_1(f) / S_2(f)]$,

$g(f,Q) = \ln[G(f,Q,z_1) / G(f,Q,z_2)]$,

$t(f) = \ln(T(f,z_1) / T(f,z_2))$

The recording system effect, $T(f,z)$, includes two parts: the instrument filter and geophone coupling. The filter from the same instrument can be assumed invariant with small depth changes. If, in addition, the coupling effect is independent of frequency or the frequency dependence does not vary, $t(f)$ is zero or a constant.

Suppose the waveform spectra have been corrected by the source signature $S(f)$. Given $K = \pi f \Delta z / QV$, we have

$$a(f,Q) = g(f,Q) + Kf + t(f) \tag{5.5}$$

We can replace $g(f,Q)$ with $g(f,Q_\infty)$ which is the spectrum where there is no intrinsic attenuation (Q_∞) and make an initial Q estimation from:

$$a(f,Q) - g(f,Q_\infty) = Kf + t(f) \tag{5.6}$$

Using this initial Q estimation from K, we can calculate the synthetic spectral ratio a' as

$$a'(f,Q) = g(f,Q_{estimate}) + K_{estimate}f \qquad (5.7)$$

This a' is different from the true spectral ratio a. Subtracting equation (5.7) from (5.5), gives

$$a(f,Q) - a'(f,Q_{estimate}) = g(f,Q) - g(f,Q_{estimate}) + (K - K_{estimate})f + t(f) \qquad (5.8)$$

Modeling shows that $g(f,Q) - g(f,Q_{estimate})$ is approximately a linear function of the frequency. Thus equation (5.8) can be rewritten as

$$a(f,Q) - a'(f,Q_{estimate}) = \Delta K f + t(f) \qquad (5.9)$$

where $Q_{estimate}$ is the attenuation parameter we wish to determine. $a'(f,Q)$ is the synthetic spectral ratio calculated assuming $Q{=}Q_{estimate}$. ΔK is the estimated slope deviation of the synthetic spectral ratio from the true spectral ratio, and

$$\Delta K = g(f,Q)/f - g(f,Q_{estimate})/f + (K - K_{estimate}) \qquad (5.10)$$

From equations (5.5) – (5.9), the intrinsic attenuation can be estimated in the following way: Assuming the impedance profile is known from well logs, the synthetic spectral ratio can be calculated. If the synthetic spectral ratio of non-intrinsic attenuation $g(f,Q_{\infty})$ is used as the scattering effect term $g(f,Q)$ in equation (5.5), an estimation of

Q from the slope K from equation (5.6) is obtained. This estimation is not exactly the true intrinsic Q, but deviates somewhat because the multiples have experienced different attenuation than primaries arriving in the same window. So, if this Q is used to calculate the synthetic amplitude spectral ratio, this ratio will be different from the correct spectral ratio, and the slope ΔK in equation (5.9) will be an estimate of the deviation from the true slope. Using this estimated deviation of slope to correct the former estimation, gives an improved estimate of Q. Applying this correction iteratively converges to the true Q value. Thus, Q can be iteratively estimated from the amplitude spectral ratio at z_1 and z_2.

The following procedure is used to estimate Q:

1. Calculate the VSP spectra within predefined analysis windows (preceding the tube wave and other non-modeled events) on the VSP data at the target depths, compute frequency spectra and perform source signature normalization.;
2. Calculate the spectral ratio between two depths from real data as S1;
3. Generate the synthetic spectra at the target depths;
4. Calculate the spectral ratio from synthetic data assuming no intrinsic attenuation as S0;
5. Subtract the logarithmic spectral ratios as $\ln(S_1)-\ln(S_0)$. This is referred to as the contrast spectral ratio.
6. Estimate the intrinsic Q using the slope K of $\ln(S_1)-\ln(S_0)$ versus f;
7. Calculate the spectral ratio from synthetic data assuming intrinsic attenuation has a value of the estimated Q from step 6 as S2 ;

8. Compare S1 and S2, if the two curves have discrepancy below a predefined threshold, the iteration stops;
9. Use the difference of $\ln(S_1) - \ln(S_2)$ to estimate the slope deviation ΔK;
10. Use ΔK to correct the former estimate of Q and repeat the procedure from step 6 using the corrected Q.

As down-going and up-going events are affected by the Q profile outside the depth range, z_1 and z_2, the iterations must proceed simultaneously for all depth ranges.

Note that this method does not use the wavelet spectrum but the spectrum of the response signal (the VSP trace) to calculate the spectral ratio. This avoids wavelet extraction difficulty. The synthetic calculation already includes the up- and down-going waves in the VSP trace; there is no need to filter out up-going waves and multiples as is done by Amundsen and Mittet (1994). In fact, all arrivals become part of the signal, and do not confound the spectral ratios by introducing spectrum notches that may vary in frequency between depths. Synthetic studies show that the technique converges without requiring an initial Q profile starting model.

It is obvious that the key to this method is the synthetic VSP. In the following the full waveform synthetic VSP modeling algorithm is described.

5.3 SYNTHETIC VSP

In Chapter 4, Claerbout's method is modified to include inelastic non-Goupillaud media for surface seismic forward modeling. Here the method is extended to permit VSP synthetics that include inelastic non-Goupillaud media and geometric spreading. Tube waves are not modeled and are assumed to be suppressed by filtering or outside the analysis window.

5.3.1 Medium model

The synthetic VSP method assumes a 1-D layered inelastic medium and normally incident waves. A layered medium can be specified by giving the reflection coefficient and the transmission coefficient at each interface and the thickness for each layer. Figure 5.1 shows the general 1-D medium, where t is the transmission coefficient, c is the reflection coefficient, x is the thickness, U refers to the up-going wave and D refers to the down-going wave. x_k is the thickness of the kth layer. t_k and c_k are the transmission and reflection coefficients at the kth interface for incidence from below the interface. t'_k and c'_k are the transmission and reflection coefficients at the kth interface for incidence from above the interface. U_k and D_k refer to the up and down-going wave at the top of the kth layer just below the (k-1)th interface. U'_k and D'_k refer to the up and down-going wave at the bottom of the kth layer just above the kth interface.

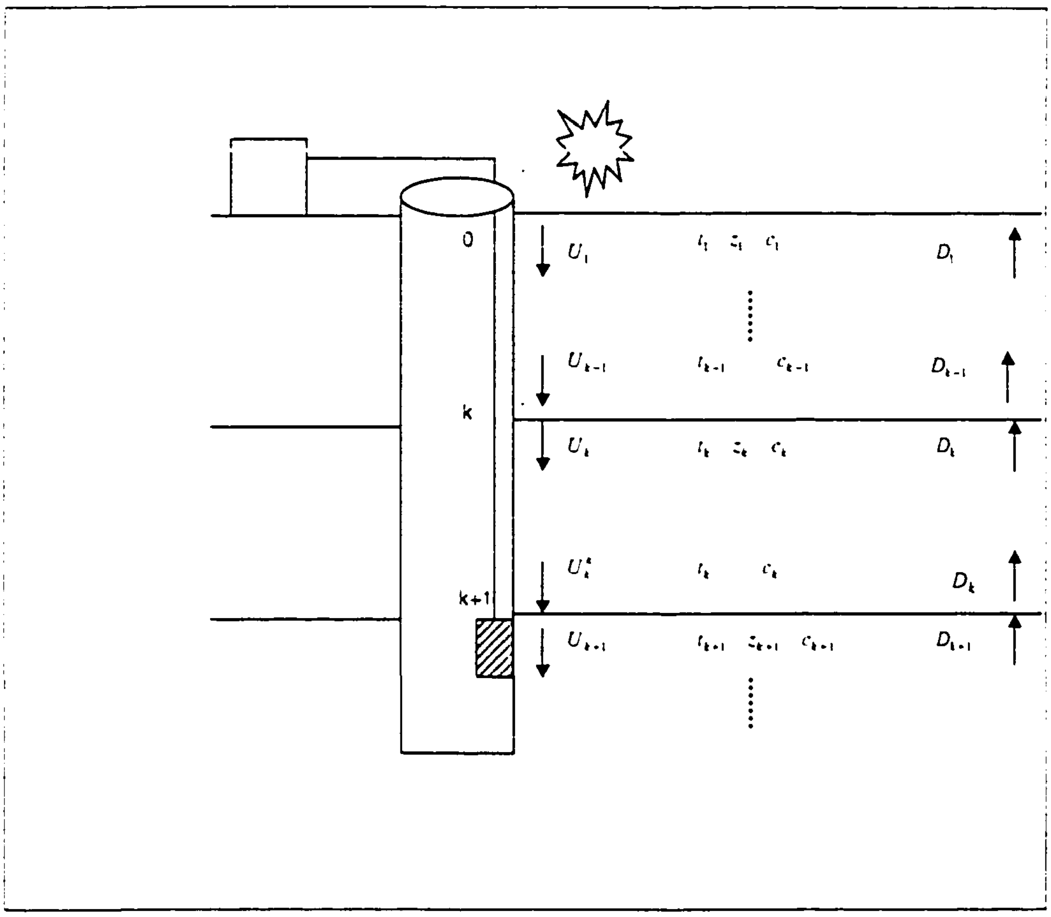

Figure 5.1. The general 1-D medium model. z_k refer to the thickness of the kth layer. t_k, c_k refer to the transmission and reflection coefficient at the kth interface from up to down. t'_k, c'_k refer to the transmission and reflection coefficient at the kth interface from down to up. U_k, D_k refer to the up and down-going wave at the top of the kth layer just below the (k-1) the interface. U'_K, D'_k refer to the up and down-going wave at the bottom of the kth layer just above the kth interface.

5.3.2 Propagation equation

According to the continuity principle and energy conservation principle.

$$\begin{bmatrix} U \\ D \end{bmatrix}_{k+1} = \frac{1}{t_k}\begin{bmatrix} 1 & c_k \\ c_k & 1 \end{bmatrix}\begin{bmatrix} U' \\ D' \end{bmatrix}_k \tag{5.11}$$

According to wave theory in an attenuating medium and geometrical spreading

$$\left.\begin{aligned} U'_k &= \frac{1}{x_k} U_k e^{-i\beta x_k} e^{\alpha x_k} \\ D'_k &= \frac{1}{x_k} D_k e^{i\beta x_k} e^{-\alpha x_k} \end{aligned}\right. \xrightarrow{z = e^{i\beta x_k} e^{-\alpha x_k}} \begin{bmatrix} U' \\ D' \end{bmatrix}_k = \frac{1}{x_k}\begin{bmatrix} 1/z & 0 \\ 0 & z \end{bmatrix}\begin{bmatrix} U \\ D \end{bmatrix}_k \tag{5.12}$$

where $\frac{1}{x_k}$ compensate the geometrical spreading, α is the attenuation coefficient and β is the wave number. The later two are related to quality factor Q and velocity V by

$$\alpha = \pi f / QV \tag{5.13}$$

$$\beta = \frac{2\pi f}{V} \tag{5.14}$$

Combining equation (5.11) with equation (5.12) gives the propagation equation including attenuation and the geometrical spreading.

$$\begin{bmatrix} U \\ D \end{bmatrix}_{k+1} = \frac{1}{t_k x_k} \begin{bmatrix} 1 & c_k \\ c_k & 1 \end{bmatrix} \begin{bmatrix} 1/z_k & 0 \\ 0 & z_k \end{bmatrix} \begin{bmatrix} U \\ D \end{bmatrix}_k$$
$$= \begin{bmatrix} 1/z_k t_k x_k & c_k z_k / t_k x_k \\ c_k / z_k t_k x_k & z_k / t_k x_k \end{bmatrix} \begin{bmatrix} U \\ D \end{bmatrix}_k \tag{5.15}$$

5.3.3 Synthetic VSP

Considering the basic seismic geometry shown in Figure 5.2, the earth sends the up-going reflectivity series -R to the surface. The surface is free and returns the down-going reflectivity R back into earth. E is the escaping wave at the bottom layer. Suppose there are k interfaces in the geometry. From the propagation equation (5.15),

$$\begin{bmatrix} 0 \\ E \end{bmatrix} = \begin{bmatrix} 1/z_k t_k x_k & c_k z_k / t_k x_k \\ c_k / t_k x_k & z_k / t_k x_k \end{bmatrix} \cdots \begin{bmatrix} 1/z_1 t_1 x_1 & c_1 z_1 / t_1 x_1 \\ c_1 / t_1 x_1 & z_1 / t_1 x_1 \end{bmatrix} \begin{bmatrix} -R \\ 1+R \end{bmatrix}$$
$$= \begin{bmatrix} F_{11} & F_{12} \\ F_{21} & F_{22} \end{bmatrix} \begin{bmatrix} -R \\ 1-R \end{bmatrix} \tag{5.16}$$

Solving equation (5.16) gives the reflected wave at the surface and the transmitted wave at the bottom in the frequency domain:

$$R = \frac{F_{12}}{F_{11} - F_{12}} \tag{5.17}$$

$$E = \frac{F_{11} F_{22} - F_{12} F_{21}}{F_{11} - F_{12}} \tag{5.18}$$

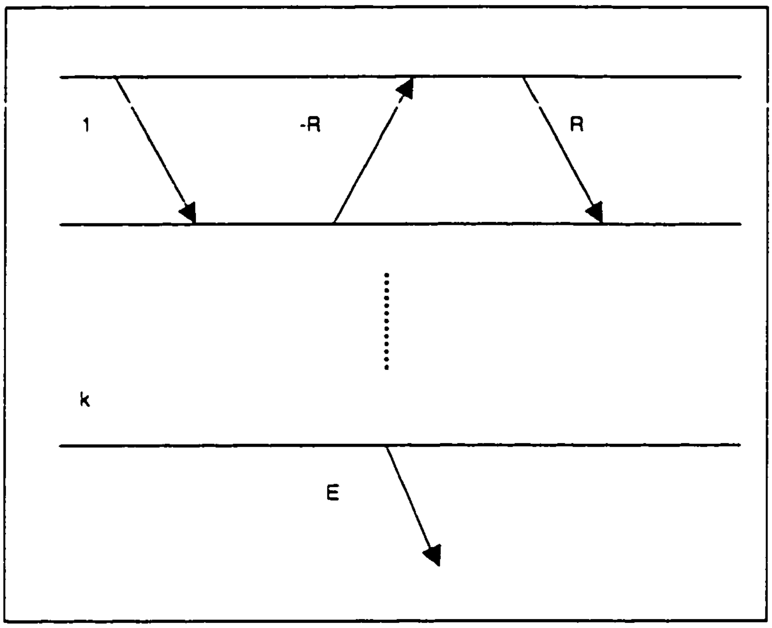

Figure. 5.2. 1-D seismology geometry. The impulse is initiated at the surface. The earth sends back refection -R to the surface. The surface is free and returns R back into earth. E is the escaping wave at the bottom layer.

Equation (5.17) and (5.18) can be transformed into the time domain by Fourier transform:

$$
\begin{aligned}
R(t) &= \frac{1}{2\pi}\int_{-\infty}^{\infty} R(\omega)e^{-i\omega t}\,d\omega \\
E(t) &= \frac{1}{2\pi}\int_{-\infty}^{\infty} E(\omega)e^{-i\omega t}\,d\omega
\end{aligned}
\tag{5.19}
$$

Equation (5.17) and (5.18) give the reflected seismic wave R at surface and transmitted wave E at the bottom if impedance and Q are known. Knowing R in the first layer, the up-going wave U and down-going wave D at any interface K can be calculated using the following equation.

$$
\begin{aligned}
\begin{bmatrix} U_{k-1} \\ D_{k-1} \end{bmatrix} &= \begin{bmatrix} 1/z_k t_k & c_k z_k / t_k \\ c_k / t_k & z_k / t_k \end{bmatrix} \cdots \begin{bmatrix} 1/z_1 t_1 & c_1 z_1 / t_1 \\ c_1 / t_1 & z_1 / t_1 \end{bmatrix} \begin{bmatrix} -R \\ 1+R \end{bmatrix} \\
&= \begin{bmatrix} F_{11} & F_{12} \\ F_{13} & F_{14} \end{bmatrix} \begin{bmatrix} -R \\ 1+R \end{bmatrix}
\end{aligned}
\tag{5.20}
$$

The VSP spectrum at interface K is equal to $\left(U_{k-1} + D_{k-1}\right)$.

5.4 NUMERICAL EXAMPLES

Two numerical examples using VSP synthetics are presented to demonstrate the performance of the proposed method. One has an infinite bandwidth source signal, while the other is band limited. In both cases, the source signal passes through a set of 300 synthetic layers that are 1 foot thick and have random velocities. The density is taken to be constant and is set to given value. Q estimation is carried out on the synthetic trace.

In the infinite band case, the source is an impulse that has an infinite frequency range and a constant amplitude. After the impulse passes through the modeled layers, its spectrum is attenuated and distorted. Figure 5.3 compares the spectra of the transmitted waves in cases of intrinsic $Q=\infty$, 100 and 10 and illustrates how attenuation and multiples are interacting. The amplitude reduction due to Q attenuation is much greater at frequencies where multiples are constructive (spectrum peaks) and less where the multiples are destructive (spectrum valleys). In this case, the transmitted wave spectrum at the bottom of the section is divided by the impulse spectrum at the top of the section to get the spectral ratio. Figure 5.4 shows the difference between the theoretical and synthetic scattering-only spectral ratios for Q=10. Note that, due to multiples, the regression fit to the contrast spectral ratio differs from the correct line. The slope of the predicted line from the contrast spectral ratio is used to obtain an initial estimate of Q. The iterative procedure described in the previous section is followed to remove the scattering effects and to get the correct Q. First, the Q obtained by linear regression of the contrast spectral ratio from Figure 5.4 is used to estimate the synthetic ratio with attenuation. This synthetic ratio is different from the theoretical ratio because the predicted Q used is not the true Q. Figure 5.5 compares the theoretical spectral ratio for Q=10 with that from the synthetic generated using the first estimated Q. The estimated slope deviation (0.0018; see Figure 5.6) is then used to correct the former Q estimate. These steps are repeated until after 6 iterations, the estimated Q is close to the correct value. Figure 5.7 shows the real spectral ratio and the last predicted synthetic spectral ratio. The iterative results are listed in Table 5.1. Figure 5.8 shows the estimated constant Q lines in each iteration, the correct constant Q line and the difference of the observed and synthetic scattering-only ($Q=\infty$) spectral ratios. The iterative procedure works effectively to remove the scattering effects.

Table 5.1. Step results of Q estimation using iterative scattering-removal method for infinite band case

Iteration #	K-slope estimated	Q estimated	ΔK-slope correction
1	0.0033	6.67	0.0018
2	0.0015	14.67	-0.0012
3	0.0027	8.15	0.0008
4	0.0019	11.6	-0.0005
5	0.0024	9.17	0.0003
6	0.0021	10.5	

In the limited band case (Figure 5.9), the iterative method also works well. The spectral ratio is calculated by dividing the transmitted wave spectrum at the bottom of the section by the wave spectrum at the top of the section. Taking the spectral ratio with Q=10 as the observed spectral ratio and the spectral ratio with $Q=\infty$ as the synthetic scattering-only spectral ratio, Figure 5.10 shows the subtraction of the observed spectral ratio and the synthetic scattering-only spectral ratio, the predicted trend from the subtracted curve and the correct line for Q=10. The scattering effects once again cause the linear regression fit to be erroneous. Following the iterative procedure, scattering is removed and a satisfactory Q value is estimated after 5 iterations. The iteration results are listed in Table 5.2. Figure 5.11 shows the estimated constant Q lines for each iteration, the correct constant Q line for Q=10 and the spectral ratio difference.

Table 5.2. Step results of Q estimation using iterative scattering-removal method for limited band case

Iteration #	K-slope estimated	Q estimated	ΔK-slope correction
1	0.0029	7.49	0.0015
2	0.0014	15.7	-0.001
3	0.0024	9.2	0.0006
4	0.00234	9.4	0.0005
5	0.0023	9.57	

To test that the method is unaffected by frequency independent coupling effects, synthetic tests were made where the VSP traces were multiplied by different scalars from location to location. The Q estimation was unaffected.

5.5 APPLICATION TO REAL DATA

The method was applied to real VSP data (Figure 5.12) from well D11 of the Eugene Island 354 Field, offshore Gulf of Mexico. This is a multi-shot VSP survey. The source signature is normalized for every trace in the frequency domain. The spectra are summed at each depth to get the average spectrum. The estimation method is applied to the average spectra from depths 4980.5 to 10175 feet where only a heavily edited sonic log is available. Some error in Q estimation is expected due to lack of impedance information above 4980.5 ft. Anomalous spectral traces are removed. Then the spectra are scanned visually. Depth zone boundaries were set by spotting locations where the spectral amplitudes were obviously attenuated differently. The iterative correction was applied simultaneously to the entire profile. That is, a gross Q-profile prediction by estimating the Q for each section from simple spectral ratio differences within that section was first obtained. Then the entire predicted Q profile was used to calculate the new synthetic VSP data. The new predicted VSP spectral ratio differences and the real spectral ratio differences gave a depth dependent profile correction, and the correction procedure was repeated. After only three repetitions, the iterative error fell below 1.0e-4. Table 5.3 lists the iterative results from each step. Figure 5.13 shows the computed intrinsic attenuation profile compared with related well log data. The attenuation profile correlates with independent well log information such as gamma ray and resistivity logs. At a depth of 6825 feet, a potential reservoir exhibits anomalously high attenuation. Q values of 10 and under are estimated in much of the section at and immediately below the prospective pay zone, which is plausible if free gas occurs in the interval.

Table 5.3. Step results of Q estimation using iterative scattering-removal method for real VSP data

	Gross Q estimation		Iteration 1		Iteration 2		Iteration 3	
Md D(KB)	K	Q	DK	Q	DK	Q	DK	Q
5325	0.0007	196.6	0	196.6	0	196.6	0	196.6
5825	0.0007	73.2	0.0002	56.9	-0.00003	58.9	7E-07	58.8
6825	0.0045	23.5	-0.0006	27.2	0.0003	25.2	-0.0001	25.8
7325	0.0126	4.7	-0.0039	6.9	0.0015	5.86	-0.0005	6.16
7825	0.006	9.5	-0.0006	10.6	0.0002	10.2	-0.00009	10.4
8325	0.0063	8.4	-0.0011	10.1	0.0003	9.58	-0.00008	9.72
8825	0.002	27.7	-0.0008	46.1	0.0004	34.6	0.00003	34
9275	0.0058	8.8	-0.0001	9.0	-0.0003	9.5	0.0001	9.33
10175	0.006	16.6	0.0004	15.5	-6E-06	15.5	-0.00002	15.6

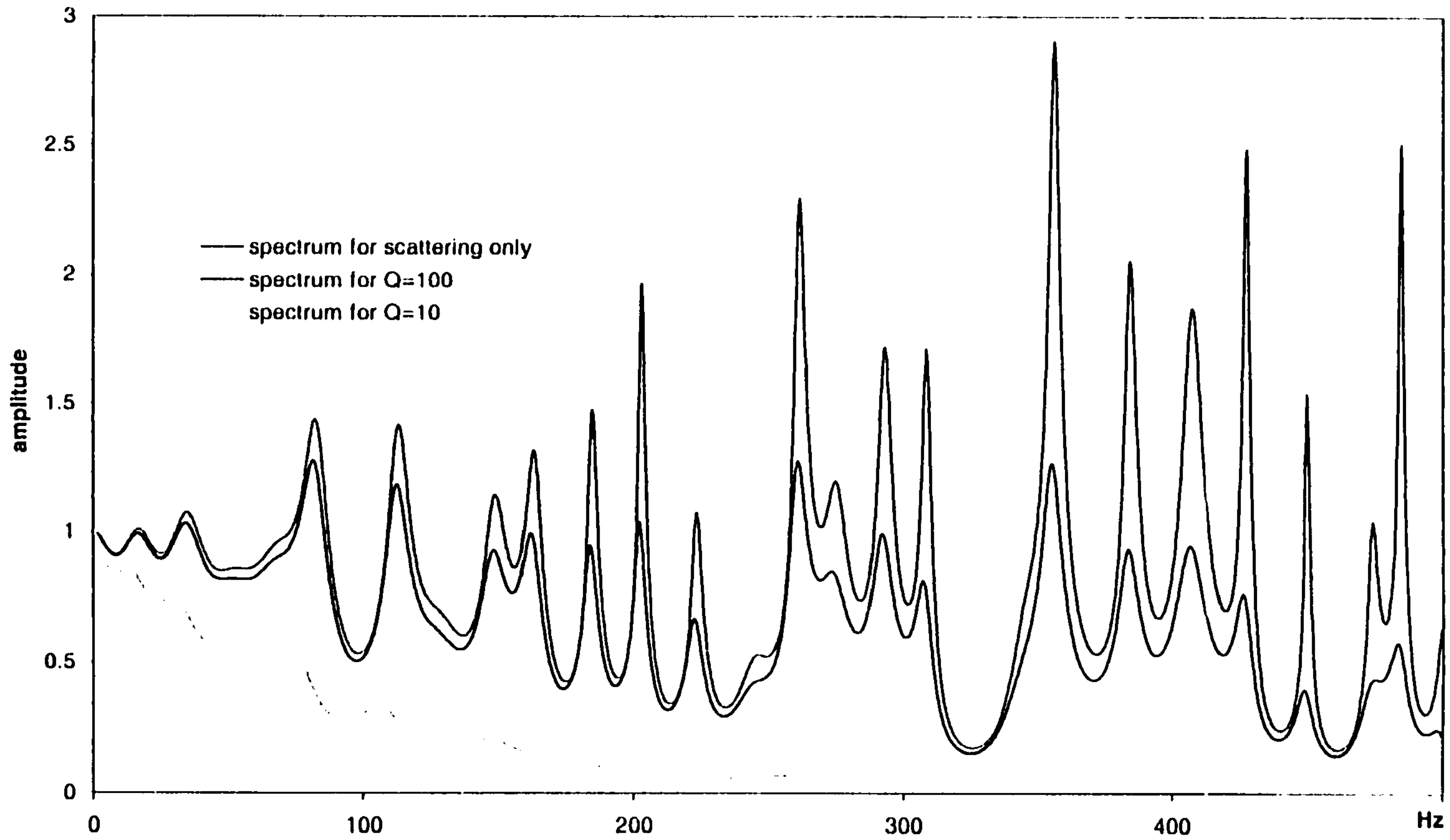

Figure 5.3. Comparison of the spectra of the transmitted waves in cases of intrinsic Q=∞, 100 and 10.

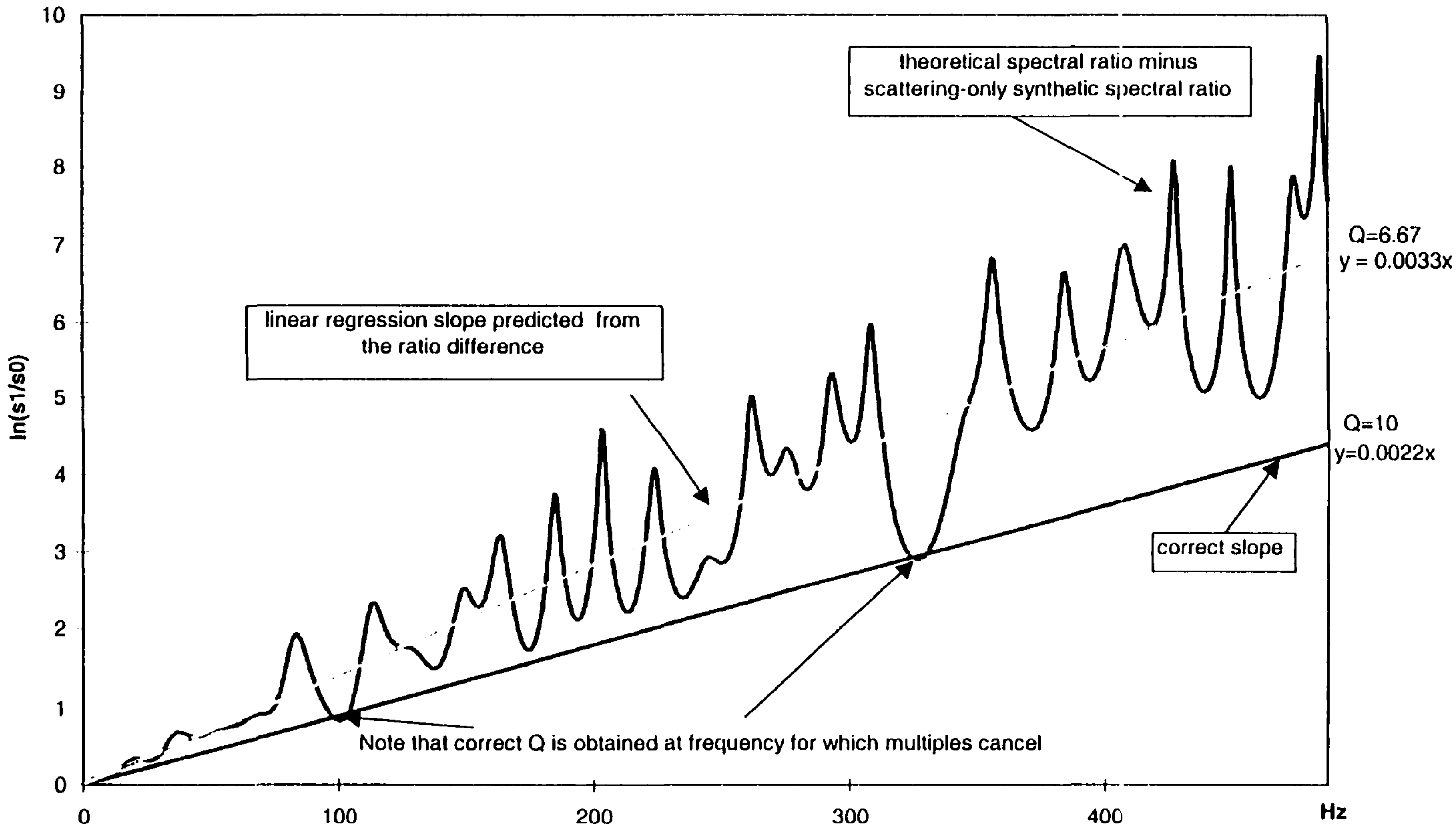

Figure 5.4. Predicted and theoretical spectral ratio differences.

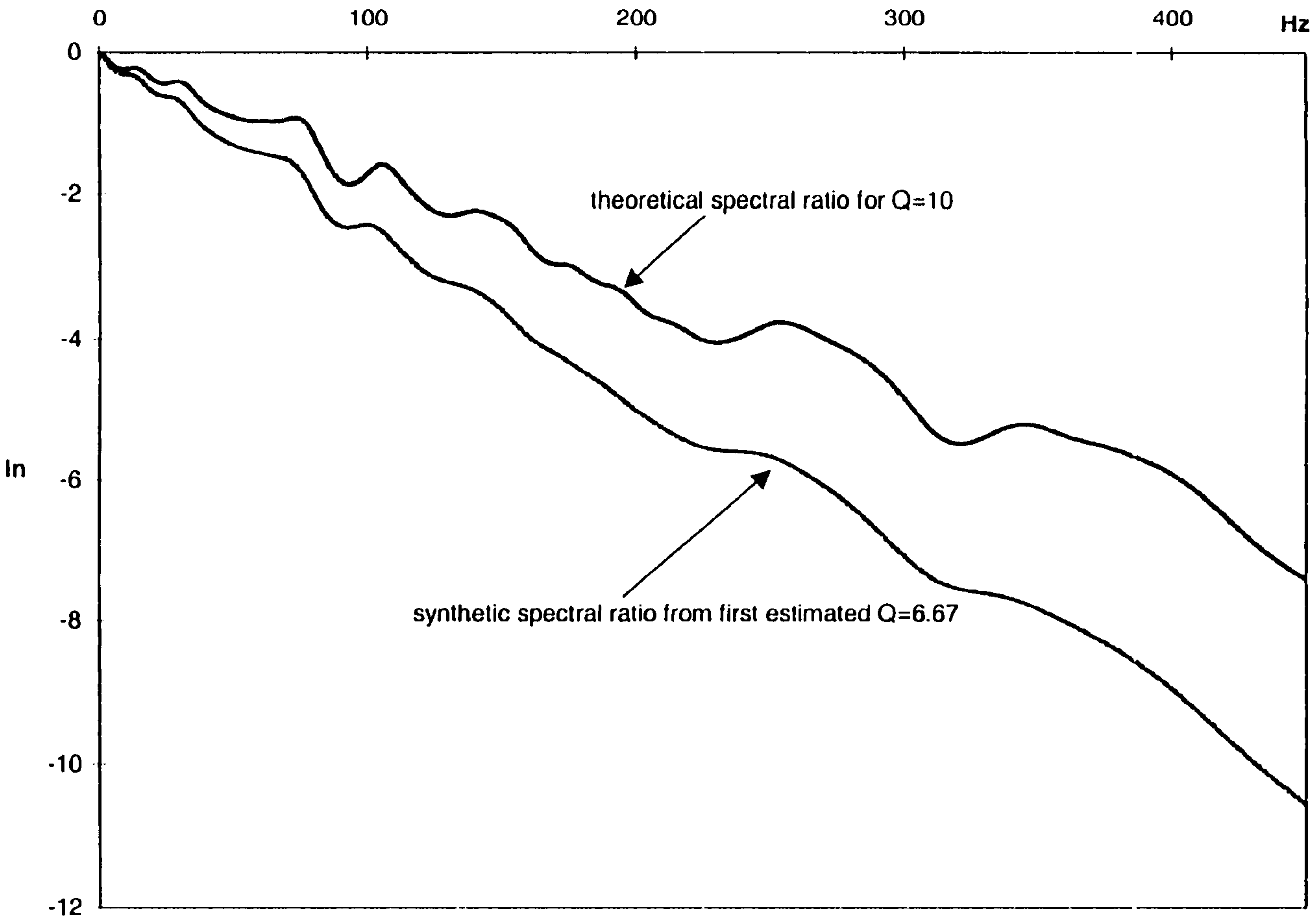

Figure 5.5. Comparison of the real and first predicted spectra.

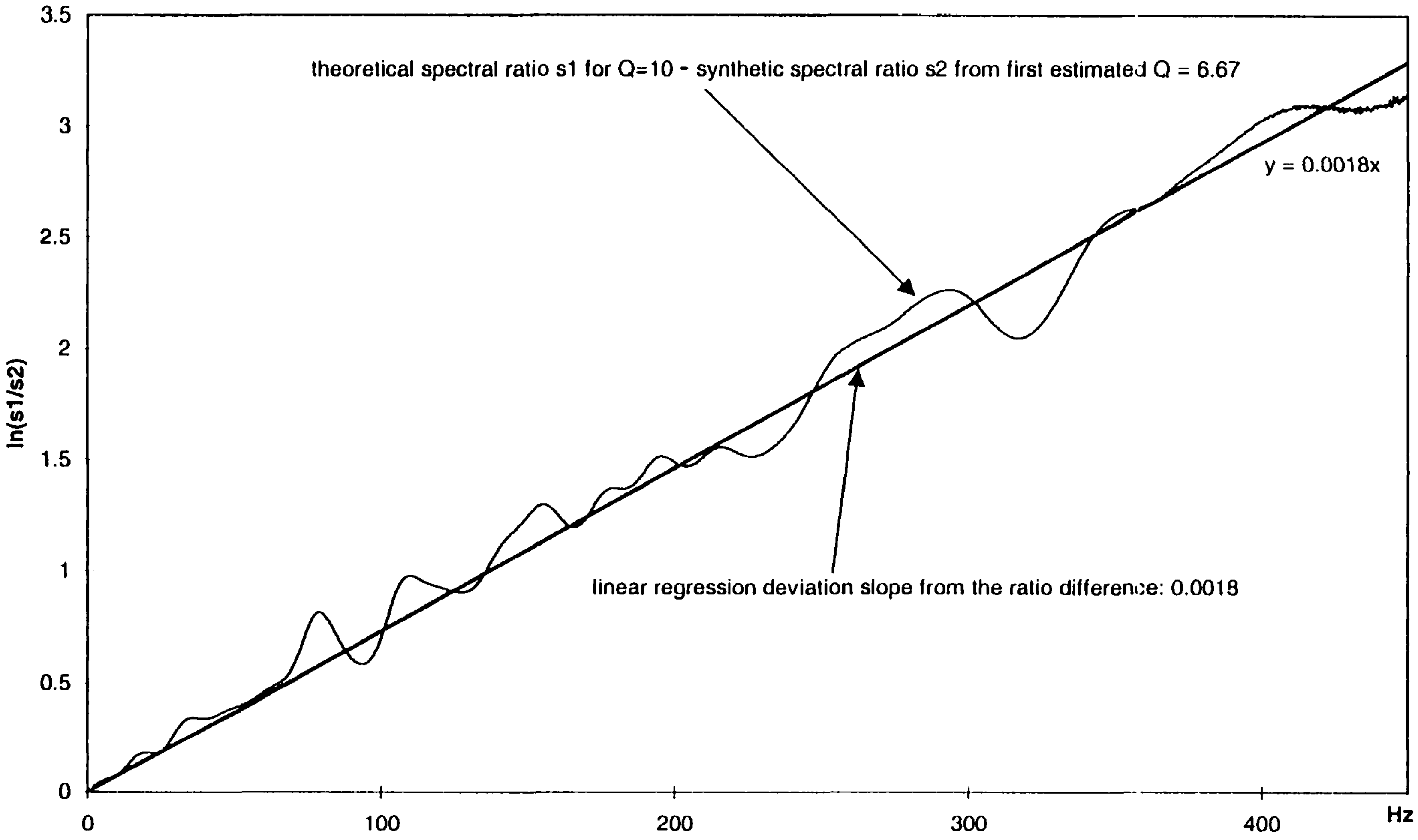

Figure 5.6. Difference of the real and first predicted spectra and estimated slope deviation.

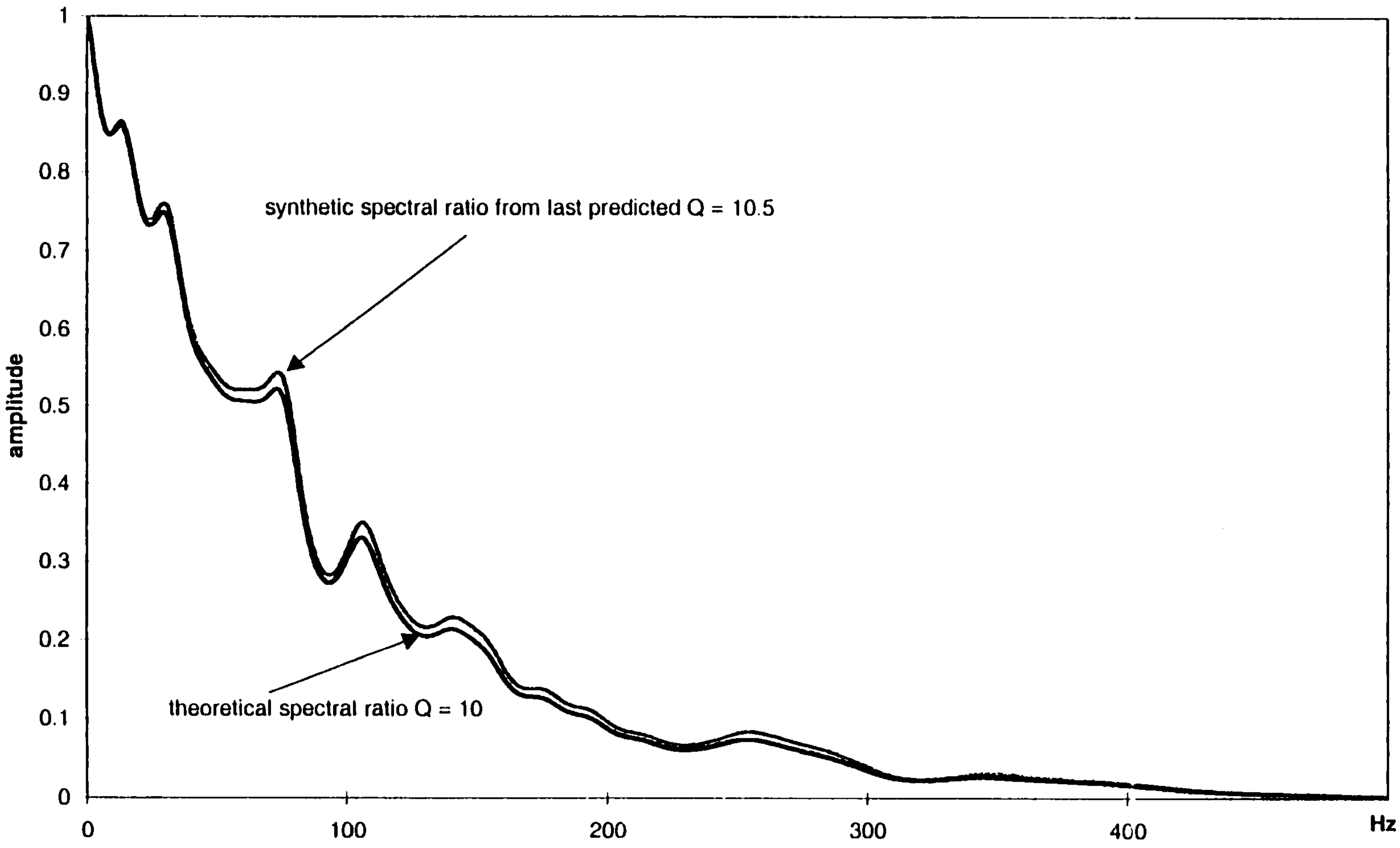

Figure 5.7. Comparison of real spectrum and final prediction .

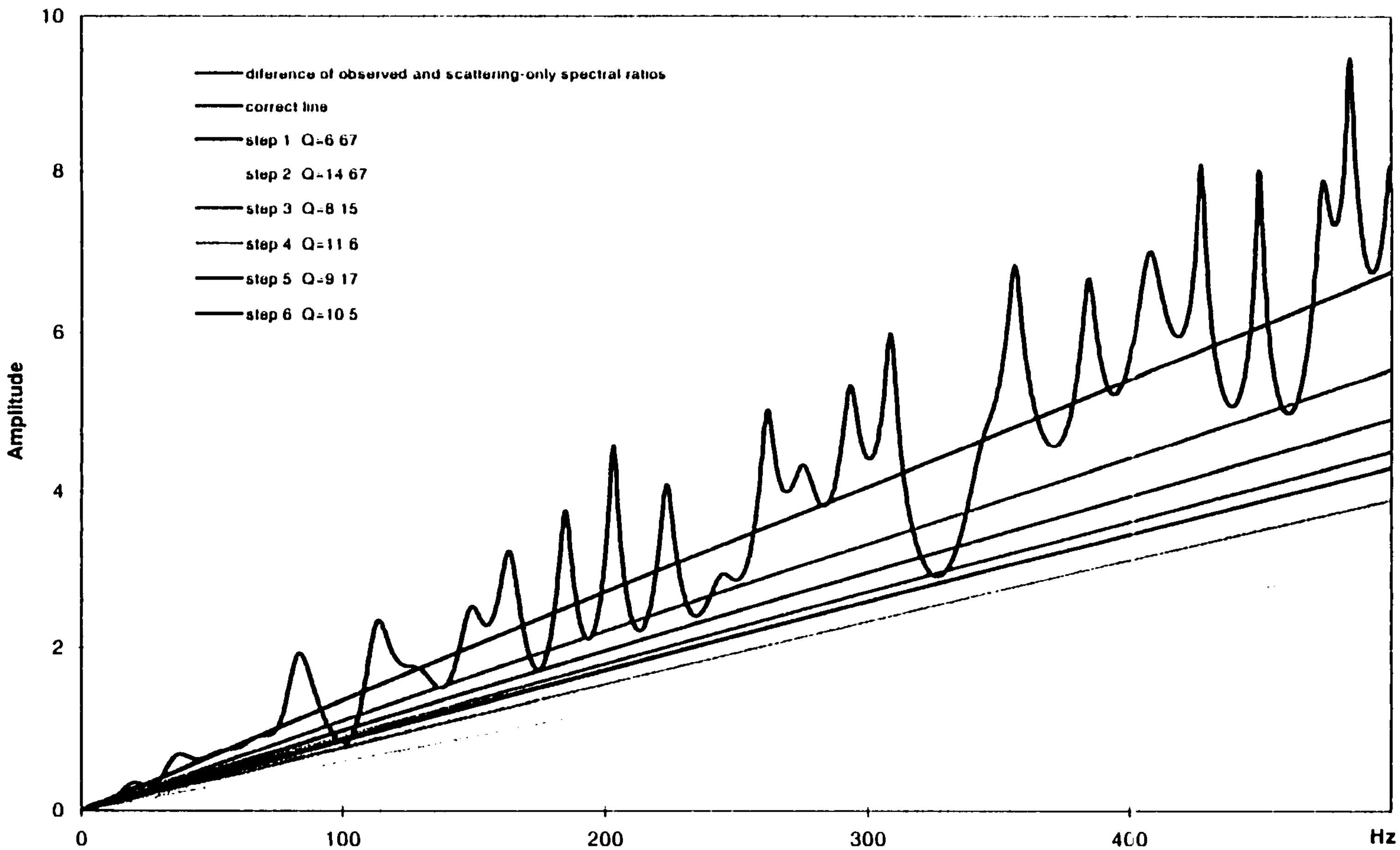

Figure 5.8. Predicted spectral ratio for each iteration and the theoretical ratio for Q=10 and impulse source.

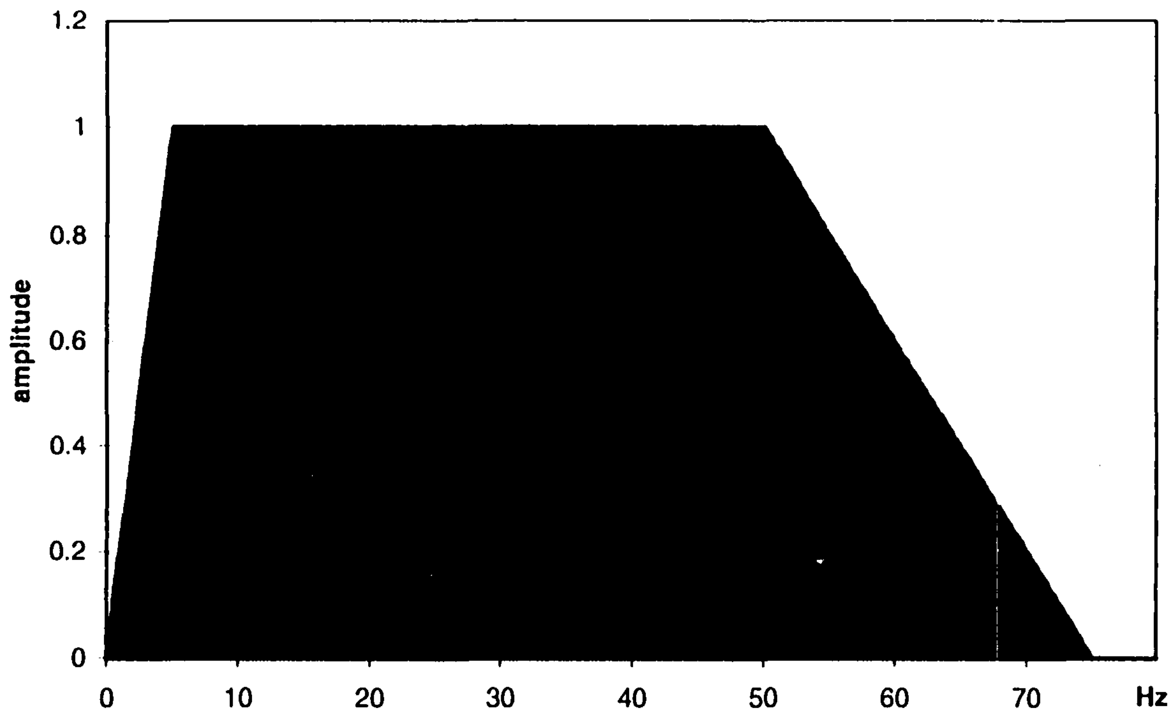

Figure 5.9. Spectrum of the limited band wavelet.

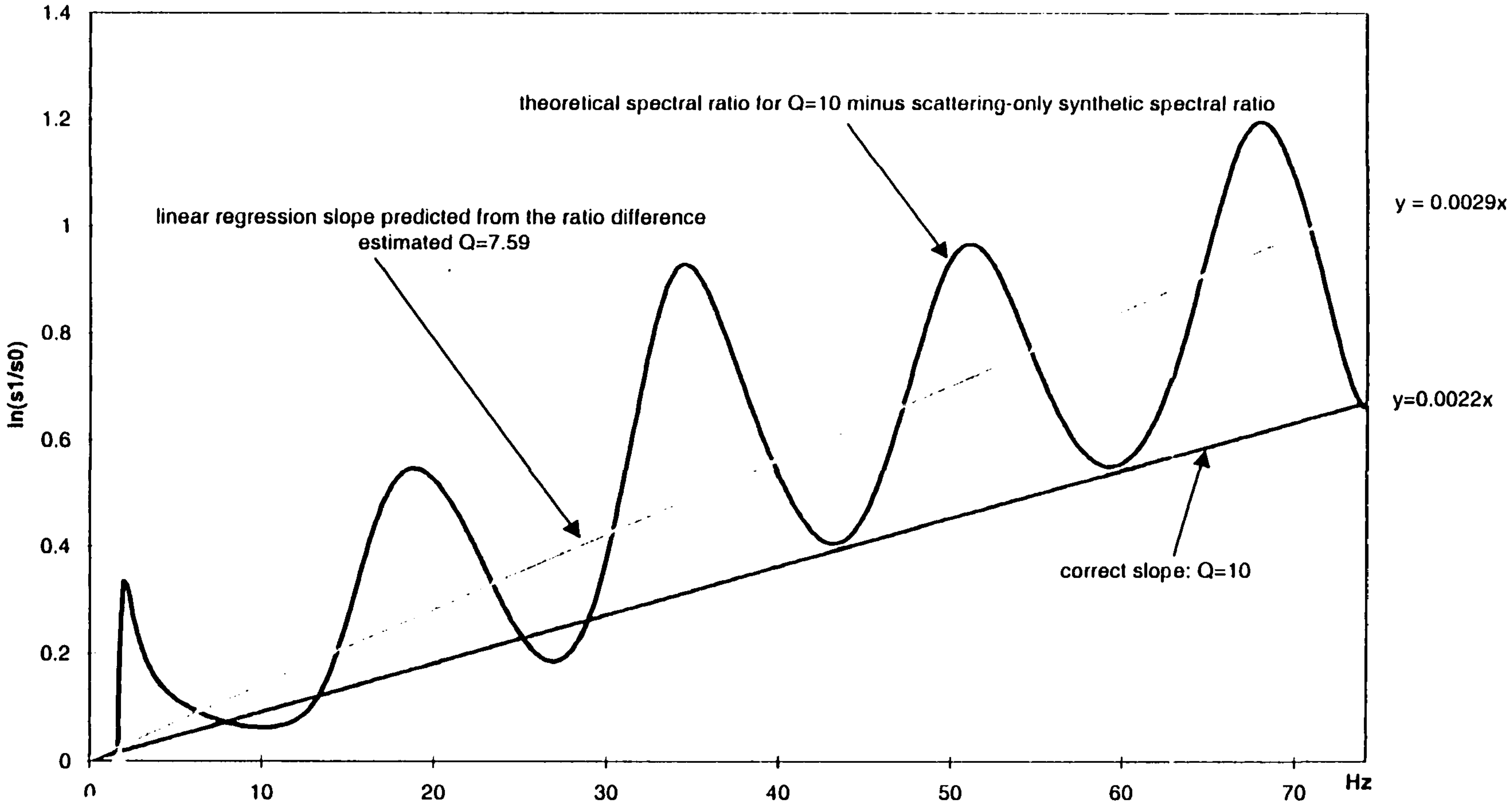

Figure 5.10. Predicted and theoretical spectral ratio differences in the limited band case.

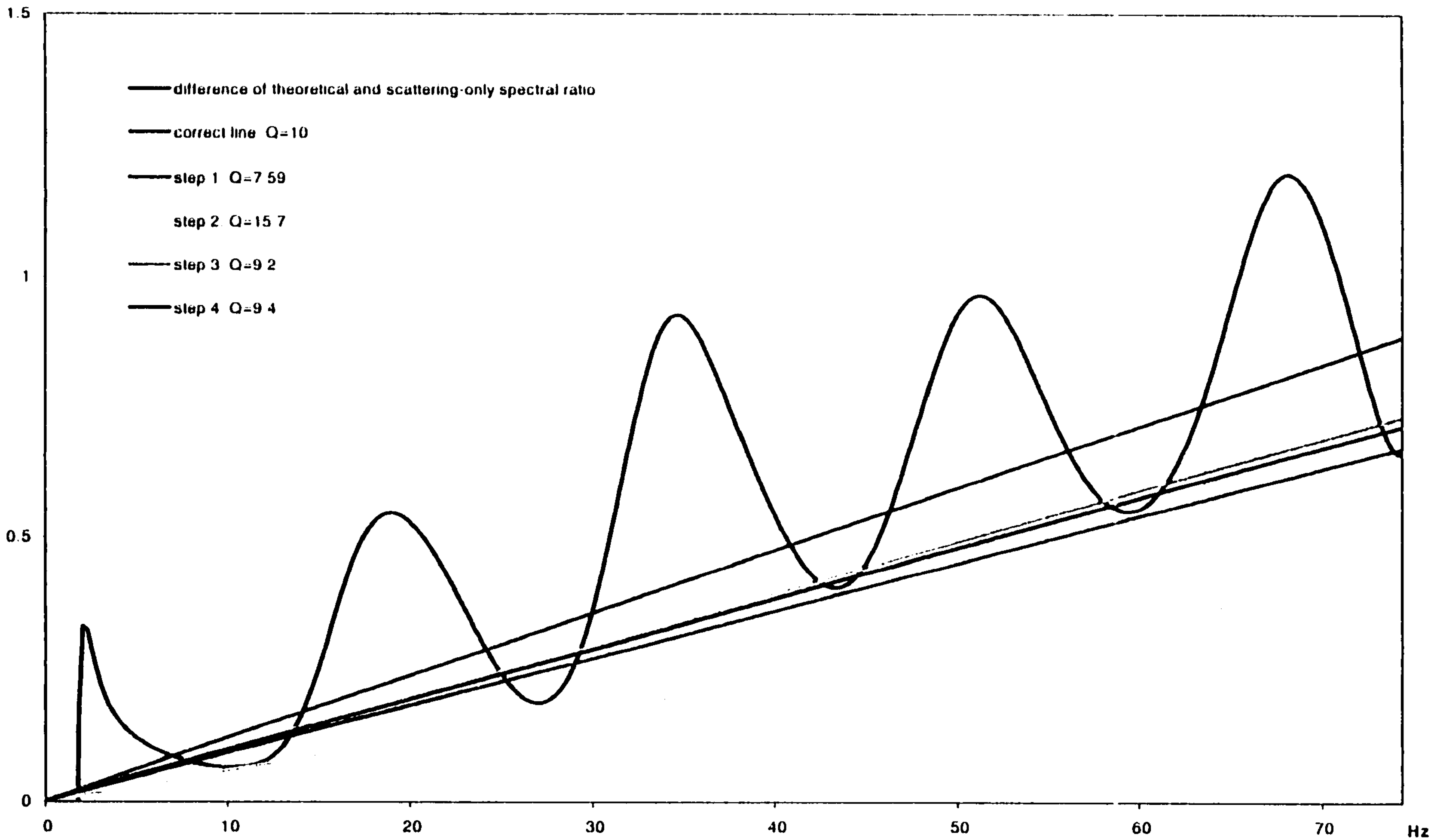

Figure 5.11. Predicted spectral ratios for each iteration and the theoretical ratio for Q=10 and band limited source

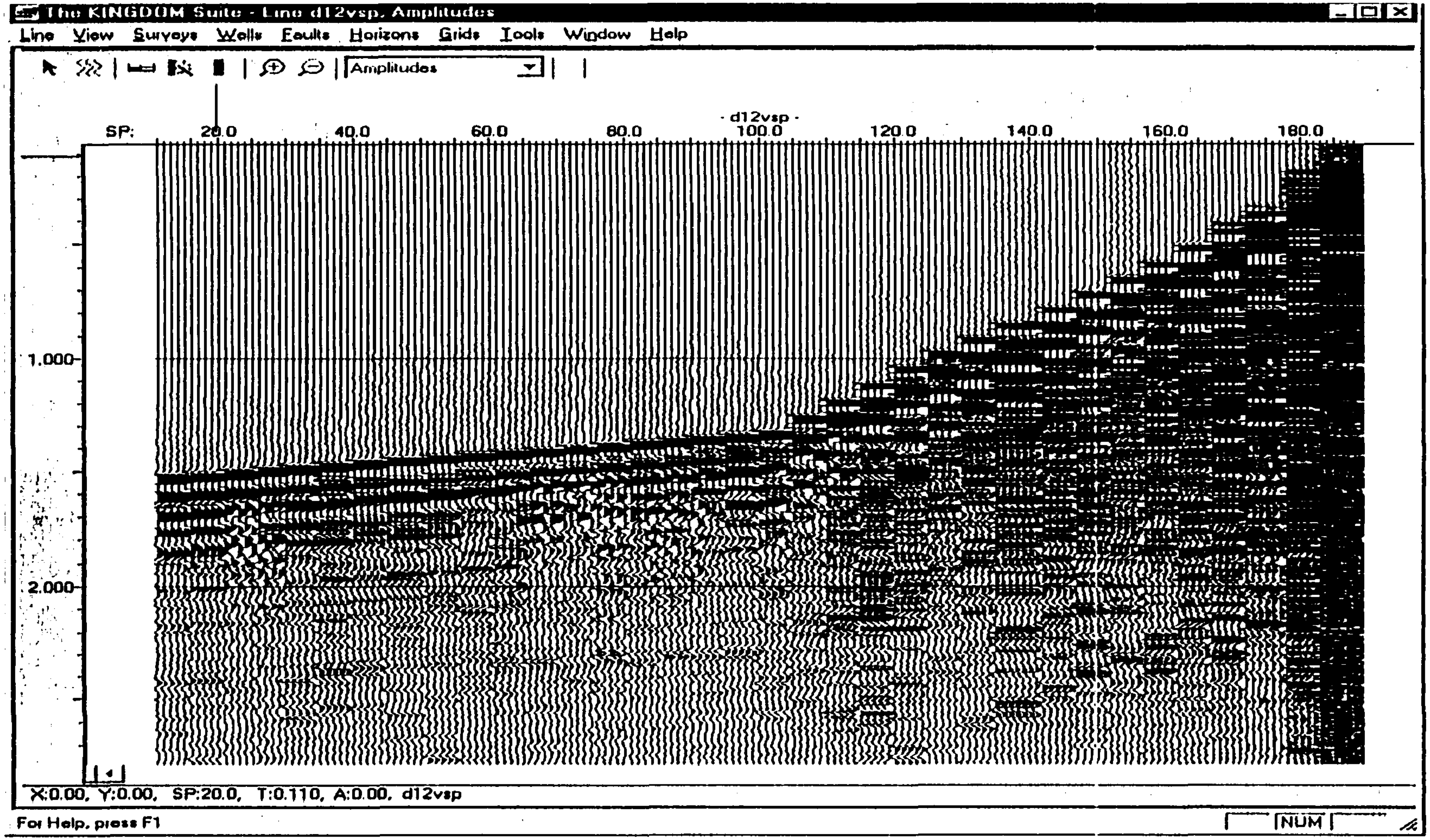

Figure 5.12. Real VSP data from the Eugene Island 354 Field at well D11.

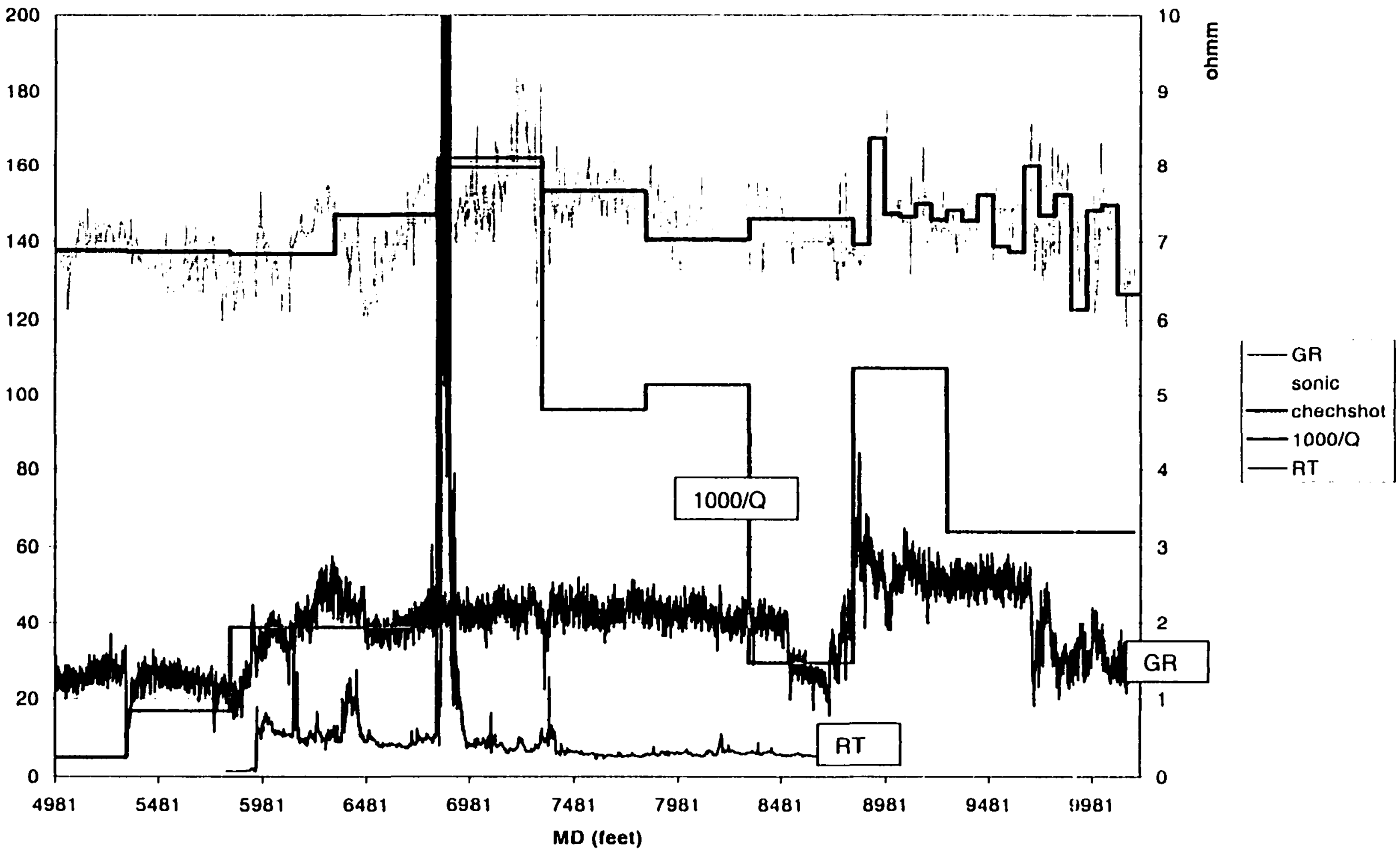

Figure 5.13. Comparison of the computed intrinsic attenuation profile and related well log data.

CHAPTER 6. DISCUSSION AND CONCLUSION

Accurate estimation of intrinsic attenuation from both surface seismic and VSP data is needed for attenuation research and calibration of attenuation based direct hydrocarbon indicators. In fact both measurements are difficult. However, as VSP data has the benefit of more information from the borehole in the form of sonic and density logs, it is easier to extract accurate estimates of intrinsic attenuation from VSP data. Accurate measurement of attenuation from VSP's can not only help us to understand the relationship between the attenuation and fluid content, but also can verify the techniques of attenuation measurement from surface seismics. Thus starting with a VSP is an easy way to combat various difficulties in attenuation measurement and application.

Since measurements in a borehole generally are accurate in the depth direction but have small lateral penetration, large errors can be introduced by interpolation between and extrapolation from well locations. In contrast, surface seismic measurements are laterally continuous. Therefore, integrated application of information from both seismics and VSP should improve the estimation of intrinsic attenuation and then reservoir properties.

The iterative scattering-removal Q estimation method from VSP data is more accurate than conventional spectral ratio methods. This method can compensate for traditional difficulties such as scattering, coupling and first arrival isolation, and at the same time allow accurate estimation of the intrinsic attenuation. The research presented here represents significant progress in attenuation measurement from VSP data. This method will be an important means of calibration of surface seismic attenuation attributes. It has already confirmed anomalously high attenuation in a likely hydrocarbon zone, and will be an effective tool for the study of attenuation using field data. Further studies to establish the statistical relationship between intrinsic attenuation and reservoir characteristics can be expected. Accurate estimation of attenuation also provides important support for attenuation estimation from surface seismic data. However, the iterative scattering-removal method is not perfect yet. It will be refined during practical application. The current method is susceptible to errors caused by early arriving tube-waves or shear-waves (due to mode conversions in the borehole), and could be improved by incorporating these events into the forward modeling. Improved understanding of how the signal/noise ratio and windowing and sampling phenomena affect the spectral ratio is needed to further improve attenuation estimates.

Application of attenuation as an exploration and development tool requires reliable measurement of Q from surface seismic data. The full waveform GLI inversion method is an important attempt in measuring Q from surface seismics. Most of the existing methods are restricted because they cannot solve the wavelet and scattering problems. The inversion method addresses these problems by directly inverting Q from the seismic trace. The method requires that multiples not be attenuated by processing. It can perfectly recover the Q values in simple models even if there is not a well-defined initial Q profile. This promising result implies that we can simplify our inversion model and focus on the formations of interest to obtain the correct intrinsic attenuation. Case studies are needed to further test the full waveform inversion method and to extend attenuation measurements from the borehole.

REFERENCES

Akbar, N., J. Dvorkin, and A. Nur, 1993, Relating P-wave attenuation to permeability, v. 58, No. 1, p. 20-29.

Amundsen, L., and Mittet., R., 1994, Estimation of phase velocities and Q-factors from zero-offset, vertical seismic profile data: Geophysics, 59, 500-517.

Aki, K., and Richards, P. G., 1980, Quantitative Seismology: Theory and Methods, p.168-169, W. H. Freeman, New York, 1980.

Anderson, R. G. and Castagna, J. P., 1984, Analysis of sonic log compressional wave amplitudes using borehole compensation techniques, APWLA Twenty-Fifth Annual Logging Symposium.

Backus, G., and Gilbert, F., 1968, The resolving power of gross earth data, Geophys. J. Roy. Astr. Soc., V. 16, p. 169-205.

Badri, M., and Mooney, H. M., 1987, Q measurements from compressional seismic waves in unconsolidated sediments, Geophysics, V. 52, No. 6, P. 772-784.

Banik, N. C., Lerche, I., and Sheuy, R. T., 1985, Stratigraphic filtering, Part I: Derivation of the O'Doherty-Anstey formula, Geophysics, V.50, No. 12, P. 2768-2774.

Batzle, M., Han, D., and Castagna, J. P., 1996, Attenuation and velocity dispersion at seismic frequencies, presented at 66th Annual Meeting of the Society of Exploration Geophysicists, Denver.

Bickel, S. H., and Natarajan, 1985, Plane-wave Q deconvolution, Geophysics, v. 50, no. 9, p. 1426-1439.

Biot, M. A., 1956, Theory of propagation of elastic waves in a fluid saturated porous solid, II, Higher frequency range, J. Acoust. Soc. Am., v. 28, p. 179-191.

Blair, D. P., 1990. A direct comparison between vibrational resonance and pulse transmission data from asseddment of seismic attenuation in rock, Geophysics, v. 55, p. 51-60.

Bourbie, T., and Zinszner, B., 1984, Saturation methods and attenuation versus saturation relationships in Fontainebleau Sandstone, 54th Ann. Internat. Mtg., Soc. Expl. Geophys., Expanded Abstracts, p.344-347.

Bracewell, R., 1965, The Fourier transform and its applications, McGraw-Hill Book Co.

Castagna, J. P., 1998, Velocity dispersion - How significant is it, 1998 EDGE Consortium Report.

Castagna, J. P., Batzle, M. L., and Kan, T. K., 1993, Rock physics - the link between rock properties and AVO response, in J. P. Castagna and M. M. Backus, Eds., Offset-Dependent Reflectivity - Theory and Practice of AVO Analysis., Society of Exploration Geophysicists, Tulsa, 348pp.

Claerbout J. F., 1976, FUNDAMENTALS OF GEOPHYSICAL DATA PROCESSING: with applications to petroleum processing, McGraw-Hill Inc.

Clark, V. A., 1980, Effects of volatiles on seismic attenuation velocity in sedimentary rocks, Ph.D. dissertation, Texas A & M University.

Clark, V. A., Spencer, T. W., and Tittmann, B. R., 1981, The effect of thermal cycling on the seismic quality factor Q of some sedimentary rocks, J. G. R., v. 86, p. 7087-7094.

Cooke, D. A., and Schneider, W. A., 1983, Generalized inversion of reflection seismic data, Geophysics, v. 48, p. 665-676.

Dainty, A. M., 1981, A scattering model to explain seismic Q observations in the lithosphere between 1 and 30 Hz. Geophys. Res. Lett., v. 8, p. 1126-1128.

Dasgupta, R. and Roger A. C., 1998, Estimation of Q from surface seismic reflection data, Geophysics, v. 63, no. 6, p. 2120-2128.

Dvokin, J., and Nur, A., 1993, Dynamic poroelastisity: a unified model with the squirt and the Biot mechanisms, Geophysics, v. 58, p. 524-523.

Frazer, L. N., 1994, A pulse in a binary sediment, Geophys. J. Int. V. 118, p. 75-93.

Frisillo, A. J., Stewart, T. J., 1980, Effect of partial gas/brine saturation on ultrasonic absorption in sandstone, J. G. R. v. 85, p. 5209-5211.

Frisillo, A. J.M And Thomsen, L., 1992, Effect of fluid microdistribution on velocity and attenuation in porous rock, 54th Ann. Internat. Mtg., Europ. Assoc. Expl. Geophys., Expanded Abstracts, p. 246-247.

Futterman, W. I., 1962, Dispersive Body Waves, J. G. R., v. 67, p. 5279-5291.

Gardner, G. H. F., Wyllie, M. R. J., and Droschak, D. M., 1964, Effects of pressure and fluid saturation on the attenuation of elastic waves in sands, J. Petr. Tech. V. 16, p. 189-198.

Gladwin, M. T., and Stacey, F. D., 1974, Anelastic degradetion of acoustic pulses in rock, Phys. Earth Planet. Int., V. 8, p. 332-336.

Harris, P. E., and White, R. E., 1991, Improving the performance of f-x prediction filtering at low signal-to-noise ratios: Presented at the 53rd Eur Assn. Expl. Geophys. Meeting, Paper A22.

Houck, R. T., 1987, Comparison of Q measurements from logs and VSPs, 57th Ann. Internat. Mtg., Soc. Explor. Geophys., Expanded Abstracts, p. 786-788.

Hough, S. E., Anderson, J. G., Brune, J., Vernon, F. III, Berger, J., Fletcher, J., Haar, L., Hanks, T., And Baker, L., 1988, Attenuation near Anza, California, Bull. Seismol. Soc. Am., v. 78, p. 672-695.

Hoshiba, M., Sato, H., And Fehler, M., 1991, Numerical basis of the separation of scattering and intrinsic absorption from full seismogram envelope--- A Monte-Carlo simulation of multiple isotropic scattering, Pap. Meteorol. Geophysics, v. 42, p.65-91.

Jacobson, R. S., 1987, An investigation into the fundamental relationships between attenuation, phase dispersion, and frequency using seismic refraction profiles over sedimentary structures, Geophysics, v. 52, p. 72-87.

Jones, T. D., 1983, wave propagation in porous rock and models for crustal structure, Ph.D. thesis, Standford Univ.

---1986 pore fluids and frequency-dependent wave propagation in rocks Geophysics, v. 51, p. 1939-1953.

Jones, T. D., And Nur, A., 1983, velocity and attenuation in sandstone at elevated temperatures and pressures, Geophysics, Res., Lett. V. 10, p. 140-143.

Kan, T. K., Corrigan, D., and Huddleston, P. D., 1981, Attenuation Measurement from Vertical Seismic Profiles, Presented at 51th Ann. Internat. Mtg, Soc. Expl. Geophys.

Kan, T. K., Batzle, M. L., and Gaiser, J. E., 1983, Attenuation measured from VSP: Evidence of frequency dependent Q, Presented at 53th Ann. Internat. Mtg, Soc. Expl. Geophys.

Kanamori, H. and Anderson, D. L., 1977, Importance of physical dispersion in surface wave and free oscillation problems, Review: Rev. Geophysics and space physics, v. 15, p. 105-112.

Kang, I. B., and McMechan, G. A., 1994, Separation of intrinsic and scattering Q based on frequency-dependent amplitude ratios of transmitted waves, J. of Geophysical Res., v. 99, no. B12, p. 23875-23885.

Kjartansson, E., 1979, Constant Q wave propagation and attenuation, J. Geophys. Res., V. 84, p. 4737-4748.

Klimentos, T., and McCann, C. , 1990, Relationships among compressional wave attenuation, porosity, clay content, and permeability in sandstones, v. 55, No. 8, p. 998-1014.

Lamb, W. J., 1998, Absorption and dispersion from Gypsy data, 1998 EDGE Consortium Report.

Lanczos, C., 1961, Linear differential operators, D. van Nostrand Co., London, p. 564.

Marquardt, D. W., 1963, An algorithm for least squares estimation of nonlinear parameters, J. Soc. Indust. Appl. Math., c.11, p. 431-441.

Mavko, G. M. and Nur, A., 1979,Wave attenuation in partially saturated rocks, Geophysics, v. 44, no. 2, p. 161-178.

Mayeda, K., Koyanagi, S., Hoshiba, M., Aki, K., And Zeng, Y., 1992, A comparative study of scattering, intrinsic, and coda Q for Hawii, Long Valley, and central California between 1.5 and 15.0 Hz, J. G. R., v. 97, p. 6643-6659.

McDonal, F. J., F. A. Angona, R. L. Mills, R. L. Sengbush, R. G. Van Nostrand, and J. E. White, 1958 Attenuation of shear and compressional waves in Pierre shale, Geophysics, v. 23, p. 421-439, 1958.

Meissner, R.. 1983, Attenuation of seismic waves in sediments, Proc. 11th World Petroleum Congress. v.2, p. 363-381.

Meju, M. A., 1994, A general program for linear parameter estimation and uncertainty analysis, Computers and Geosciences, v. 20, no. 2, p. 197-220.

Mitchell, J. T., Derzhi, N., Lichman, E., and Lanning, E. N., 1996, Energy absorption analysis: a case study, presented at 66th nnual Meeting of the Society of Exploration Geophysicists, Denver.

Murphy, W. F., III, 1982, Effects of microstructure and pore fluids on acoustic properties of granular sedimentary materials, Ph.D. Thesis, Standford University.

---1983, Effects of partial water saturation on attenuation in Massilon Sandstone and Vycor porous Glass, J. Acoust. Soc. Am., v. 71. No. 6, p. 1458-1468.

Murphy, W. F., III, Winkler, K. W., and Kleinberg, R. L., 1986, Acoustic relaxation in sedimentary rocks: Dependence on grain contacts and fluid saturation, Geophysics, v. 51, p. 757-766.

O'Connell, R. J., and Budiansky, B., 1977, Viscoelastic properties of fluid-saturated cracked solids, J. Geophys. Res., v. 76, p. 2022-2034.

O'Doherty, R. F., and Anstey, N. A., 1971, Reflections on amplitudes, Geophysical Prospecting, v. 19, p.430-458.

Palmer, I. D., and Traviolia, M. L., 1980, Attenuation by squirt flow in undersaturated gas sands, Geophysics, v. 45, p. 1780-1792.

Raikes, S. A., And White, J. E., 1984, Measurements of earth attenuation from downhole and surface seismic recording, Geophys. Prosp., v. 32, p. 892-919.

Richards, P. G., and Menke, W., 1983, The apparent attenuation of a scattering medium, Bull. Seismol. Soc. Am., v. 73, p. 1005—1-21.

Ricker, Norman, 1952, The form and laws of propagation of seismic wavelets, Geophysics, v.18, p. 10-40.

Rovelli, A., 1982, On the frequency dependence of Q in Friulli from short-period digital records, Bull. Seismol. Soc. Am., v. 72, p. 2369-2372.

Sams, M. S., Neep, J. P., Worthington, M. H., and King, M. S., 1997, The measurement of velocity dispersion and frequency-dependent intrinsic attenuation in sedimentary rocks, Geophysics, v. 62, no. 5, p. 1456-1464.

Shapiro, A. S., and Ziem, H., 1993, The O'Doherty-Anstey formula and localization of seismic waves, Geophysics, V. 58, No. 5, P. 736-740.

Spncer, J. W., 1979, Bulk and shear attenuation in Bera Sandstone: The effects of pore fluids, J. G. R., v. 84, p. 7521-7523.

--- 1981, Stress, relaxations at low frequencies in fluid saturated rocks: Attenuation and modulus dispersion, J. G. R., v. 86, p. 1803-1812.

--- 1985, Measurement and interpretation of seismic attenuation, Chapter 3 in Fitch, A. A., Developments in geophysical exploration methods - 6: Elservier Applied Science, London, 71-109.

Tang, X., and Burns D. R., 1992, Seismic scattering and velocity dispersion due to heterogeneous lithology, paper presented at Technical Program, 1992 Annual Meeting, (abstract), Soc. Explor. Geophys., New Orleans.

Tittmann, B. R., Bulua, J. R., and Abdel-Gawad, M. 1983, Dissipation of elastic waves in fluid saturated rocks, Am. Inst. Phys. conference on physics and chemistry of porous media, Schlumberger-Doll Research, Johnson, D. L., and Sen, P.N., Eds., Am. Inst. Phys., 131-143.

Turgut, A., and Yamamoto, T., 1990, Measurements of acoustic wave velocities and attenuation in marine sediments, J. Acoustic. Soc. Am., v. 87, p. 2376-2383.

Tutuncu, A. N., Sharma, M. M., and Podio, A. L., 1995, An experimental investigation of the role of pore fluids on the nonlinear behavior of rocks, Absts., SEG annual meeting, Houston, 886-889.

White, J. E., 1975, Computed seismic speeds and attenuation in rocks with partial saturation, Geophysics, 40, p. 224-232

White, R. E., 1973, The estimation of signal spectra and related quantities by means of the multiple coherence function, Geophysical Prospecting, v. 21, p. 660-703.

---1980, Partial coherence matching of synthetic seismograms with seismic traces, Geophysical Prospecting , V. 28, p. 333-358.

Winkler, K. W., and Nur, A., 1979, pore fluids and seismic attenuation in rocks, Geophys. Res. Lett., v. 61, p. 1-4.

---- 1982, Seismic attenuation: Effects of pore fluids and frictional sliding, Geophysics, v. 47, p. 1-15.

Yamamoto, T., Thomas, N., and Murat, K., 1995, Imaging the permeability structure of a limestone aquifer by crosswell acoustic tomography, Geophysic, v. 60, no. 6, p. 1634-1645.